

Cover Page



Universiteit Leiden



The handle <http://hdl.handle.net/1887/74368> holds various files of this Leiden University dissertation.

Author: Crisafi,E.

Title: In vitro investigation of the photoprotection mechanism of Light Harvesting Complex II

Issue Date: 2019-06-25

*In vitro investigation of the
photoprotection mechanism of
Light Harvesting Complex II*

Emanuela Crisafi

*In vitro investigation of the photoprotection
mechanism of Light Harvesting Complex II*

PROEFSCHRIFT

ter verkrijging van
de Graad van Doctor aan de Universiteit Leiden,
op gezag van Rector Magnificus Prof. Mr. C. J. J. M. Stolker,
volgens besluit van het College voor Promoties
te verdedigen op dinsdag 25 juni 2019
klokke 13:45 uur

door

Emanuela Crisafi

Geboren te Brindisi, Italië
in 1988

PROMOTIECOMMISSIE

Promotor: Prof. dr. Huub J.M. de Groot

Co-promotor: Dr. Anjali Pandit

Overige leden: Prof. dr. Hermen S. Overkleeft
Prof. dr. Alexander Kros
Prof. dr. Bruno Robert
(*University of CEA Saclay, France*)
Prof.dr. Roberta Croce
(*University of VU Amsterdam*)

Emanuela Crisafi

In vitro investigation of the photoprotection mechanism of Light Harvesting Complex II.
Ph.D. thesis, Leiden University

ISBN: 9789463325165

Cover and bookmark designed by Nicola Francesco Toro.

This research was financed by a CW-VIDI grant from the Netherlands Organization of Scientific Research (NWO) under grant nr. 723.012.103.

Table of contents

LIST OF ABBREVIATIONS.....	8
CHAPTER 1.....	9
Introduction	9
PHOTOSYNTHESIS.....	10
PHOTOPROTECTION	12
LIGHT-HARVESTING ANTENNAS.....	13
LIGHT-HARVESTING COMPLEX II.....	14
PHOTOSYNTHETIC PIGMENTS AND THEIR CHARACTERISTICS.....	15
PsbS.....	18
MIMICKING A MEMBRANE ENVIRONMENT	19
SCOPE OF THE THESIS.....	22
REFERENCES.....	23
CHAPTER 2.....	26
Disentangling protein and lipid interactions that control a molecular switch in photosynthetic light harvesting	26
ABSTRACT.....	27
INTRODUCTION.....	28
MATERIALS AND METHODS.....	29
RESULTS AND DISCUSSIONS	35
GENERAL DISCUSSION	46
CONCLUSIONS.....	47
REFERENCES.....	48
CHAPTER 3.....	51
Fluorescence lifetimes of LHCII in a lipid environment: aggregation, low pH and the presence of PsbS.....	51
ABSTRACT.....	52
INTRODUCTION.....	53
MATERIALS AND METHODS.....	55
RESULTS	58
DISCUSSION.....	65
CONCLUSIONS.....	66
REFERENCES.....	67
APPENDIX	69
CHAPTER 4.....	72
Production of ¹³C Lutein rLhcb1 for NMR studies.....	72
ABSTRACT.....	73
INTRODUCTION.....	74
LARGE SCALE OVEREXPRESSION AND PURIFICATION OF Lhcb1 APOPROTEIN IN <i>E. coli</i>	75
¹³ C LABELLING OF CHLAMYDOMONAS REINHARDTII.....	78
PIGMENT EXTRACTION	79
HPLC ISOLATION	79
REFOLDING AND CHARACTERIZATION OF ¹³ C LUTEIN rLhcb1	84
CONCLUSIONS.....	90
REFERENCES.....	91
CHAPTER 5.....	93
NMR studies on ¹³C lutein- rLhcb1.....	93
ABSTRACT.....	93

<i>INTRODUCTION</i>	95
<i>MATERIALS AND METHODS</i>	97
<i>RESULTS AND DISCUSSION</i>	101
<i>CONCLUSIONS</i>	112
<i>REFERENCES</i>	113
<i>A.5 Liquid and Solid-State NMR of lutein</i>	115
CHAPTER 6	120
CONCLUSIONS and OUTLOOK	120
CONCLUSIONS.....	121
OUTLOOK.....	121
<i>SUMMARY</i>	124
<i>SAMENVATTING</i>	125
<i>RIASSUNTO</i>	127
<i>CURRICULUM VITAE</i>	128
<i>PUBLICATIONS</i>	129
<i>ACKNOWLEDGEMENTS</i>	130

LIST OF ABBREVIATIONS

ATP	Adenosine Triphosphate
β -DM	n-dodecyl- β -D-maltoside
CD	Circular dichroism
CP	Crosspolarization
Chl	Chlorophyll
<i>E. coli</i>	<i>Escherichia coli</i>
Fd	Ferredoxin
HEPES	4-(2-hydroxyethyl)-1-piperazineethanesulfonic acid
HPLC	High performance liquid chromatography
HETCOR	Heteronuclear correlation spectroscopy
IPTG	Isopropyl- β -D-thiogalactoside
LDS	Lithium dodecyl sulfate
LHCII	Light harvesting complex II
Lhcb	Light harvesting complex b
Lut	Lutein
MAS	Magic angle spinning
NADPH	Nicotinamide adenine dinucleotide phosphate
Neo	Neoxanthin
NMR	Nuclear magnetic resonance
OD	Optical density
OEG	Oxygen evolving complex
OG	Octyl- β -Glucoside Detergent
PARIS	Phase Alternated Recoupling Irradiation Schemes
PC	Plastocyanin
PLR	Protein to lipid ratio
PQ	Plastoquinone
PsbS	Photosystems subunit S
PSI	Photosystem I
PSII	Photosystem II
TAP	Tris-acetate-phosphate
Tris	Tris(hydroxymethyl)aminomethane
TRF	Time resolved fluorescence
SDS	Sodium dodecyl sulfate,
UV-Vis	Ultra violet, visible spectroscopy
Vio	Violaxanthin
Zea	Zeaxanthin

CHAPTER 1

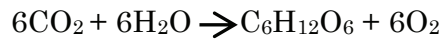
Introduction

PHOTOSYNTHESIS

“Photosynthesis is a process in which light energy is captured and stored by an organism, the stored energy is used to drive energy-requiring cellular processes [1]”

This definition of photosynthesis includes all kind of systems that use solar energy to survive, from algae to plants to bacteria.

The oxygenic photosynthetic process can be described by this minimal equation:



Julius Robert Mayer, in 1864, discovered that carbohydrates, in the form of starch, were accumulated in the portion of the leaf directly exposed to the light. The understanding of this observation was that, under illumination, the absorbed carbon dioxide in the presence of water was converted into organic carbon, in the form of carbohydrates, with O_2 as a side product.

As displayed in Figure 1.1, photosynthesis takes place in the chloroplast, within the thylakoid membrane compartments and in the soluble phase named stroma. Two components of the thylakoid membrane have been identified: a cylindrical stacked system called granum and the un-stacked interconnecting region named stroma lamellae [2]. The thylakoid membrane is a lipid bilayer, mainly composed of galactolipids and phospholipids, which hosts protein complexes and cofactors [1].

The photosynthetic process consists of two phases which are the light and dark reaction respectively described below:

- Light reaction: involves harvesting of the light energy, which is converted to chemical energy and temporarily stored in the form of ATP and NADPH.
- Dark reaction: involves the conversion of CO_2 using the energy of ATP and NADPH into other compounds used for long-term energy storage, via reactions involved in the Calvin-Benson cycle.

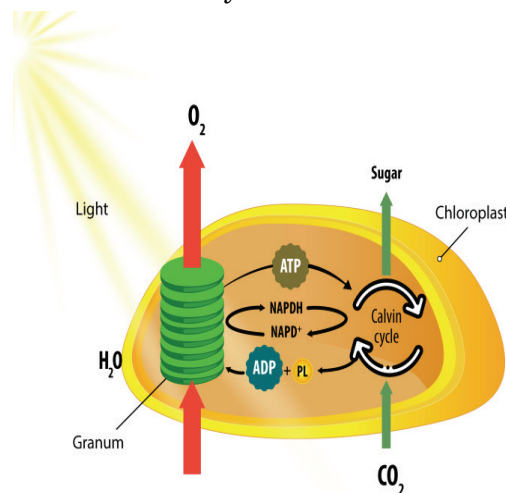
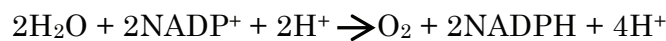


Figure 1.1 Representation of the two main stages of photosynthesis. On the left side, the light reactions are presented and, on the right side the dark reactions carried out in the chloroplast are shown.

Solar energy is primarily absorbed by two groups of pigments, chlorophylls (Chls) and carotenoids (Cars). These pigments are bound to Light-Harvesting Complexes (LHCs) and to both reaction centre complexes, Photosystem I (PSI) and Photosystem II (PSII). The representation in Figure 1.2 shows the linear electron flow upon light absorption. Excitation energy is transferred to the PSII reaction centre Chl special pair (P680), creating a charge-separated state. An electron is donated from P680 to pheophytin and consequently to the plastoquinone (PQ) bound to the complex, Q_A . P680⁺ is reduced back to P680 via the active Tyr (Y_z) of PSII. Y_z is reduced back using electrons extracted from water at the oxygen-evolving complex (OEC) while protons are released into the lumen. The electron, from the Q_A site, is transferred to a PQ in the Q_B site. After two turnovers, the reduced Q_B -PQ accepts two protons from the stroma and is released from the PSII complex in the form of PQH₂ [3,4]. This molecule, after diffusion through the membrane, reaches the Cyt b₆f in which the Q-cycle takes place. The two electrons are donated to the blue copper plastocyanin (PC) which is a redox protein able to diffuse to PSI that similarly to the PSII has a reaction centre Chl special pair P700, and the four protons are released into the lumen. Excitation of PSI leads to charge separation from the P700 special pair producing an electron that is used to reduce ferredoxin (Fd). P700⁺ is then reduced back accepting electrons, from the PC while the Fd electrons are donated to NADP⁺-oxide reductase to produce NADPH. The net reaction can be written as:



The electron flow involves the generation of reducing power used to produce ATP. The protons, which accumulated at the lumen, generate a ΔpH used by the ATP synthase complex to drive the conversion of ADP with inorganic phosphorus into ATP. The ATP and NADPH produced are used to fixate CO₂ into carbohydrates.

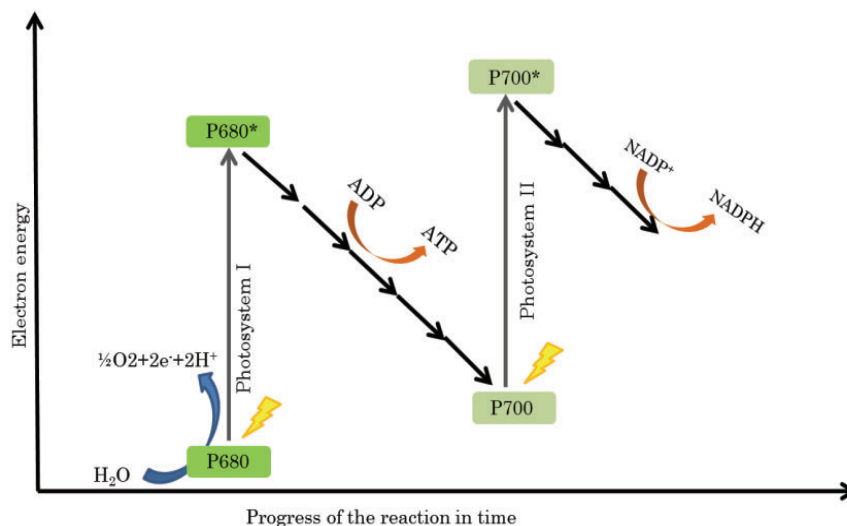


Figure 1.2 Representation of the linear electron flow in the light reactions process according to Hohmann-Marriot et al. [1].

PHOTOPROTECTION

Photosynthetic systems are exposed to intermittent sunlight. Sudden changes in the sunlight exposure can saturate quickly the electron transport chain preventing further use of the absorbed energy. The consequence of the unused energy is the formation of triplet $^3\text{Chl}^*$, after inter-system crossing (ISC) of $^1\text{Chl}^*$, which can react with oxygen to produce singlet oxygen $^1\text{O}_2$ causing oxidative damage to proteins, lipids, and pigments [5,6]. To reduce the negative effect of light stress, plants and algae have developed a variety of photoprotective mechanisms that can be activated in the long and in the short term. The first group is characterized by an acclimation of the system to stressful conditions. The second group is, instead, characterized by a short-term response to sudden changes in the light exposure known as non-photochemical quenching (NPQ), which are the mechanisms of interest in this dissertation.

With the increase of irradiation, the electron flow increases and with it, the ΔpH across the membrane. The system responds to ΔpH with various mechanisms aimed to avoid overload of the electron flow. The ΔpH activates the regulatory protein PsbS and the xanthophyll-cycle in which de-epoxidase enzymes convert violaxanthin to zeaxanthin [7,8].

Figure 1.3 shows the differences between the utilized energy and absorbed. In the case of high light, photosynthetic systems keep absorbing energy photons but only a fraction will be actually involved in the photosynthetic cycle while the rest is dissipated as heat to prevent overexcitation. At the molecular level, the absorbed energy, when in excess compared to what is the capacity of the carbon fixation, leads to lumen acidification, which initiates processes that down-regulate photosynthesis [9].

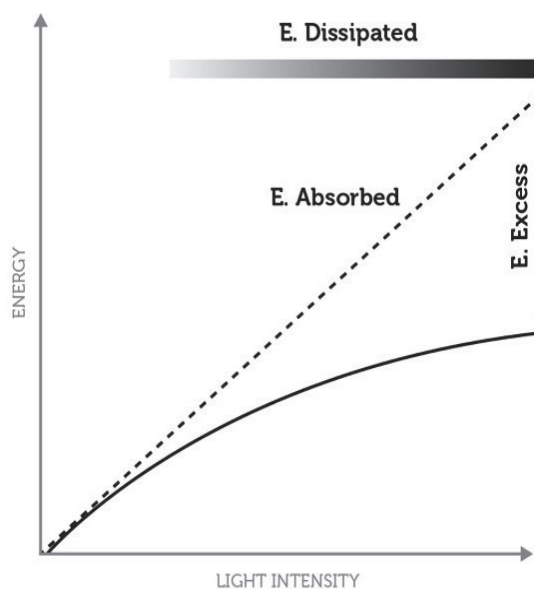


Figure 1.3 The graphic illustration, according to Ruban et al., shows how in high light condition is necessary the photoprotection of the photosystem II. The 'excess energy' is defined as the difference between the light absorbed and the utilized, which can cause photo-oxidative damage to the photosynthetic system. This excess will be dissipated via NPQ processes as heat [10].

Examples of such down-regulating processes are excitation quenching and the xanthophyll cycle [9].

Several mechanisms of photoprotection have been identified involving different components, among which the major Light-Harvesting antenna Complex (LHCII) plays a central role. NPQ can be differentiated into three processes as described below:

- qI slow relaxing process related to photoinhibition, which is defined as a light-induced decrease of the quantum yield of photosynthetic carbon fixation [11].
- qZ is related to the presence of zeaxanthin (Zea). When NPQ is activated, a significant amount of epoxide carotenoids, predominantly violaxanthin, (Vio) is converted into non-epoxide zeaxanthin (Zea) via the de-epoxidase enzyme, in a process known as the xanthophyll cycle. This VDE cycle is reversible in the dark [12-15]. The full understanding of the role of this pigment in the photoprotection is still under investigation.
- qE is the fastest component of NPQ that is activated and relaxes very quickly [16]. As for qZ, this mechanism is activated by the acidification of the thylakoid lumen. The qE process is called energy-dependent quenching and is a nonphotochemical quenching, through which the excess absorbed light energy is safely dissipated as heat [16,17].

This dissertation will focus on the molecular mechanisms involved in the fast component of NPQ, qE. Researchers have proposed different mechanisms involving either Chl–Cars [18-22], or Chl–Chl interaction [23,24] to explain the photophysical cause of excitation energy dissipation. Molecular models for non-photochemical quenching involving Chl–lutein interactions, and consequently quenching of lutein excited states, have been supported recently by *in silico* models predicting that small changes in orientation of the lutein might be sufficient to tune excitation quenching [25].

LIGHT-HARVESTING ANTENNAS

The primary function of the antenna is to absorb light and transfer the energy to the RC, which is a trap. In 1936 Gaffron and Wohl imagined that the energy was transferred from one pigment to the other, but pigments are not capable to carry out the photosynthesis by themselves [26]. Therefore, it was conjectured that a photosynthetic unit must consist of a collection of pigments. This was later confirmed by Franck and Teller in 1938 [27].

A variety of antennas have been identified in organisms able to perform photosynthesis. Antenna complexes can be divided into two main classes: integral membrane antenna complexes and extrinsic antenna complexes. The first class consists of proteins with buried pigments and are embedded in the lipid bilayer of photosynthetic membranes. The second class, instead, consists of extrinsic antenna complexes that are associated with transmembrane elements. The energy absorbed by the extrinsic complexes is first transferred to the integral membrane from which it is redirected to the reaction centre [1].

The existence of an antenna is essential for sufficient light collection and photoprotection in photosynthesis. Not only the antennas are necessary to harvest photons and efficiently transfer the energy to the reaction center, but for oxygenic photosynthetic organisms that are exposed to full sunlight, the energy excess has to be dissipated to avoid photodamage. Examples of proteins that have both light-harvesting and photoprotective functions are the LHC pigment-protein complexes [1]. This class of proteins is still under investigation to understand how the molecular mechanism of photoprotection is activated and which kind of structural rearrangements are needed to promote this function.

LIGHT-HARVESTING COMPLEX II

Light-Harvesting Complex II (LHCII) associates with PSII to form a multisubunit pigment-protein complex located in the thylakoid membrane of algae and higher plants. LHCII is the first chlorophyll-binding protein to be identified and the most abundant membrane protein on Earth [28,29]. The protein belongs to the multi-gene family of LHC proteins. All LHC proteins are encoded by Lhc genes and form complexes containing three membrane-spanning helices, with the exception of Psbs that has four helices, with three invariant amino acids Glu, Arg, several well conserved Gly residues and a conserved sequence for the generic LHC motif in the stretch ELINGRLAMLGFLGFLVPELIT, which is the transmembrane core of the complex [30]. Two of the transmembrane helices are kept together by Arg-Glu salt bridges and contain the majority of the binding sites for chlorophylls and carotenoids [31]. The LHCII trimeric complexes of higher plants are assembled from polypeptides encoded from three genes, Lhcb1, Lhcb2, and Lhcb3, while Lhcb4, Lhcb5, and Lhcb6 encode for the monomeric core antenna complexes.

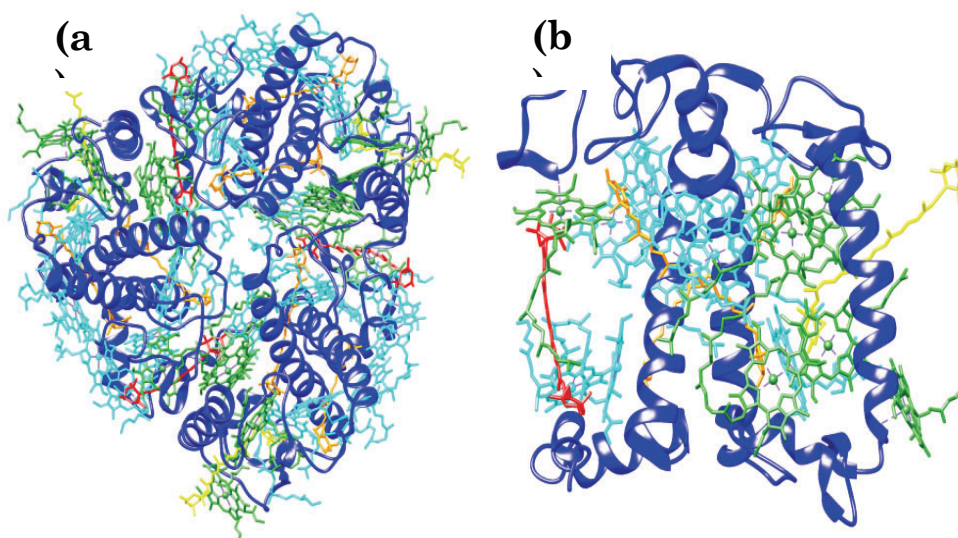


Figure 1.4 LHCII trimeric crystal structure (a) and monomeric (b) from spinach (PDB- 1RWT). In green Chl b, in cyan Chl a, in orange Lut1 and Lut2, in red Vio and in yellow Neo.

As shown in the paper of Caffarri *et al.*, Lhcb1 and Lhcb2 have similar but non-identical pigment binding and spectral properties, and the presence of Lhcb3 together with the other holoproteins lead to the formation of a heterotrimer [32].

The primary function of the LHCII protein is to bind pigments in an arrangement that ensures efficient absorption and excitation transfer of solar energy. In the case of excess of light, in order to prevent photodamage, the LHCII protein switches from a light-harvester function into a photoprotector function [33].

PHOTOSYNTHETIC PIGMENTS AND THEIR CHARACTERISTICS

In the following paragraph Chlorophylls and carotenoids, which are the active components involved in light harvesting, are described.

CHLOROPHYLLS

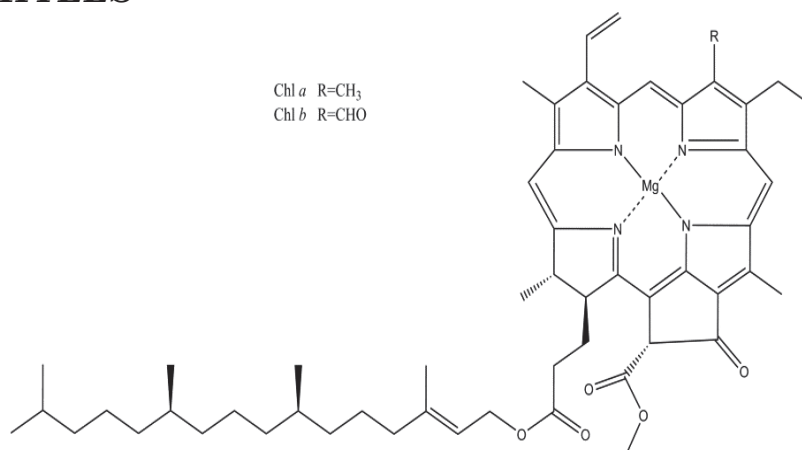


Figure 1.5 Chl chemical structure. The difference between Chl a and Chl b lies in the group R in C-7 which is respectively a methyl or a formyl group.

The first researchers investigating Chl pigments were Pelletier and Caventou in 1818 [1]. Several kinds of Chl pigments have been discovered in higher plants and algae, which are named in order of discovery from *a-f*. The Mg²⁺ coordinates the four nitrogen atoms, which are the part of a pyrrole ring, as represented in Figure 1.5 [34]. The hydrocarbon tail is attached to the fifth ring, isocyclic ring, which derived from protoporphyrin.

Chl *a* and Chl *b* are abundant in the eukaryotic photosynthetic organisms. As illustrated in Figure 1.5 the two pigments differ only for the group in the C-7 position. Both pigments absorb in the blue and red region of the visible spectrum. These properties are correlated to the conjugation system, given by the π -electrons, which extends over the planar chlorine macrocycle. The electronic transitions can be explained with the theory of the four orbitals model [35].

The presence of the formyl group gives more symmetry to the macrocycle, which means that the absorption spectrum is more similar to the porphyrin one, and is responsible for the spectral shift to shorter wavelengths compared to Chl *a*. The two types of Chls are not uniformly distributed and in fact, while Chl *a* is present in the reaction centre, Chl *b* not. In the absorption spectra of Chl *a*, as shown in Figure 1.6, the excited state is populated by blue light absorption, the Soret band in the region 400-480 nm, and relaxes, via heat loss, to the energy level accessed by red light absorption for the Q bands in the region 600-700 nm [36].

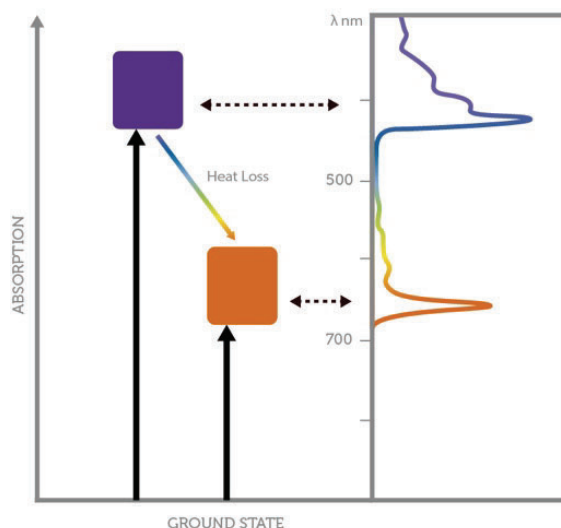


Figure 1.6 Simplified absorption energy level diagram for Chl *a* according to what proposed from Blankenship et al. [36].

CAROTENOIDS

Cars have in common the delocalization of the π -electrons. The Cars family is divided into two subgroups, unoxygenated and oxygenated. β -Carotene and α -Carotene are part of the first group, in which no oxygen atoms are present in the structure [37]. In the other subgroup, at the end of each chain there are usually ring structures containing one or more oxygen atoms as part of a hydroxyl group or epoxide group. Figure 1.7 shows the chemical structures of the most common carotenoids which are bound to the LHCs.

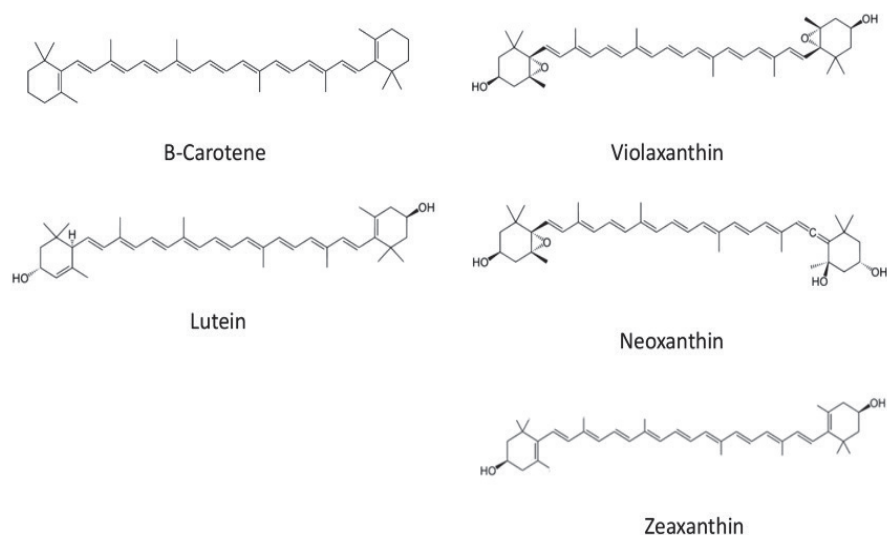


Figure 1.7 Chemical structures of carotenoids with different conjugation lengths. Neo has $N=8$, Vio has $N=9$, Lut has $N=10$ and Zea has $N=11$ double bonds

Carotenoids have the primary function of increasing the absorption of LHCs in the blue-green region (400-500 nm) with their conjugated polyene chain. The transition from S_0 to S_2 is promoted by light absorption, while the direct transition to S_1 is forbidden due to the molecular symmetry of the S_0 and S_1 state. The S_2 excited-state lifetime is in the order of femtoseconds and the S_2 state decays by internal conversion to S_1 from which the molecule relaxes to the ground state via non-radiative internal conversion.

The excitation energy levels of carotenoids are inversely dependent on their conjugation length (N). Longer conjugation lengths lower the energy of the S_1 states [38]. Carotenoids increase the energy absorption cross section of the protein but also play an important role in the promotion of the protein folding, as will be further discussed in Chapter 5 [39]. Indisputably, another important role of these molecules resides in the participation to the photoprotection mechanism because they are strong antioxidants. Excess of energy promotes the formation of harmful long-lived $^3\text{Chl}^*$ which reacts with O_2 forming $^1\text{O}^*$ [5]. This mechanism is prevented owing to the proximity of Cars to Chls, which allows the transfer of the Chl triplet energy to the carotenoid and consequently the energy is dissipated via a non-radiative process [40].

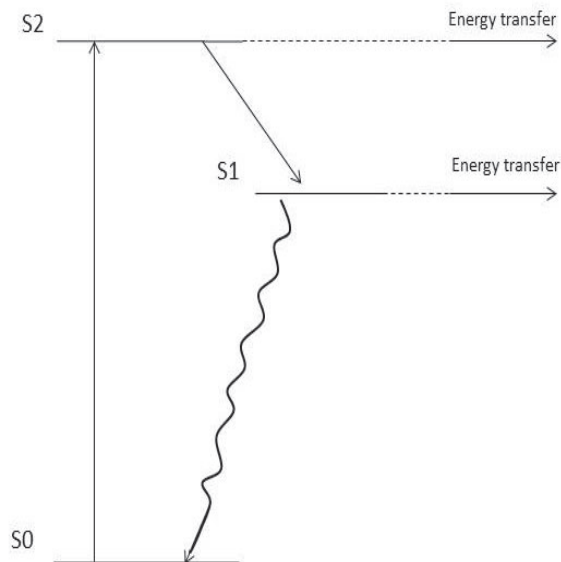


Figure 1.8 Schematic energy level diagram of carotenoids according to Blankenship [1].

PsbS

The photosystem II subunit S protein (PsbS) is an active participant in qE-type non-photochemical quenching, which protects plants from photodamage under excess light conditions. The activation of PsbS, triggered from low pH that protonates the two glutamates in the luminal loop, initiates qE processes [41]. PsbS, as mentioned before, is part of the LHCs family. The protein structure is characterized by four transmembrane helices, as shown in Figure 1.9, which determine a compact structure that is unable to selectively bind any pigments. Fan *et al.* have proposed that *in vivo* the active form of PsbS during qE, at pH 5.0, most probably is a stable dimer [41]. No clear explanation of how PsbS is exactly involved in the NPQ has been commonly agreed upon so far and the molecular mechanism of PsbS is still unresolved [8,10,42].



Figure 1.9 PsbS crystal structure (PDB-4RI2) from spinach. In cyan are underlined the 2 glutamate sites active in the protection mechanism. Glu 173 is in the loop while Glu 69 is in the helix.

One hypothesis is that PsbS is originally associated with the PSII core, and under high-light conditions migrates toward LHCs [42]. Considering that the protein does not bind any pigment molecules, the activated dimeric PsbS protein, located among the antennae, might play the role of an attenuator slowing down the energy flow amongst the LHCs. It has been conjectured that PsbS is able to promote thylakoid membrane reorganization, responsible for the promotions of the quenching states [41,43]. Evidence for direct interaction between PsbS and LHCs during qE has been validated with pull-down assays [44] and by *in vitro* reconstitution of a proteoliposome system containing PsbS, LHCII, and Zea [45]. This interaction is analysed in Chapter 3. It is also possible that in qE processes PsbS acts as pH-sensing trigger or as a catalyst [45].

MIMICKING A MEMBRANE ENVIRONMENT

For structural and functional studies, the membrane environment plays an essential role in membrane proteins [46-48]. It would be ideal to be able to study a protein of interest in its native environment but due to the membrane complexity, alternatives have to be found [49]. For membrane protein analysis, it is, therefore, a standard procedure to isolate the one of interest to avoid any interferences with other proteins or membrane constituents [50].

This dissertation focuses on the membrane protein LHCII, which in the native systems is located in the thylakoid membrane. LHCII is a hydrophobic protein and for this reason, the isolated protein can be studied either in detergent micelles or can be inserted in model membranes, such as liposomes and nanodiscs.

As mentioned earlier in this chapter, LHCII can switch between two functions. *In vitro*, it is possible to reproduce these two activities by inserting the protein in nanodiscs or in liposomes as is presented and discussed in Chapters 2 and 3. In nanodiscs, due to the relatively large size of the LHCII pigment-protein complex compared to the nanodiscs sizes, only one protein per disc is inserted [51], preventing LHCII-LHCII interactions, while in liposomes, LHCII aggregates can be formed.

Membrane proteins tend to be hydrophobic and can be solubilized only by agents, detergents, which are defined as amphipathic molecules forming micelles in water.

In the mixture of biological membrane and detergent, the latter brings the membrane proteins into solution as detergent-protein complexes, although some lipid molecules may remain attached to the protein [50].

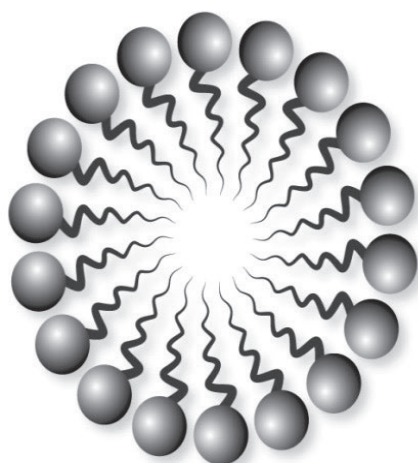


Figure 1.10 Cross section of a detergent micelle. The circle of hydrophilic heads point toward the water solution, while the hydrophobic tails are buried inside the micelle.

The structural biology of membrane proteins occupies a central place in current biophysics, biochemistry and cell biology investigations. Membrane proteins often display altered or loss of activity and function outside the phospholipid environment. For many systems, it is possible to reproduce the native behaviour in a membrane model [52].

In the 1970s the pioneering work of Racker and colleagues, started a new era for membrane protein characterization started [49,53]. Similarly to detergent molecules, lipids interact with the hydrophobic portions of the membrane protein, usually are the α helices, so that the protein is embedded in the phospholipid bilayer, as it is *in vivo* [50].

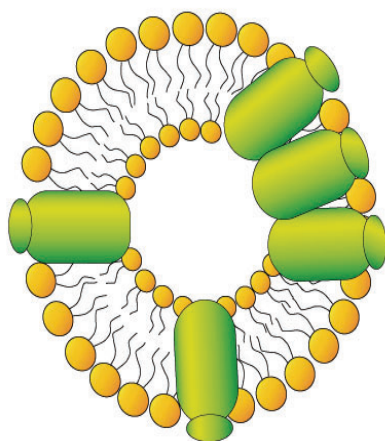


Figure 1.11 A liposome is a system formed by lipids, organized in a double layer similar to a natural biological membrane, creating a cavity filled by an aqueous solution [54]. This is a schematic cross-section representation of a proteoliposome. In yellow, the lipids are shown that are assembled via hydrophobic interactions between their acyl chains, which allows forming the characteristic bilayer. In green, a schematic representation of reconstituted protein is displayed. The "empty" cavity inside the proteoliposome is filled with a water-based solution which is often the buffer applied for protein solubilisation.

Reconstitution of purified membrane proteins into liposomes makes possible to have accurate control of several factors such as lipid composition and proteins interaction which affect the function of the target protein [49].

Alternative to liposomes is possible to use nanodiscs. As displayed in Figure 1.12, a nanodisc consists of a membrane patch that has been solubilized by two amphipathic proteins, called membrane scaffold proteins (MSPs). MSPs wrap around the hydrophobic core of the lipids, effectively creating a soluble portion of the membrane. When prepared properly, nanodiscs are uniform in size and allow the study of isolated membrane proteins *in vitro*, while maintaining a native-like membrane environment [55].

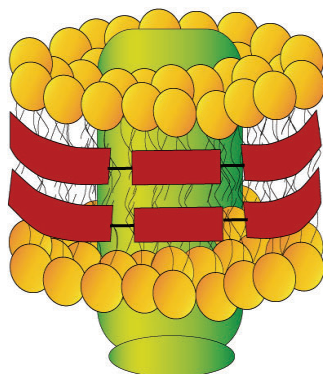


Figure 1.12 Representation of a nanodisc with inserted protein. In yellow the lipids forming the bilayer, in green, the inserted protein and in red the MSPs are shown which embrace the phospholipids bilayer. The size of the disc is determined by the length of the MSP and the lipids stoichiometry.

Nanodiscs have proven to be an invaluable tool for revealing the structure and function of isolated membrane proteins. There are several advantages of using nanodiscs over liposomes. In nanodiscs, both the C- and N-terminus of the protein are accessible and it is possible to have only one protein per disc, avoiding aggregation. Nanodiscs are increasingly being used as 'cassettes' that allowing investigation of membrane proteins without denaturation through a variety of analytical methods [52].

SCOPE OF THE THESIS

The scope of this thesis is to investigate *in vitro* the photoprotection mechanism of Light Harvesting Complex II. In Chapter 2 we aimed to study and differentiate the effect of the protein environment in the fluorescence quenching. Further investigation, whether the LHCII fluorescence quenching is the results of solo LHCII-PsbS interaction were performed in Chapter 3 by studying the two proteins co-inserted in a model membrane. In Chapter 4 we described the NMR quantity overproduction of recombinant Lhcb1, in *E. coli*, refolded in presence of pigments of which only lutein is ^{13}C labelled. With this selective labelling, the aim was to obtain a simplified protein NMR spectra from which only peaks relative to the labelled lutein are visible. Next up in Chapter 5 we focused in solid state NMR analysis of ^{13}C lutein-rLhcb1 in the unquenched and quenched state, respectively in detergent and in the aggregate state. The aim was to follow how lutein chemical shift is influenced upon conformational changes that undergo in the transition from unquenched to quenched state. Conclusion and future outlook of the thesis are discussed in Chapter 6.

REFERENCES

1. Blankenship RE. Molecular Mechanism in Photosynthesis. (2014).
2. Murphy DJ. The molecular organisation of the photosynthetic membranes of higher plants. *Biochim. et Biophys. Acta*, 864, 33-94 (1986).
3. Croce R, van Amerongen H. Light-harvesting and structural organization of Photosystem II: from individual complexes to thylakoid membrane. *J Photochem Photobiol B*, 104(1-2), 142-153 (2011).
4. Goussias C, Boussac A, Rutherford W. Photosystem II and photosynthetic oxidation of water: an overview. *Phil. Trans. R. Soc. Lond. B*, 357, 1369–1381. (2002).
5. Siefermann-Harms D. The light-harvesting and protective functions of carotenoids in photosynthetic membranes. *Physiologia Plantarum*, 69, 561-568 (1987).
6. Long SP, Humphries S, and Falkowski PG. Photoinhibition of photosynthesis in nature. *Annu. Rev. Plant Physiol Plant Mol. Biol.*, 45, 633-662 (1994).
7. Demmig-Adams B. Carotenoids and photoprotection in plants: A role for the xanthophyll zeaxanthin. *Biochim. et Biophys. Acta*, 1020, 1-24 (1990).
8. Li XP, Gilmore AM, Caffarri S, Bassi R, Golan T, Kramer D and Niyogi KK. Regulation of Photosynthetic Light Harvesting Involves Intrathylakoid Lumen pH Sensing by the PsbS Protein. *JBC Papers in Press.*, 279, 22866–22874 (2004).
9. Kramer DM, Sacksteder CA, Cruz JA. How acidic is the lumen? *Photosynthesis Research*, 60, 151-153 (1999).
10. Ruban AV, Johnson MP, Duffy CD. The photoprotective molecular switch in the photosystem II antenna. *Biochimica Biophysica Acta*, 1817(1), 167-181 (2012).
11. Krause GH. Photoinhibition of photosynthesis. An evaluation of damaging and protective mechanisms. *Physiologia Plantarum* 74: 566-574, 74, 566-574 (1988).
12. Demmig-Adams B and Adams WW III. Photoprotection and other responses of plants to high light stress. *Annu. Rev. Plant Physiol. Plant Mol. Biol.* , 43, 599-626 (1992).
13. Yamamoto HY, Nakayama TOM, Chichester CO. Studies on the Light and Dark Interconversions Leaf Xanthophylls. *Archives of Biochemistry and Biophysics*, 97,168-173, (1962).
14. Haager A. Die Zusammenhänge zwischen lichtinduzierten Xanthophyll-Umwandlungen und Hill-Reaktion. *Berichte der Deutschen Botanischen Gesellschaft*, 79,94-107 (1966).
15. Muller P, Li X-P, and Niyogi KK. Non-Photochemical Quenching. A Response to Excess Light Energy. *Plant Physiol.*, 125, 1559-1566 (2001).
16. Horton P, Ruban AV, and Walters RG. Regulation of light harvesting in green plants. *Annu. Rev. Plant Physiol. Plant Mol. Biol.*, 47, 655–684 (1996).
17. Caffarri S, Kouřil R, Kerešič S, Boekema EJ, Croce R. Functional architecture of higher plant Photosystem II supercomplexes, *EMBO J.*, 28, 3052–3063. (2009).
18. Shi LX, Hall M, Funk C, Schroder WP. Photosystem II, a growing complex: updates on newly discovered components and low molecular mass proteins, *Biochim. et Biophys. Acta* 1817, 13-25 (2012).
19. Dekker JP, Boekema EJ. Supramolecular organization of thylakoid membrane proteins in green plants. *Biochim. et Biophys. Acta- Bioenergetics*, 1706, 12-39 (2005).
20. Umena Y, Kawakami K, Shen JR, Kamiya N. Crystal structure of oxygen-evolving Photosystem II at a resolution of 1.9 angstrom. *Nature*, 473, 55-U65 (2011).
21. Nield J, Kruse O, Ruprecht J, da Fonseca P, Buchel C, Barber J. Three-dimensional structure of *Chlamydomonas reinhardtii* and *Synechococcus elongatus* Photosystem II complexes allows for comparison of their oxygen-evolving complex organization. *J. Biol. Chem.*, 275, 27940–27946 (2000).
22. Büchel C, Kühlbrandt W. Structural differences in the inner part of Photosystem II between higher plants and cyanobacteria. *Photosynth. Res*, 85, 3-13 (2005).

23. Dau H, Zaharieva I, Haumann M. Recent developments in research on water oxidation by Photosystem II. *Curr. Opin. Chem. Biol.*, 16, 3–10 (2012).
24. Balevičius V Jr., Fox KF, Bricker WP, Jurinovich S, Prandi IG, Mennucci B & Duffy CDP. Fine control of chlorophyll-carotenoid interactions defines the functionality of light-harvesting proteins in plants. *Sci Rep*, 7(1), 13956 (2017).
25. Gaffron H and Wohl K. Zur theorie der assimilation. *De naturewissenschaften*, 24, 81-90, 103-107 (1936).
26. Franck J, Teller E. Migration and Photochemical Action of Excitation Energy in Crystals. *The Journal of Chemical Physics*, 6(12), 861-872 (1938).
27. Ogawa T, Obata F, Shibata T. Two pigment proteins in spinach chloroplasts. *Biochim. Biophys. Acta*, 112, 223-234 (1966).
28. Thornber JP. Comparison of a chlorophyll *a*-Protein complex isolated from *aa* blue-green alga with chlorophyll proteins obtained from green bacteria and higher plants. *Biochim. et Biophys. Acta*, 172, 230-241 (1969).
30. Kühlbrandt W, Wang DN, Fujiyoshi Y. Atomic model of plant light-harvesting complex by electron crystallography. *Nature*, 367, 614-620 (1994).
31. Jansson S. A guide to the Lhc genes and their relatives in *Arabidopsis*. *Trends in plant science perspectives*, 4(6), 236-240 (1999).
32. Alpes H, Apell H-J, Knoll G, Plattner H and Riek R. Reconstitution of Na⁺/K⁺-ATPase into phosphatidylcholine vesicles by dialysis of nonionic alk maltoside detergents. *Biochim. et Biophys. Acta* 946, 379-388 (1988).
33. Krüger TPJ, Novoderezhkin VI, Iliaia C, Grondelle R. Fluorescence spectral dynamics of single LHCII trimers. *Biophysical Journal*, 98, 12, 3093–3101 (2010).
34. Cabral BJC, Coutinho K, Canuto S. Born-Oppenheimer molecular dynamics and electronic properties of chlorophyll-*c*₂ in liquid methanol. *J Chem Phys*, 138(22), 225102 (2013).
35. Gouterman M, Wagnier GH, Snyder LC. Spectra of Porphyrins: Part II. Four Orbital Model. *Journal of molecular spectroscopy*, 11, 108-127 (1963).
36. Blankenship RE, Tiede DM, Barber J, Brudvig GW, Fleming G, *et al.* Comparing Photosynthetic and Photovoltaic Efficiencies and Recognizing the Potential for Improvement. *Science*, 332, 805-809 (2011).
37. Umena Y, Kawakami K, Shen JR, Kamiya N. Crystal structure of oxygen-evolving photosystem II at a resolution of 1.9 Å. *Nature*, 473(7345), 55-60 (2011).
38. Frank HA, Cua A, Chynwat V, Young A, Gosztola D & Wasielewski MR. Photophysics of the carotenoids associated with the xanthophyll cycle in photosynthesis. *Photosynthesis Research*, 41, 389-395 (1994).
39. Paulsen H, Finkenzeller B, Kühlein N. Pigments induce folding of light-harvesting chlorophyll *a/b*-binding protein. *Eur. J. Biochem*, 215, 809-816 (1993).
40. Krinsky NI. Carotenoid protection against oxidation. *Pure & Appl. Chem*, 51, 649-660 (1979).
41. Fan M, Li M, Liu Z *et al.* Crystal structures of the PsbS protein essential for photoprotection in plants. *Nat Struct Mol Biol*, 22(9), 729-735 (2015).
42. Bergantino E, Segalla A, Brunetta A, Teardo E, Rigoni F, Giacometti GM & Szabò I. Light- and pH-dependent structural changes in the PsbS subunit of photosystem II. *PNAS*, 100(25), 15265–15270 (2003).
43. Ware MA, Giovagnetti V, Belgio E, Ruban AV. PsbS protein modulates non-photochemical chlorophyll fluorescence quenching in membranes depleted of photosystems. *J Photochem Photobiol B*, 152(Pt B), 301-307 (2015).
44. Teardo E, de Laureto PP, Bergantino E *et al.* Evidences for interaction of PsbS with photosynthetic complexes in maize thylakoids. *Biochim Biophys Acta*, 1767(6), 703-711 (2007).
45. Wilk L, Grunwald M, Liao PN, Walla PJ, Kuhlbrandt W. Direct interaction of the major light-harvesting complex II and PsbS in nonphotochemical quenching. *Proc Natl Acad Sci U S A*, 110(14), 5452-5456 (2013).
46. Long SB, Tao X, Campbell EB, MacKinnon R. Atomic structure of a voltage-dependent K⁺ channel in a lipid membrane-like environment. *Nature*, 450(7168), 376-382 (2007).

47. Schmidt D, Jiang QX, MacKinnon R. Phospholipids and the origin of cationic gating charges in voltage sensors. *Nature*, 444(7120), 775-779 (2006).
48. Gonen T, Cheng Y, Sliz P *et al.* Lipid-protein interactions in double-layered two-dimensional AQP0 crystals. *Nature*, 438(7068), 633-638 (2005).
49. Wang L, Tonggu L. Membrane protein reconstitution for functional and structural studies. *Sci China Life Sci*, 58(1), 66-74 (2015).
50. Alberts B, Johnson A, Lewis J, *et al.* Molecular Biology of the Cell. 4th edition. *New York: Garland Science*, (2002).
51. Pandit A, Shirzad-Wasei N, Wlodarczyk LM *et al.* Assembly of the major light-harvesting complex II in lipid nanodiscs. *Biophys J*, 101(10), 2507-2515 (2011).
52. Denisov IG, Sligar SG. Nanodiscs for structural and functional studies of membrane proteins. *Nat Struct Mol Biol*, 23(6), 481-486 (2016).
53. Eytan GD, Matheson MJ, Racker E. Incorporation of Mitochondrial Membrane Proteins into Liposomes containing acidic phospholipids. *The Journal of Biological Chemistry*, 251(21), 6831-6837, (1976).
54. Podolsky RJ. Protein Degradation in Bacteria 327-340 (1953).
55. Miao Y, Cross TA. Solid state NMR and protein-protein interactions in membranes. *Curr Opin Struct Biol*, 23(6), 919-928 (2013).

CHAPTER 2

Disentangling protein and lipid interactions that control a molecular switch in photosynthetic light harvesting

This chapter is published as E. Crisafi, A. Pandit, *Biochimica et Biophysica Acta Biomembranes*, 2017

Cryo-electron microscopy experiments were performed in collaboration with the Electron Microscopy Department, Groningen Biomolecular Sciences and Biotechnology, Univ. of Groningen.

ABSTRACT

In the photosynthetic apparatus of plants and algae, the major Light-Harvesting Complexes (LHCII) collect excitations and funnel these to the photosynthetic reaction centre where charge separation takes place. In high-light, remodelling of the photosynthetic membrane and protein conformational changes produce a photoprotective state in which excitations are rapidly quenched to avoid photodamage.

The quenched states are associated with protein aggregation in the membrane, however, the LHCII complexes are also proposed to have an intrinsic capacity to shift between light harvesting and fluorescence-quenched conformational states. To disentangle the effects of protein-protein and protein-lipid interactions on the LHCII photoprotective switch, we compared the structural and fluorescent properties of LHCII lipid nanodiscs and proteoliposomes with very low protein to lipid ratios. We demonstrate that LHCII proteins adopt a fully fluorescent state in nanodiscs and in proteoliposomes with highly diluted protein densities. The increase of protein density induces a transition to a mildly-quenched state that reaches a fluorescence quenching plateau at a molar protein-to-lipid ratio of 0.001 and has a fluorescence yield reminiscent of the light-harvesting state *in vivo*. The low onset for quenching strongly suggests that LHCII-LHCII attractive interactions occur inside membranes. The transition at low protein densities does not involve strong changes in the excitonic circular dichroism spectrum and is distinct from a transition occurring at very high protein densities that comprises strong fluorescence quenching and circular dichroism spectral changes involving chlorophyll *a*611 and *a*612, correlating with proposed quencher sites of the photoprotective mechanisms.

INTRODUCTION

Photosynthetic light-harvesting antennae form supra-molecular arrays with strong connectivity that capture sunlight and transfer the excitations over long distances towards the photosynthetic reaction centres, where charge separation takes place [1]. In contrast to artificial solar antennae, natural light-harvesting structures are dynamic assemblies that continuously adapt to the light conditions for prevention of photodamage [2]. In the excess of light, extensive remodelling of the photosynthetic thylakoid membranes takes place. The ability of the peripheral Light-Harvesting Complexes of plants and photosynthetic algae to adapt fluorescent, light harvesting, versus photoprotective, excitation-quenched states under excess light conditions, is a phenomenon that has been studied extensively *in vivo* and *in vitro* over the last decades [3-9]. LHCII proteins have the intrinsic capacity to switch between light-harvesting, fluorescent, or photoprotective, quenched conformational states [4,10]. The formation of quenched states is associated with LHCII aggregation in the membrane and the balance between light harvesting and photoprotection is regulated by membrane remodelling in high light conditions [8,11]. Mild dilution with thylakoid lipids of overcrowded mutant thylakoid membranes has shown to increase the LHCII chlorophylls (Chls) fluorescence lifetimes, while further dilution functionally uncouples the LHCII antenna proteins from the photosystem reaction-center units [12,13]. Thus, the functional roles of the light-harvesting proteins to transfer excitations to the photosynthetic reaction centres or dissipate excess excitations under high light critically depend on the respective protein to lipid densities within strong- or weak-coupling regimes. The strong correlation between quenching and protein aggregation *in vivo* and *in vitro* together with the notice that individual LHCII complexes can adopt different fluorescent states, suggests a mechanistic process in which external pressure and protein or lipid changes in the LHCII microenvironment bring about a molecular conformational change. This change should involve altered Chl-Cars or Chl-Chl interactions to be able to quench the light excitations [5,14,15]. While several models have been proposed for the photophysical quenching mechanisms [5,14-16] involving the protein-bound Chls, lutein and/or zeaxanthin, there is no clear view on the mechanistic process or on the protein conformational switch that is associated with a twist in the protein-bound neoxanthin (Neo), a change in Chl *b* hydrogen bond strength [14], subtle changes in the Chl *a* ground-state electronic structures [17,18] or conformational changes in one of the luteins (Lut1) [19]. Upcoming methods, like single-molecule fluorescence and nuclear magnetic resonance (NMR), are being explored to comprehend the conformational switch of LHCII and its associated mechanistic process [4,17]. The relevance of such studies strongly relies on the chosen *in vitro* conditions to mimic the *in vivo* membrane environment. In addition, new kinetic models have been proposed that describe excitation, diffusion, and quenching in small LHCII aggregates, that benefit from experimental data describing the behaviour of single and aggregated LHCII under controlled, membrane-mimicking conditions [20,21]. Model lipid membranes form suitable tools for the investigation of protein structure, dynamics and lipid interplay in a controlled environment and open the possibility to

create artificial minimal protein networks with functional connectivity. LHCII-reconstituted proteoliposomes and protein-lipid aggregates have been investigated to determine inter-protein connectivity and protein-lipid interactions under various conditions [22-24]. Comparing the structural and functional properties of aggregated membrane proteins in proteoliposomes with those of isolated proteins embedded in detergent micelles, however, creates a bias because the protein microenvironment changes when proteins are transferred from detergent micelles to lipid membranes. Lipid nanodiscs form attractive alternative model systems that prevent protein aggregation while providing a lipid environment. We demonstrated that LHCII proteins could be reconstituted in asolectin lipid nanodiscs, capturing the proteins in their fluorescent, light-harvesting state [25].

In this chapter, we compared both structure and fluorescence properties between LHCII in lipid nanodiscs and LHCII in proteoliposomes, thereby disentangling protein-protein and protein-lipid interactions in minimal membrane models to investigate the LHCII mechanistic, functional switch. The LHCII pigment-protein complexes are unique in possessing Chls and xanthophylls that form intrinsic probes, reporting changes in the microenvironment. By adjusting the protein to lipid ratio (PLR) in the proteoliposomes, we determined the onset ratio for protein aggregation in membranes, bridging the gap between properties of isolated proteins and of their aggregated states. Liposome and nanodisc models were prepared from plant thylakoid or from soybean asolectin lipids to investigate the influence of specific lipid microenvironments. Thylakoid lipids were used to mimic the lipid composition of native thylakoid membranes. Preparations of soybean asolectin lipids were used as easily controllable lipid model systems and for comparison of our data with previous results obtained in an earlier study on LHCII lipid nanodiscs [25]. Circular dichroism (CD) experiments were carried out to characterize LHCII pigment interactions for the different membrane model systems.

MATERIALS AND METHODS

LHCII EXTRACTION

Light-Harvesting Complexes were purified from *Spinacia oleracea* leaves as previously described [25]. In short, LHCII trimer complexes were isolated using a sucrose gradient. The green band of LHCII trimers was manually collected with a long needle. The purified LHCII complexes were characterized by absorption spectroscopy. The sucrose buffer was exchanged into buffer containing HEPES 50 mM, NaCl 100 mM, pH 7.5, *n*-Dodecyl β -D-maltoside (β -DM, Sigma) 0.03%. The solution was concentrated using Amicon Ultra 2 mL centrifugal filters with a cut off of 30 kDa (Millipore). The protein complexes were stored at -80°C until use.

PREPARATION OF ASOLECTIN LIPOSOMES

Chloroform was added to asolectin from soybean lipids (Sigma) to a concentration of 5 mg/ml. The chloroform/asolectin solution was collected in a round-bottom flask, and all solvent was evaporated with a stream of N₂ followed by evaporation in a rotary evaporator (R3000, Buchi). The phospholipid bilayer was then hydrated using the reverse phase method [26]. A solution was poured to the dried film containing the buffer (HEPES 50 mM, NaCl 100 mM, pH 7.5) and diethyl ether in the ratio 1 to 3, and gently mixed and sonicated (2210, Branson). The diethyl ether was evaporated using the rotary evaporator and the last traces of solvent were removed using a stream of N₂. The liposome suspensions were exposed to 10 freeze/thaw cycles followed by extrusion through polycarbonate membranes of 400 and 200 nm pore size, using a mini-extruder (Avanti polar lipids). Sizes of liposome preparations were determined by dynamic light scattering (DLS, Malvern Zetasizer Nano ZS) equipped with a thermostatic cell holder controlled by a Peltier element.

PREPARATION OF THYLAKOID-LIPID LIPOSOMES

Thylakoid lipids phosphatidylglycerol (PG), digalactosyldiacylglycerol (DGDG), monogalactosyldiacylglycerol (MGDG) and sulphoquinovosyl diacylglycerol (SQDG) were purchased from Lipid Products Company (Redhill). Unilamellar liposomes were prepared according to [27]. Lipid mixtures containing 47% MGDG, 27% DGDG, 12% SQDG and 14% PG were dried into a thin film using a rotary evaporator at 40°C, to remove all traces of chloroform. The lipid film was hydrated using a reconstitution buffer (HEPES 50 mM, NaCl 100 mM, pH 7.5 and 0.03% β -DM) to a final lipid concentration of 0.25 mg/ml. Detergent was extracted by incubation for 48 hrs with polystyrene beads (Bio-beads, SM-2, Bio-Rad). The liposome suspensions were exposed to 10 freeze-thaw cycles followed by extrusion through polycarbonate membranes with 200 nm and 100 nm pore sizes.

PROTEIN INSERTION IN LIPOSOMES

To determine the onset of liposome solubilisation by detergent, liposome preparations were titrated with β -DM and DLS and 90° light scattering were used to monitor the solubilisation of liposomes into lipid-detergent micelles.

Liposome solubilisation curves were obtained by mixing liposomes with increased amounts of β -DM. Solubilisation of the liposome vesicles into lipid-detergent micelles upon detergent titration was followed by the decrease of 90° light scattering measured with a fluorescence spectrometer (Varian) with the excitation and detection wavelength both set at 500 nm (Figure 2.1). Particle sizes of the liposome-detergent preparations were determined by DLS. The onset value for solubilisation was determined as 0.01% β -DM for liposome preparations containing 0.95 mM lipid, which converts to 5 lipids per detergent molecule.

For protein insertion, preformed liposomes were destabilized by the addition of 0.03% of β -DM to facilitate the insertion of LHCII into the membranes. LHCII complexes were added to the suspension and incubated for 30 min. For proteoliposomes preparations with

high PLRs (1:65), instead of insertion into preformed liposomes, the LHCII complexes in β -DM were directly mixed with detergent-solubilized lipids. Bio-beads were added to the suspensions in several steps and solutions were incubated overnight. The proteoliposomes suspension was centrifuged at 15000 x g for 30 minutes at 4°C using a table-centrifuge (5430 R, Eppendorf) to remove non-incorporated LHCII that forms aggregate pellets.

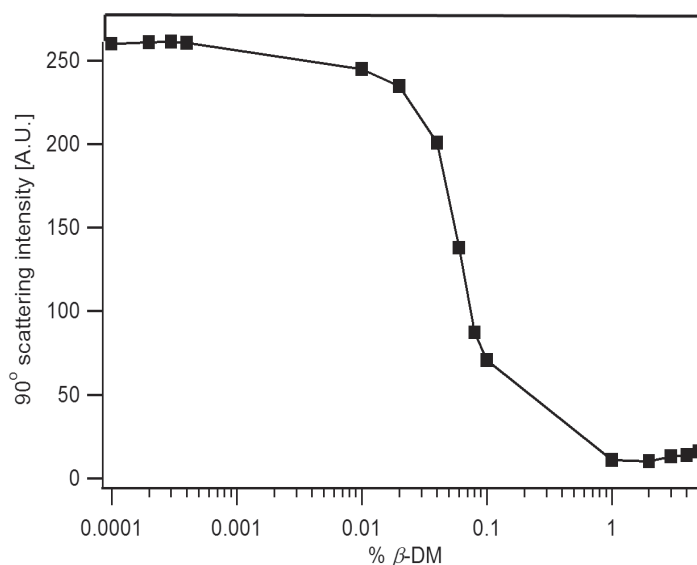


Figure 2.1 Solubilisation of asolectin liposomes (lipid 0.95 mM) upon β -DM titration. The onset of solubilisation starts at β -DM 0.01%.

Preparations of LHCII in 0.03% β -DM and of LHCII proteoliposomes were loaded on sucrose gradients 10-45% and run overnight at 200000 x g at 4 °C in an SW41 rotor (Beckmann). Figure 2.2 shows that LHCII proteoliposomes form two bands on the sucrose gradient, while there are no visible LHCII aggregates at the bottom of the tube, confirming that all of the LHCII were incorporated.

The proteoliposome preparations were characterized by cryo-electron microscopy (cryo-EM, FEI Technai T20 electron microscope, operating at 200 keV). The reported PLR is defined as moles of LHCII trimers per moles of total lipids. The concentration of LHCII was determined from the molar extinction coefficient for trimers at 670 nm, $\epsilon=1638000 \text{ M}^{-1} \text{ cm}^{-1}$ [28].

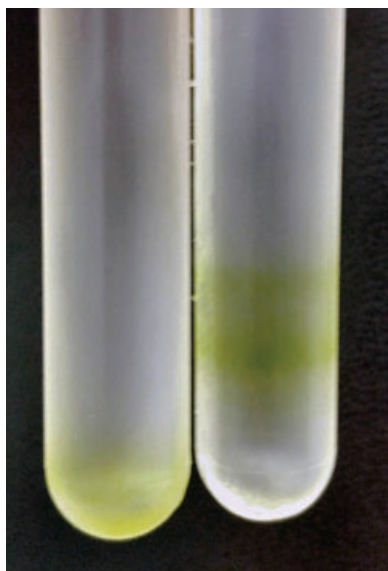


Figure 2.2 Sucrose gradient of LHCII aggregates (bottom left) and LHCII proteoliposomes with PLR = 1:65 (right).

PREPARATION OF LHCII ASOLECTIN NANODISCS

For incorporation of LHCII in lipid nanodiscs, we used the membrane scaffold protein 1E3D1 (MSP 1E3D1) [29]. MSPs are amphipathic helices and are genetically engineered apolipoproteins (A-1). The MSP1E3D1 overexpressed in *E. coli* was purification and consequently stored at -80°C . Lipid nanodiscs are formed spontaneously upon detergent extraction of lipid: detergent: MSP mixtures. In lipid nanodiscs, the lipid molecules associate as a bilayer domain while two molecules of MSP wrap around the edges of the discoidal structure in a belt-like configuration, one MSP covering the hydrophobic alkyl chains of each leaflet (see Figure 1.11, Chapter 1). For the preparation of LHCII asolectin nanodiscs, a 5 mg/ml solution of asolectin was prepared according to Pandit *et al.*, in buffer (HEPES 50 mM, NaCl 100 mM, pH 7.5) with nonyl β -D-glucopyranoside 40 mM (Sigma) [25]. LHCII complexes were mixed with the lipid/ detergent solution and incubated at 4°C while shaking for 15 min. The MSP1E3D1 was added to the mixture and incubated for another 15 min [25]. To allow the reconstitution of protein in nanodiscs, the detergent was removed using Bio-beads (SM-2). Samples were diluted to a final volume of 2 ml and ultra-centrifuged at $120000 \times g$ at 4°C to remove lipid and protein pellets, in an Ultracentrifuge (Optima L-90K, Beckman) using a 70.1 Ti rotor. Because we observed that for some preparations small aggregates remained in the lower part of the supernatant, the upper and lower volumes of the 2 ml supernatant solution were collected separately from the centrifuge tubes. Sizes of empty nanodisc and liposome preparations were determined by DLS. The illumination wavelength of the DLS apparatus, 632.8 nm, was not suitable for measuring scattering profiles of LHCII-containing samples because LHCII fluorescence upon illumination at 632.8 nm interfered with the scattering profile.

PREPARATION OF LHCII THYLAKOID-LIPID

NANODISCS

Nanodiscs consisting of plant thylakoid lipids were prepared as described above for asolectin lipid nanodiscs, except for the initial step. Native thylakoid membranes contain the non-bilayer lipid MGDG that makes up ~40-50% of the lipid constituents [30]. The addition of MGDG to our lipid preparations prevented the formation of nanodiscs and resulted in the formation of LHCII lipid aggregates. MGDG is a non-bilayer lipid that changes the membrane lateral pressure profile and has a preference for hexagonal membrane phases [31]. The cone-shaped MGDG lipids might prevent the formation of flat lipid membrane discs that are stabilized by the MSP proteins. Lipid mixtures containing 47% MGDG, 27% DGDG, 12% SQDG and 14% PG or lacking MGDG, containing 61.9% DGDG, 16.7% SQDG and 21.4% PG were dried with a rotary evaporator for 45 minutes at 40°C. The lipid film was hydrated with buffer (HEPES 50 mM, NaCl 100 mM, pH 7.5) containing 40 mM nonyl β -D-glucopyranoside. The remaining steps were performed following the protocol described above for asolectin lipids.

CIRCULAR DICHROISM MEASUREMENTS

CD spectra of the LHCII nanodiscs and proteoliposome suspensions were recorded with a J-815 spectropolarimeter (Jasco) equipped with a Peltier element temperature control. The wavelength range was from 350 to 750 nm, data pitch 1 nm, response 2 s, bandwidth 4 nm, and scanning speed 50 nm/min at 20°C using a 0.2 or 0.5 cm quartz cuvette (Hellma).

ABSORPTION MEASUREMENTS

Absorption spectra were recorded with a UV-1700 PharmaSpec UV-Vis spectrophotometer (Shimadzu) over a wavelength range from 350 to 750 nm

FLUORESCENCE MEASUREMENTS

Fluorescence measurements were performed with a Cary Eclipse fluorescence spectrophotometer (Varian), collecting emission spectra from 660 to 720 nm using 3 mm quartz cuvettes. The optical density of the sample preparations varied from 0.03 to 0.07 cm^{-1} at 650 nm. The excitation wavelength (λ_{ext}) was set at 650 nm or at 475 nm. Fluorescence quantum yields of LHCII proteoliposome and nanodisc preparations were determined relative to the fluorescence yield of LHCII in β -DM. Data were corrected for the number of absorbed photons by dividing the fluorescence intensities by $1 - T$ (1-T).

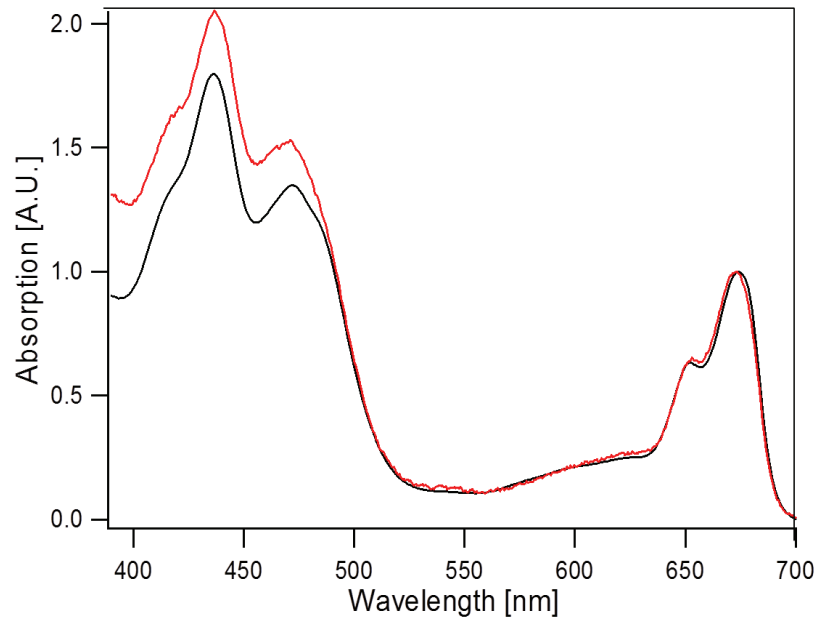


Figure 2.3 UV-VIS Absorption spectra of LHCII proteoliposomes with protein to lipid ratios of $5 \cdot 10^{-5}$ (red) and of LHCII in 0.03% β -DM (black). Spectra are normalized at the Chl a Q_y maximum.

To minimize errors caused by liposome scattering, which causes a scattering background signal at the blue side of the absorption spectra, as shown in Figure 2.1, liposome samples were excited at the red side in the Q_y band of Chl *b* ($\epsilon_{exc} = 650$ nm) and fluorescence emission spectra were corrected for the number of absorbed photons dividing the fluorescence intensities by $1 - T_{650}$.

RESULTS AND DISCUSSIONS

FLUORESCENCE ANALYSIS OF LHCII IN NANODISCS COMPOSED OF ASOLECTIN OR THYLAKOID- LIPIDS

Sample	LHCII: MSP: lipid	Φ/Φ_r (%)
1	1:4:427	100
2	1:4:213	100
3	1:12:870	70
4	1:24:870	75
5	1:12:120	90
6	1:18:180	90
7	1:20:120	74
8	1:5:120	80

Table 2.1 Fluorescence yields relative to LHCII in β -DM of LHCII nanodiscs preparations, composed of DGDG: SQDG: PG lipid mixtures (sample 1 to 4) or of soybean asolectin lipids (sample 5-8).

At optimized LHCII: MSP: lipid ratios, LHCII lipid nanodiscs prepared using asolectin or DGDG: SQDG: PG lipids had fluorescence intensities that were comparable to the fluorescence intensities of LHCII in β -DM micelles as reported in Table 2.1, while with sub-optimal LHCII: MSP: lipid ratios, lower fluorescence yields were observed, caused by the presence of small amounts of LHCII aggregates that quench the fluorescence.

Note that in lipid membranes where the LHCII proteins would not be prevented from protein-protein interactions by the MSPs, protein to lipid ratios of 1:120 or 1:180 as were used for the asolectin nanodiscs would induce quenched states of LHCII by protein aggregation [32]. In contrast, the fluorescence yields in Table 2.1 confirm that the nanodisc scaffolds prevent LHCII aggregation. In earlier work, it was already demonstrated that LHCII retains its fluorescent state upon reconstitution in asolectin nanodiscs [25]. Here we conclude that LHCII also adapts an unquenched, fully fluorescent state in nanodiscs composed of thylakoid lipids.

FLUORESCENCE ANALYSIS OF LHCII PROTEOLIPOSOMES AT LOW PROTEIN TO LIPID RATIOS

In artificial and in native membranes, the fluorescence of LHCII is reduced compared to the fluorescence of LHCII in detergent micelles. The LHCII-nanodisc experiments, however, show that the transition from a detergent to a lipid environment in itself does not produce quenched states. We reasoned that quenching of LHCII in membranes is caused by their aggregation and that very diluted concentrations of LHCII complexes in proteoliposome membranes should reproduce the fluorescence yields of the LHCII lipid nanodiscs. To test this assumption, we prepared LHCII asolectin proteoliposomes with PLRs in the range 2×10^{-5} to 2×10^{-3} . At the lowest ratios, the fluorescence yield indeed equals the fluorescence yields of LHCII in lipid nanodiscs or detergent micelles as shown in Figure 2.4. The fluorescence yield decreases with increased PLR until a plateau is reached where the yield is reduced to ~50% relative to the fluorescence of LHCII in lipid nanodiscs. This reduced yield is comparable with the reduction in fluorescence that is observed for LHCII in dark-adapted leaves *in vivo* [8,25,33].

For clarity, the x-axis in Figure 2.4 has a logarithmic scale. Data were fit with a standard sigmoidal curve to determine the midpoint PLR value, using the fit function:

$$y = F_{max} - F / \{1 + \exp[(x_{half}-x)/x_0]\}$$

The fit would give a midpoint PLR value $x_{half} = 0.0001$ (Figure 2.4). Exponential fitting was also performed and would give a half-life PLR of 0.00015 and offset $y_0 = 0.49$ (fluorescence at plateau level). The fits at this point do not represent a functional model for concentration quenching but were used to estimate the PLR values at which mild quenching occurs and the fluorescence yield at the plateau level.

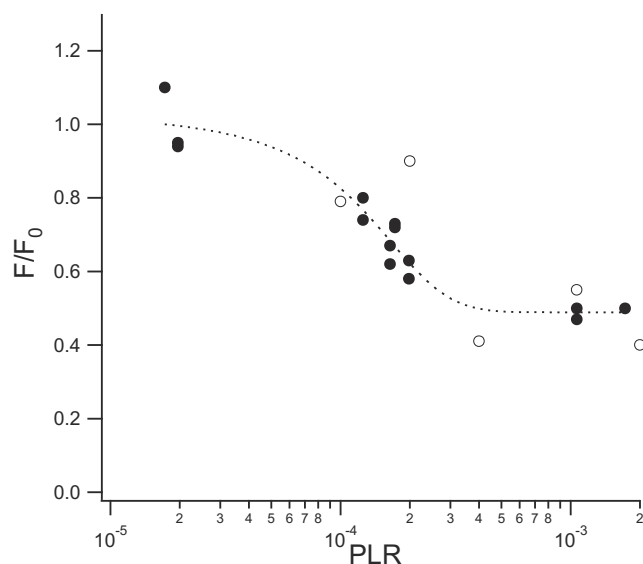


Figure 2.4 Fluorescence yield (F/F_0) of LHCII asolectin proteoliposomes (black circles) and thylakoid MGDG: DGDG: SQDG: PG proteoliposomes (open circles) relative to the fluorescence of LHCII in β -DM micelles (F_0) at a different PLR. To determine the midpoint PLR value, data were fit with a standard sigmoidal curve using the following fit parameters: half at $PLR = 1.0 \cdot 10^{-4} \pm 8.2 \cdot 10^{-5}$, maximal fluorescence reduction = -0.67 ± 0.31 and $F_{max} = 1.16 \pm 0.30$.

The asolectin LHCII proteoliposomes in our preparations had varying sizes according to different EM micrographs in Figure 2.5.

Assuming that (1) liposomes contain double-leaflet membranes in which each asolectin lipid molecule occupies a surface area of 70 \AA [34], (2) the mean diameter of the liposomes as determined by EM ranges from 60 nm to 80 nm, and (3) discarding any losses of LHCII or lipids during our preparations, we estimate that preparations with a PLR of 1×10^{-4} , which corresponds to the midpoint value of the quenching curve in Figure 2.4, contain 1 to 2 LHCII trimers *per vesicle*.

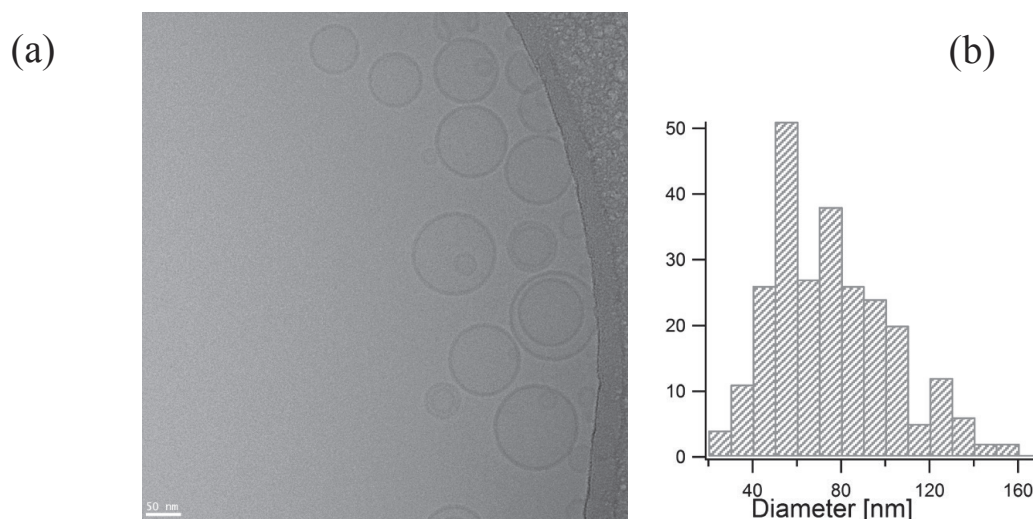


Figure 2.5 (a): Cryo-electron micrograph of asolectin LHCII proteoliposomes (scale bar 50 nm). (b): size distribution of asolectin liposomes, extracted from several electron micrographs.

The curve reaches a plateau value of ~50% quenching with on average 8-14 LHCII *per vesicle*, assuming vesicle sizes of 60-80 nm (Figure 2.5). Interestingly, the estimated average number of LHCII per vesicle at which the fluorescence quenching reaches a plateau (8–14 trimers) approaches the experimentally determined range for functional domain sizes of LHCII *in vivo* of 12–24 trimers, according to Lambrev *et al.* [35]. Although the calculations are a rough estimate, the numbers imply that the onset for fluorescence quenching starts when only a few LHCII complexes *per vesicle* are present, suggesting that the LHCII proteins have attractive interactions and form small aggregate clusters. Our previous study on LHCII-lipid nanodiscs showed that LHCII-lipid preparations containing disc particles with diameter sizes ranging from 12 to 50 nm, already display considerable quenching characteristics, the fluorescence yields were reduced to 40% compared to LHCII in detergent micelles [25]. Hence, small clusters of LHCII are capable of significantly reducing the fluorescence.

LHCII proteoliposomes prepared from thylakoid MGDG: DGDG: SQDG: PG lipid mixtures displayed similar quenching characteristics. For these lipid mixtures, however, it was more difficult to control the PLR without loss of protein and lipids, which was sometimes observed as small LHCII pellets after the centrifugation step, and only a few PLR values are compared (open circles in Figure 2.4). For consistency with the lipid compositions of the thylakoid lipid nanodiscs, we also prepared liposomes without MGDG. These preparations, however, contain mixtures of lipid vesicles and planar lipid sheets, as shown in Figure 2.6, and the sample was strongly quenched with a fluorescence intensity of ~20% compared to LHCII in β -DM. Summarizing, the LHCII proteoliposome data confirm that LHCII fluorescence quenching is induced by LHCII-LHCII interactions and not by a (specific) lipid microenvironment.

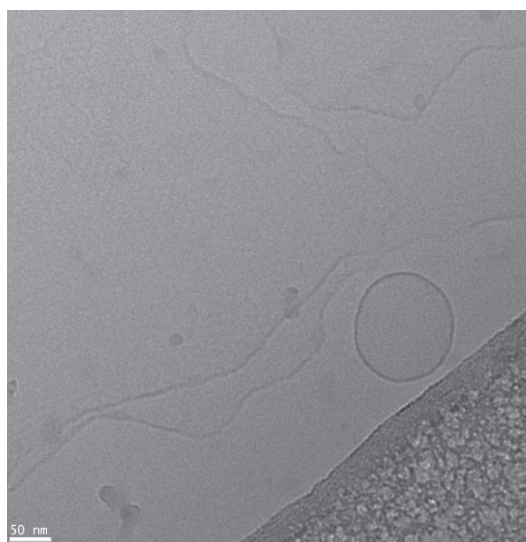


Figure 2.6 Cryo-electron micrograph of DGDG: SQDG: PG, LHCII proteoliposomes with PLR of 1.6×10^{-3} . The picture shows the co-existence of proteoliposomes and lamellar sheets.

The non-bilayer lipid MGDG has been suggested to play a role in controlling the photoprotective states of LHCII. Here we show that LHCII reconstituted in thylakoid

lipid membranes with MGDG proteoliposomes, or without MGDG nanodiscs, both adapt unquenched states. Molecular interactions between LHCII and MGDG lipids apparently do not induce fluorescence quenching. The MGDG lipids however clearly have an effect on the mesoscale organization, disturbing the thermodynamic equilibrium that stabilizes the MSP-lipid nanodisc scaffolds and counteracting the formation of large two-dimensional flat lipid-bilayer sheets. In native, highly crowded thylakoid membranes, LHCII aggregation is associated with reversible supramolecular membrane phase transitions [11]. In liposomes, MGDG and DGDG promote LHCII aggregation [22] and in LHCII-Photosystem II (PSII) liposomes, MGDG lipids increase the light-harvesting cross-section, promoting LHCII-PSII interactions [23]. These studies strongly suggest a functional role for MGDG in controlling the supramolecular interplay between light-harvesting proteins *in vivo*.

CD CHARACTERIZATION OF LHCII-NANODISCS AND LHCII-PROTEOLIPOSOMES

In LHCII pigment-protein complexes, excitonic Chl-Chl and carotenoid-Chl interactions give rise to pronounced exciton bands in the CD spectrum in the visible region [36]. The CD spectral shapes are very sensitive to the LHCII pigment-protein folds and their microenvironment [37,38]. To gain insight in the pigment-protein folds in different microenvironments and the influence of protein-lipid versus protein-protein interactions, we compared the excitonic CD spectra of LHCII in β -DM detergent micelles, lipid nanodiscs, and proteoliposomes. Figure 2.7 presents the CD spectra of LHCII in β -DM, LHCII in DGDG: SQDG: PG and asolectin nanodiscs and LHCII in MGDG: DGDG: SQDG: PG proteoliposomes with PLR of 1:555. In the Soret region, the peaks at (-)469 nm and (-)489 nm have similar intensities in the spectrum of thylakoid lipid nanodiscs, while in the spectrum of proteoliposomes, the (-)469 nm band clearly has gained more strength relative to the 489 nm band. Increase in strength of the (-)469 nm band combined with a decrease of the (-)489 nm band has been attributed to stronger inter-monomer interactions within the LHCII trimers [39,40]. The change in the 469/489 ratio observed for proteoliposomes suggests that LHCII-LHCII interactions in the membrane stabilize the trimers. The CD spectrum of asolectin nanodiscs also has a stronger (-)469 nm band than the spectrum of thylakoid lipid nanodiscs, indicating that the environment of the asolectin lipids increases the stability of the LHCII trimers.

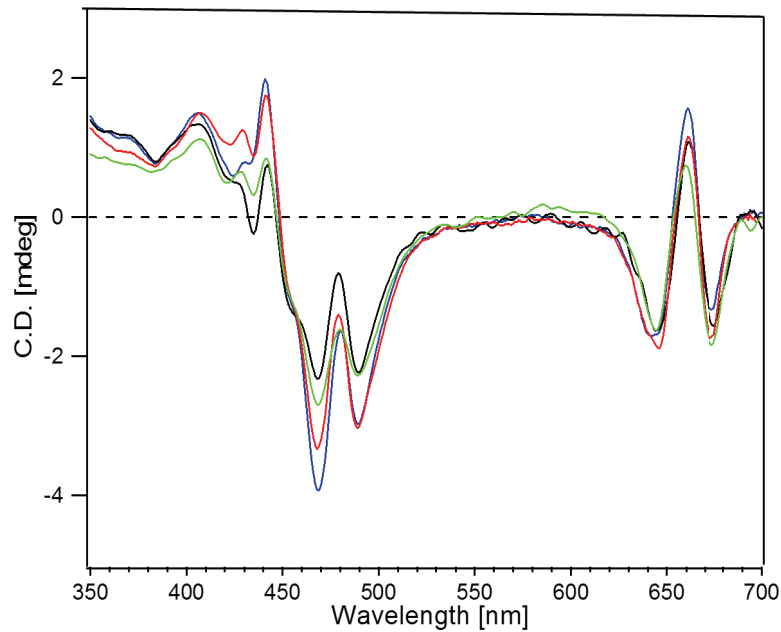


Figure 2.7 CD spectra of LHCII in β -DM (red), LHCII in MGDG: DGDG: SQDG: PG proteoliposomes (PLR 1:555, blue), LHCII in DGDG: SQDG: PG nanodiscs (black) and LHCII in asolectin nanodiscs (green).

Figure 2.8 shows CD difference spectra of LHCII thylakoid lipid nanodiscs minus LHCII in β -DM, and nanodiscs minus proteoliposomes. Remarkably, both difference spectra contain pronounced bands at (+)470 nm and (-)438 nm. The similar dispersive difference signal of the two difference spectra suggests that the nanodisc *itself* influences the LHCII pigment microenvironments. Considering the size of the LHCII trimer complexes, a triangular-shaped protein complex of ~ 6 nm wide, relative to the nanodisc dimensions of ~ 12 nm in diameter, the surrounding MSP proteins could be in contact with the exterior xanthophyll and Chl pigments of LHCII. These pigments are the neoxanthin (Neo) that protrudes from the protein complexes, and the Chls *b601*, *b605*, *b606*, *b608* and *a610*, *a611*, *a612* and *a614* (nomenclature according to Liu *et al.* [41]). Previous work demonstrated that changes occur in the Soret and Q_y band of absorption spectra of LHCII in lipid nanodiscs compared to detergent-solubilized LHCII, uncorrelated to fluorescence quenching [25]. These changes may also be explained by LHCII pigment interactions with the surrounding MSPs.

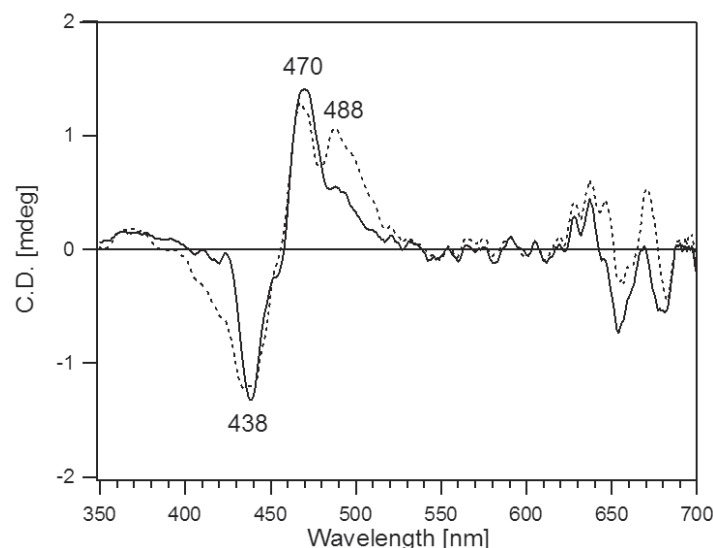


Figure 2.8 CD difference spectrum of LHCII nanodiscs minus LHCII in β -DM (dashed) and LHCII nanodiscs minus LHCII MGDG: DGDG: SQDG: PG proteoliposomes (solid line). Proteoliposomes were prepared with three different PLRs: 1:2222, 1:555 and 1:65. The two lowest PLRs are in the regime described in Figure 2.1, where the fluorescence quenching is maximal \sim 50%, reminiscent of the light-harvesting states in vivo in the weak-coupling regime. Instead, the fluorescence intensity of the densely packed proteoliposome preparations with PLR 1:65 is reduced to 10-15% compared to LHCII in β -DM micelles (Figure 2.9), which is comparable to photoprotective states in vivo [33].

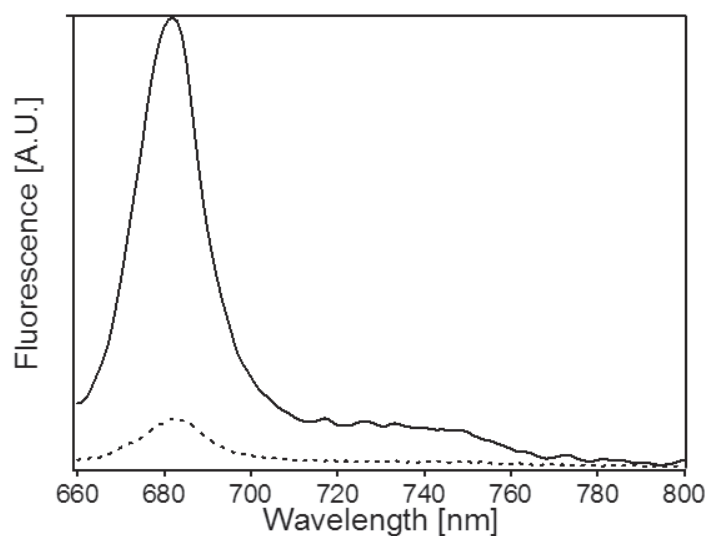


Figure 2.9 Fluorescence emission of LHCII proteoliposomes with PLR of 1:65 (dotted line) compared to LHCII in β -DM (solid line) upon 650 nm excitation. Fluorescence intensities were scaled according to their relative transmission (T) at 650 nm, by dividing by the fluorescence intensities by $(1-T)$.

Figure 2.10 compares the CD spectra of LHCII proteoliposomes with different PLRs. The samples with PLRs of 1:2222 and 1:555 have similar excitonic CD spectra. As demonstrated in Figure 2.4, changing the PLR in this regime also has only a moderate effect on the fluorescence yields. For the sample with PLR 1:65, however, spectral changes are observed that are indicated with the black arrows. The CD spectrum of proteoliposomes with PLR 1:65 resembles reported CD spectra of LHCII proteoliposomes in other work [40]. A comparison of proteoliposomes with low and high PLRs allows us to

detect the CD changes that are associated with the transition from a mild to a strong fluorescence-quenched state.

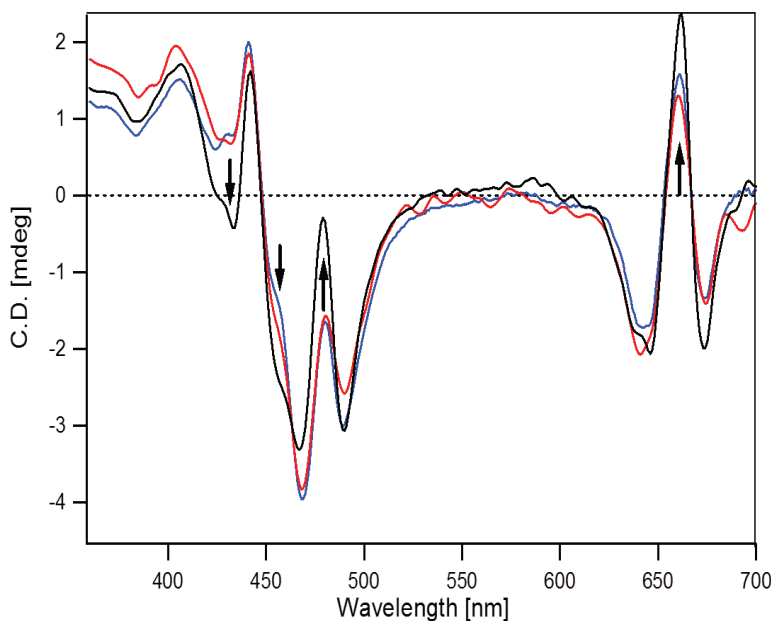


Figure 2.10 CD spectra of LHCII in MGDG: DGDG: SQDG: PG proteoliposomes; PLR of 1:2222, in red, PLR of 1:555, in blue and PLR of 1:65, in black. Arrows indicate the most significant changes for PLR 1:65.

Figure 2.11 presents the CD difference spectrum of proteoliposomes with PLR 1:65 minus PLR 1:555. In the referred CD spectra in Figure 2.10, we can exclude changes due to transitions from a detergent to a lipid environment. We presume that at a PLR of 1:555 the LHCII complexes are involved in weak protein-protein contacts. The CD difference spectrum in Figure 2.11 then shows changes in LHCII conformation and microenvironment that are associated with the transition from a weak to a strong protein-coupling regime. These changes occur at LHCII sites that have been proposed as quencher sites in earlier studies and involve the pigments Chl α 610, α 611, α 612 and Lut1 as will be explained below [4,14,18]. In the CD Q_y region, the bands at (+)662 nm and (-)673 nm are dominated by Chl α 611-Chl α 612 interactions [39]. The CD difference spectrum in Figure 11 indicates that those interactions are enhanced at high PLR. The extensive CD study of Akhtar et al. on LHCII in liposomes and detergent micelles concluded that CD changes at (-)437 nm and (+)484 nm are specific to LHCII-LHCII interactions [42]. A negative band at 437 nm, however, is also prominent in the difference spectrum of nanodiscs minus proteoliposomes (Figure 2.8), where the band actually is more pronounced in the nanodisc spectrum. This can be explained by proposing that not only LHCII-LHCII contacts but also LHCII-MSP protein-protein contacts will induce this signature. The 437 nm signature does not correlate with fluorescence quenching since LHCII in nanodiscs retains its fully fluorescent state. The Soret region of the CD difference spectrum in Figure 2.11 further contains additional bands at (-)455, (-)492 and (+)503 nm, of which the latter two signatures have tentatively been attributed to changes in the configuration or micro-environment of lutein 1 (Lut1) [43]. Increased Chl α 612-Lut1 excitonic interactions could explain the negative contribution to the CD signal at

(-)492 nm [39]. On the other hand, the (-)492 nm band has been attributed to changes in the Neo xanthophyll that protrudes from the LHCII complexes [42] and it is known that the formation of LHCII aggregates is associated with distortion of the Neo polyene chain [14].

Summarizing, the transition from a mild to strong fluorescence-quenched state, reminiscent of the transition from a light-harvesting to a photoprotective state *in vivo*, is associated with CD changes involving enhanced Chl *a*611-*a*612 and Lut1-Chl*a* *a*612 interactions or changes in the Neo environment. These sites correspond with quenching-associated structural changes that have been proposed in various studies [14,17,18,44]. Our results suggest that aggregation-induced LHCII fluorescence quenching at very low protein densities, however, is a different process that does not involve those characteristic CD features and does not reduce the fluorescence more than ~50%. This observation is in agreement with the observation of Holleboom *et al.* that in addition to a Car-Chl coupling-dependent quenching mechanism acting at high protein densities, another Car-Chl independent quenching mechanism is involved in a weak-coupling regime [13]. In the earlier study by Moya *et al.* aggregation-induced LHCII fluorescence quenching was studied in proteoliposomes with much higher protein densities than in our study [32]. They showed aggregation-dependent shortening of the LHCII fluorescence lifetimes from 1.7 to 0.9 ns [32]. We presume that their results reflect the transition from a mild to strong fluorescence-quenched state occurs, and not the transition occurring at the onset of aggregation that we followed in Figure 2.4.

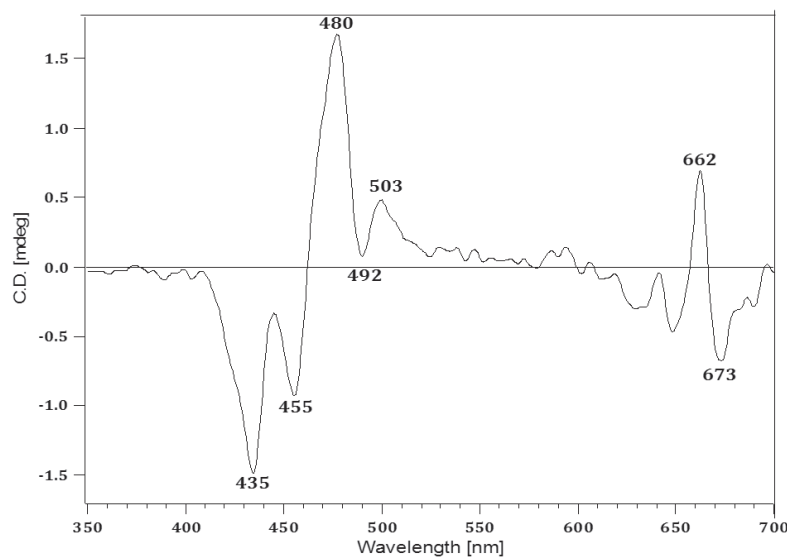


Figure 2.11 CD difference spectrum of LHCII MGDG: DGDG: SQDG: PG proteoliposomes with PLR 1:65-PLR 1:555.

THE ORIENTATION OF LHCII INSERTION IN PREFORMED LIPOSOMES

Finally, we tested if, with our liposome reconstitution method that follows the method of Rigaud, the LHCII complexes would insert in membranes with a preferential orientation [45]. LHCII proteoliposomes with low protein to lipid ratios and LHCII in β -DM as a control were exposed to trypsin or chymotrypsin cleavage. Trypsin is known to cleave part of the N-terminal site of LHCII, while for well-folded LHCII complexes the C-terminal cleavage sites are shielded from cleavage and buried in the hydrophobic membrane phase. Random orientation of LHCII in liposomes should lead to 50% cleavage if half the LHCII have their N-terminal sites oriented inward in the liposome interiors. In contrast, the interactions of trypsin with LHCII in β -DM micelles should lead to 100% cleavage since all LHCII N-terminal sites are accessible. The cleavage experiments were repeated under different trypsin incubation conditions, varying the temperature and incubation times. Figure 2.14 shows a typical SDS-page analysis of a cleavage experiment. Strikingly, for LHCII proteoliposomes only a cleaved product band is observed, suggesting that all proteins are cleaved. For LHCII in β -DM micelles, two cleavage products are found, which indicates that the protein is more exposed in detergent micelles. The two trypsin cleavage products are identified as 25 kDa and 23.5 kDa fragments of N-terminal-cleaved LHCII [46]. The results suggest a strong preferential orientation of LHCII in membranes, with its C-terminal site inserted and its N-terminal site exposed to the liposome exterior. No cleavage products were detected from chymotrypsin, that cleaves the two aromatic-type amino acids tryptophan and phenylalanine, instead of the polar residues lysine and arginine that are cleaved by trypsin as indicated in Figures 2.12 and 2.13.

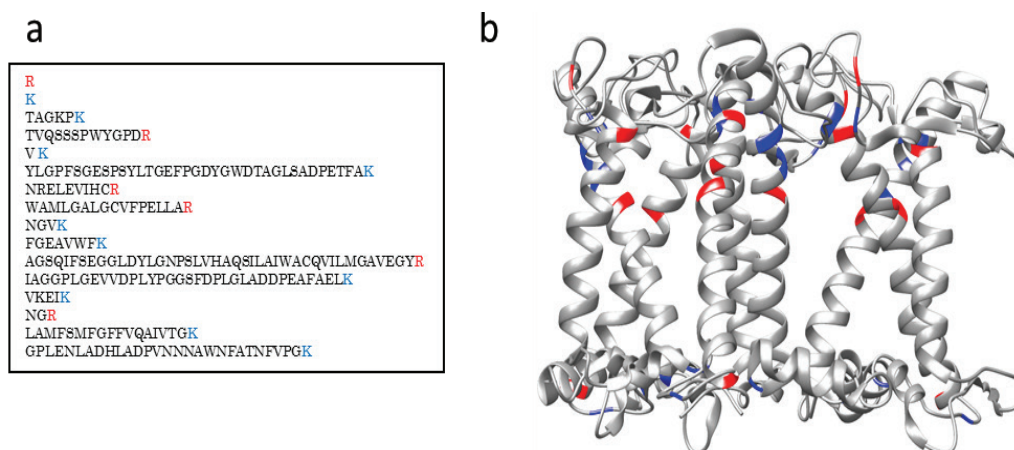


Figure 2.12 Trypsin cleavage sites in LHCII. Arginine (R) in red and lysine (K) in blue.

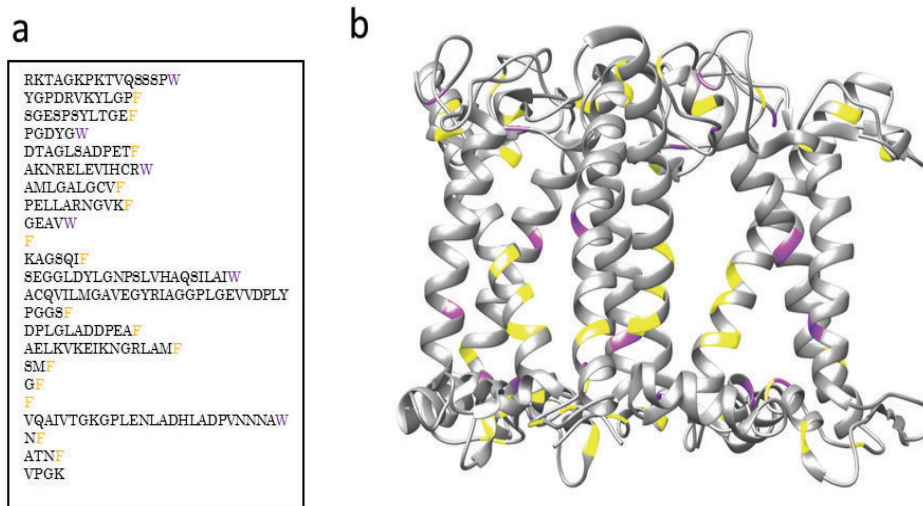


Figure 2.13 Chymotrypsin cleavage sites in LHCII sequence. Tryptophan (W) in purple and phenylalanine (F) in yellow.

Chymotrypsin is unable to cleave the designated sites because the aromatic residues are buried in the hydrophobic phase of the membrane or detergent micelles.

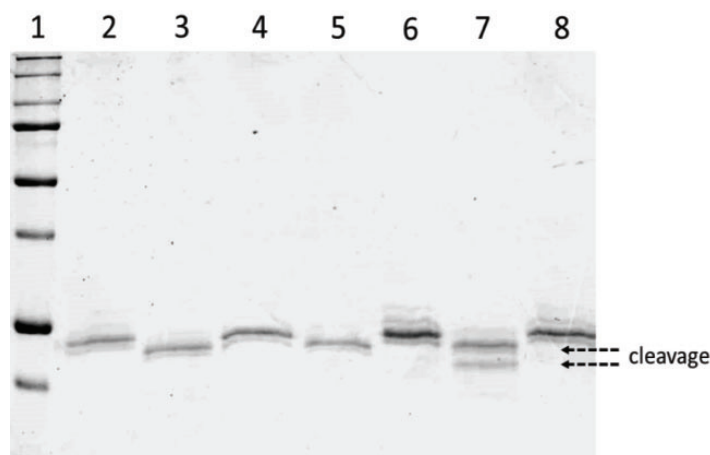


Figure 2.14 SDS-page analysis of enzymatic cleavage experiments. From left to right: 1, marker; 2, LHCII proteoliposomes; 3, LHCII proteoliposomes + trypsin; 4, LHCII proteoliposomes + chymotrypsin; 5, LHCII proteoliposomes with trypsin and chymotrypsin; 6, LHCII in β -DM; 7, LHCII in β -DM + trypsin; 8, LHCII in β -DM + chymotrypsin. Arrows indicate the height of cleavage product bands.

In native thylakoid membranes and in *in vitro* membrane refolding studies, LHCII apoproteins insert in the membrane starting from their C-terminal site that is exposed to the lumen interior [46,47]. To the best of our knowledge, we are the first to observe preferential insertion of folded, native LHCII pigment-protein complexes upon membrane reconstitution. Preferential insertion of membrane proteins from mixed protein-detergent micelles into liposome membranes, as well as membrane insertion of membrane α -helices during folding and assembly *in vivo*, is driven by the hydrophobicity of the protein terminal sites [48,49]. LHCII pigment-protein complexes contain several polar groups at both protein sites, but while at the C-terminal site positively- and negatively-charged residues are in the close distance and may neutralize the net charges, the N-terminal site contains a distinct pattern of positive and negative patches [50]. Such a pattern could

prevent insertion via the N-terminal site. Trypsin cleavage experiments unfortunately only detect interactions at the LHCII N-terminal site. Adding a C-terminal tag by using recombinant LHCII could help to further clarify the direction of LHCII insertion using our reconstitution method.

GENERAL DISCUSSION

The low PLR onset for aggregation-induced LHCII quenching demonstrates that strong attractive forces exist between the LHCII proteins in the membrane. In native membranes, the formation of membrane domains and the presence of MGDG could further promote aggregation by controlling membrane curvature. The low onset for quenching implies that studies using diluted LHCII proteoliposomes should take into account the vesicle dimensions in addition to the PLR because quenched states are already produced when more than one LHCII protein *per vesicle* is present. For larger liposomes, these occasions will occur at lower PLRs. Strong attractive forces in LHCII *in vitro* aggregates are often attributed to head-tail interactions, in which proteins make non-native interfacial protein contacts. Our results however strongly suggest that also under experimental conditions where membrane-embedded LHCII complexes are uniformly oriented attractive protein interactions occur.

We demonstrate that excitation quenching in LHCII membranes is not induced by protein-lipid molecular interactions, but is controlled by the effects of aggregation. At low protein densities, attractive forces between the LHCII complexes cause mild quenching. At very high protein densities, the effect of lateral pressure caused by membrane crowding might produce the conformational changes into more strongly quenched states. While simple LHCII-lipid model systems have many limitations in mimicking native thylakoid membranes, it is interesting to note that they can reproduce the connectivity that is essential for active light-harvesting as well as the strong excitation quenching of photoprotective states [23,32,51]. This notion suggests that lipid physicochemical parameters and the molecular design of LHC complexes are sufficient elements to govern a flexible light-harvesting antenna.

CONCLUSIONS

We demonstrate that LHCII fluorescence quenching is not the result of a specific thylakoid lipid microenvironment, but is driven by LHCII protein-protein interactions. Increasing the PLR of LHCII proteoliposomes decreased the fluorescence and stabilized at a ~50% reduced yield at a PLR of 10^{-3} , indicating (1) that strong LHCII-LHCII attractive interactions occur and (2) that this mild quenching process reaches equilibrium at protein densities of only tens of LHCII trimers per vesicle. The quenching process at the onset of aggregation is distinct from a second transition that occurs at much higher protein densities. A comparison of LHCII proteoliposomes with low and very high protein densities allowed us to detect the excitonic CD changes that are correlated with the second transition from mild to strongly quenched states. The CD changes in the infrared region are attributed to Chl α_{611} - α_{612} enhanced interactions, while alterations in the Soret band could originate from Chl-Lut1 or Chl-Neo enhanced interactions. Those sites correlate well with the quencher sites that have been proposed for the LHCII photoprotective switch.

REFERENCES

1. Blankenship RE. Molecular Mechanisms of photosynthesis. (2014).
2. Sunku K, de Groot HJ, Pandit A. Insights into the photoprotective switch of the major light-harvesting complex II (LHCII): a preserved core of arginine-glutamate interlocked helices complemented by adjustable loops. *J Biol Chem*, 288(27), 19796-19804 (2013).
3. Ruban AV, Johnson MP, Duffy CD. The photoprotective molecular switch in the photosystem II antenna. *Biochim Biophys Acta*, 1817(1), 167-181 (2012).
4. Kruger TP, Ilioaia C, Johnson MP *et al.* Controlled disorder in plant light-harvesting complex II explains its photoprotective role. *Biophys J*, 102(11), 2669-2676 (2012).
5. Bode S, Quentmeier CC, Liao PN *et al.* On the regulation of photosynthesis by excitonic interactions between carotenoids and chlorophylls. *Proceedings of the National Academy of Sciences of the United States of America*, 106(30), 12311-12316 (2009).
6. Pandit A, Wawrzyniak P, van Gammeren A, Buda F, Ganapathy S. Nuclear Magnetic Resonance Secondary Shifts of a Light-Harvesting II Complex Reveal Local Backbone Perturbations Induced by Its Higher-Order Interactions. *Biochemistry*, 49(3), 478-486 (2010).
7. Cruz J, Avenson T, Kanazawa A, Takizawa K, Edwards G, Kramer D. Plasticity in light reactions of photosynthesis for energy production and photoprotection. *Journal of experimental botany*, 56(411), 395-406 (2005).
8. Tian L, Dinc E, Croce R. LHCII Populations in Different Quenching States Are Present in the Thylakoid Membranes in a Ratio that Depends on the Light Conditions. *The Journal of Physical Chemistry Letters*, 6(12), 2339-2344 (2015).
9. Petrou K, Belgio E, Ruban AV. pH sensitivity of chlorophyll fluorescence quenching is determined by the detergent/protein ratio and the state of LHCII aggregation. *Biochim Biophys Acta - Bioenergetics*, 1837(9), 1533-1539 (2014).
10. Ilioaia C, Johnson M, Horton P, Ruban A. Induction of Efficient Energy Dissipation in the Isolated Light-harvesting Complex of Photosystem II in the Absence of Protein Aggregation. *Journal of biological chemistry*, 283(43), 29505-29512 (2008).
11. Kirchhoff H. Structural changes of the thylakoid membrane network induced by high light stress in plant chloroplasts. *Philos Trans R Soc Lond B Biol Sci*, 369(1640) (2014).
12. Haferkamp S, Haase W, Pascal AA, van Amerongen H, Kirchhoff H. Efficient Light Harvesting by Photosystem II Requires an Optimized Protein Packing Density in Grana Thylakoids. *The Journal of Biological Chemistry*, 285(22), 17020-17028 (2010).
13. Holleboom C-P, Yoo S, Liao P-N *et al.* Carotenoid-Chlorophyll Coupling and Fluorescence Quenching Correlate with Protein Packing Density in Grana-Thylakoids. *J Phys Chem B*, 117(38), 11022-11030 (2013).
14. Ruban AV, Berera R, Ilioaia C *et al.* Identification of a mechanism of photoprotective energy dissipation in higher plants. *Nature*, 450(7169), 575-578 (2007).
15. Miloslavina Y, Wehner A, Lambrev P *et al.* Far-red fluorescence: A direct spectroscopic marker for LHCII oligomer formation in non-photochemical quenching. *FEBS letters*, 582(25-26), 3625-3631 (2008).
16. Holt NE, Zigmantas D, Valkunas L, Li XP, Niyogi KK, Fleming GR. Carotenoid cation formation and the regulation of photosynthetic light harvesting. *Science*, 307(5708), 433-436 (2005).
17. Pandit A, Reus M, Morosinotto T, Bassi R, Holzwarth A, Holzwarth AR. An NMR comparison of the light-harvesting complex II (LHCII) in active and photoprotective states reveals subtle changes in the chlorophyll a ground-state electronic structures. *Biochim Biophys Acta -Bioenergetics*, 1827(6), 738-744 (2013).

18. Duffy CDP, Pandit A, Ruban A. Modeling the NMR signatures associated with the functional conformational switch in the major light-harvesting antenna of photosystem II in higher plants. *PCCP. Physical chemistry chemical physics*, 16(12), 5571-5580 (2014).
19. Ilioaia C, Johnson MP, Liao P-N *et al.* Photoprotection in Plants Involves a Change in Lutein 1 Binding Domain in the Major Light-harvesting Complex of Photosystem II. *The Journal of Biological Chemistry*, 286(31), 27247-27254 (2011).
20. Chmeliov J, Gelzinis A, Songaila E *et al.* The nature of self-regulation in photosynthetic light-harvesting antenna. *Nature Plants*, 2, 16045 (2016).
21. Chmeliov J, Trinkunas G, van Amerongen H, Valkunas L. Light Harvesting in a Fluctuating Antenna. *Journal of the American Chemical Society*, 136(25), 8963-8972 (2014).
22. Schaller S, Latowski D, Jemiola-Rzemińska M *et al.* Regulation of LHCII aggregation by different thylakoid membrane lipids. *Biochim Biophys Acta - Bioenergetics*, 1807(3), 326-335 (2011).
23. Zhou F, Liu S, Hu Z, Kuang T, Paulsen H, Yang C. Effect of monogalactosyldiacylglycerol on the interaction between photosystem II core complex and its antenna complexes in liposomes of thylakoid lipids. *Photosynthesis Research*, 99(3), 185-193 (2009).
24. Wilk L, Wilk L, Grunwald M, Walla PJ, Walla PJ, Kuhlbrandt W. Direct interaction of the major light-harvesting complex II and PsbS in nonphotochemical quenching. *Proc. Natl. Acad. Sci. USA*, 110(14), 5452-5456 (2013).
25. Pandit A, Pandit N, Shirzad Wasei L *et al.* Assembly of the Major Light-Harvesting Complex II in Lipid Nanodiscs. *Biophysical journal*, 101(10), 2507-2515 (2011).
26. F. Szoka J, AND D. Papahadjopoulos. Procedure for preparation of liposomes with large internal aqueous space and high capture by reverse-phase evaporation. *Proc. Natl. Acad. Sci. USA*, 75(9), 4194-4198, (1978).
27. Graham JM, Harris JR, Rickwood D. In Vitro Techniques Cell Biology Protocols. 201-378 (2006).
28. Butler PJG, Kuhlbrandt W. Determination of the aggregate size in detergent solution of the light-harvesting chlorophyll a/b-protein complex from chloroplast membranes. *Proceedings of the National Academy of Sciences*, 85(11), 3797-3801 (1988).
29. Bayburt TH, Sligar SG. Membrane protein assembly into Nanodiscs. *FEBS Letters*, 584(9), 1721-1727 (2010).
30. Webb MS, Green BR. Biochemical and biophysical properties of thylakoid acyl lipids. *Biochim Biophys Acta - Bioenergetics*, 1060(2), 133-158 (1991).
31. Jouhet J. Importance of the hexagonal lipid phase in biological membrane organization. *Frontiers in Plant Science*, 4, 494 (2013).
32. Moya I, Silvestri M, Vallon O, Cinque G, Bassi R. Time-Resolved Fluorescence Analysis of the Photosystem II Antenna Proteins in Detergent Micelles and Liposomes. *Biochemistry*, 40(42), 12552-12561 (2001).
33. Belgio E, Johnson Matthew P, Jurić S, Ruban Alexander V. Higher Plant Photosystem II Light-Harvesting Antenna, Not the Reaction Center, Determines the Excited-State Lifetime-Both the Maximum and the Nonphotochemically Quenched. *Biophysical Journal*, 102(12), 2761-2771 (2012).
34. Mansoor SE, Palczewski K, Farrens DL. Rhodopsin self-associates in asolectin liposomes. *Proc. Natl. Acad. Sci. USA*, 103(9), 3060-3065 (2006).
35. Lambrev PH, Schmitt F-J, Kussin S *et al.* Functional domain size in aggregates of light-harvesting complex II and thylakoid membranes. *Biochim Biophys Acta - Bioenergetics*, 1807(9), 1022-1031 (2011).
36. Lambrev PH, Varkonyi Z, Krumova S *et al.* Importance of trimer-trimer interactions for the native state of the plant light-harvesting complex II. *Biochim. et Biophys. Acta*, 1767(6), 847-853 (2007).
37. Hobe S, Pytulla S, Kuhlbrandt W and Paulsen H. Trimerization and crystallization of reconstituted light-harvesting chlorophyll a/b complex. *The EMBO Journal*, 13(15), 3423-3429 (1994).

38. Yang C, Boggasch S, Haase W, Paulsen H. Thermal stability of trimeric light-harvesting chlorophyll a/b complex (LHCIIb) in liposomes of thylakoid lipids. *Biochim. et Biophys. Acta*, 1757(12), 1642-1648 (2006).
39. Georgakopoulou S, van der Zwan G, Bassi R, van Grondelle R, van Amerongen H, Croce R. Understanding the Changes in the Circular Dichroism of Light Harvesting Complex II upon Varying Its Pigment Composition and Organization. *Biochemistry*, 46(16), 4745-4754 (2007).
40. Yang C, Boggasch S, Haase W, Paulsen H. Thermal stability of trimeric light-harvesting chlorophyll a/b complex (LHCIIb) in liposomes of thylakoid lipids. *Biochim. et Biophys. Acta - Bioenergetics*, 1757(12), 1642-1648 (2006).
41. Liu Z, Yan H, Wang K *et al.* Crystal structure of spinach major light-harvesting complex at 2.72 Å resolution. *Nature*, 428(6980), 287-292 (2004).
42. Akhtar P, Pawlak K, Kovacs L *et al.* Pigment Interactions in Light-harvesting Complex II in Different Molecular Environments. *Journal of biological chemistry*, 290(8), 4877-4886 (2015).
43. Iliaia C, Johnson MP, Horton P, Ruban AV. Induction of Efficient Energy Dissipation in the Isolated Light-harvesting Complex of Photosystem II in the Absence of Protein Aggregation. *The Journal of Biological Chemistry*, 283(43), 29505-29512 (2008).
44. Chmeliov J, Bricker W, Lo C, Jouin E, Valkunas L, Ruban A. An 'all pigment' model of excitation quenching in LHCII. *PCCP. Physical chemistry chemical physics*, 17(24), 15857-15867 (2015).
45. Rigaud J-L, Lévy D. Reconstitution of Membrane Proteins into Liposomes. In: *Methods in Enzymology*. (Academic Press, 2003) 65-86.
46. Zapf T, Tan C-W, Reinelt T *et al.* Synthesis and Functional Reconstitution of Light-Harvesting Complex II into Polymeric Membrane Architectures. *Angewandte Chemie (International ed.)*, 54(49), 14664-14668 (2015).
47. Kuttkat A, Grimm R, Paulsen H. Light-harvesting chlorophyll a/b-binding protein inserted into isolated thylakoids binds pigments and is assembled into trimeric light-harvesting complex. *Plant Physiology*, 109(4), 1267-1276 (1995).
48. Rigaud J-L, Pitard B, Levy D. Reconstitution of membrane proteins into liposomes: application to energy-transducing membrane proteins. *Biochimica et Biophysica acta. Bioenergetics*, 1231(3), 223-246 (1995).
49. Engelman DM, Steitz TA. The spontaneous insertion of proteins into and across membranes: The helical hairpin hypothesis. *Cell*, 23(2), 411-422 (1981).
50. Standfuss R, van Scheltinga ACT, Kuhlbrandt W, Standfuss J, Lamborghini M, Kühlbrandt W. Mechanisms of photoprotection and nonphotochemical quenching in pea light-harvesting complex at 2.5 Å resolution. *EMBO Journal*, 24(5), 919-928 (2005).
51. Sun R, Liu K, Dong L, Wu Y, Paulsen H, Yang C. Direct energy transfer from the major antenna to the photosystem II core complexes in the absence of minor antennae in liposomes. *Biochim Biophys Acta - Bioenergetics*, 1847(2), 248-261 (2015).

CHAPTER 3

Fluorescence lifetimes of LHCII in a lipid environment: aggregation, low pH and the presence of PsbS

This Chapter is submitted as: E. Crisafi, M. Krishnan & A. Pandit, Time-resolved fluorescence analysis of LHCII in the presence of PsbS at neutral and low pH.

ABSTRACT

Plant Light-Harvesting Complexes have a built-in capacity to switch function between light harvesting and quenching of excitation energy, protecting the photosynthetic apparatus against over-excitation via a regulatory feedback response. In their chloroplast thylakoid membranes, non-photochemical quenching (NPQ) is activated as a response to a low luminal pH and controlled by the pH-sensing protein Photosystem II subunit S, PsbS. Several studies proposed that PsbS could directly interact with the peripheral light-harvesting complexes (LHCII) at low pH. In this study, we systematically tested the influence of low pH and PsbS on the fluorescence lifetimes of membrane-embedded spinach LHCII. The proteoliposome preparations contained LHCII in mild quenched states, aimed to mimic the fluorescence conditions of dark-adapted leaves. We found that under those conditions, neither acidification nor the presence of PsbS or the combination of both did have a significant effect on the LHCII Chl fluorescence lifetimes. The results support a view in which the functional role of PsbS consists of re-organizing the thylakoid membrane under stress, rather than creating direct quencher states.

INTRODUCTION

In naturally fluctuating light conditions, plants need to constantly adjust their photosynthetic antenna to the incoming light intensities to prevent themselves from over-excitation and photodamage. They have developed sophisticated feedback mechanisms that regulate light harvesting. In high-light conditions, NPQ processes are activated to dissipate a large part of the incoming excitations as heat [1].

Light-Harvesting Complexes (LHCs) that are associated with PSII have the ability to reversibly switch their conformation into a quenched state, which is assumed to be the cause of excitation quenching during NPQ [2]. Single-molecule experiments have shown that individual LHCs can fluctuate between fluorescent and quenched states [3,4]. In bulk experiments, the quenched state is produced upon aggregation of LHCs [5,6]. Aggregation-dependent quenching has also been observed in native thylakoid membranes, where aggregates of the peripheral Light-Harvesting Complex, LHCII, are formed under high-light conditions [7,8].

The fast energy component of NPQ, called qE, in plants is reversibly controlled via the pH-sensing protein Photosystem II subunit S (PsbS), of which the action is triggered by acidification of the inner compartments of chloroplasts, the thylakoid lumen [9,10]. Switching back from high to moderate light conditions, PsbS also accelerates fast de-activation of the quenching process [11]. The fast qE process is connected to a slower quenching process, termed qZ [12]. In qZ, lumen acidification activates the enzyme violaxanthin de-epoxidase (VDE) to catalyse the conversion of the carotenoid violaxanthin (Vio) to zeaxanthin (Zea). qZ quenching likely occurs due to the binding of Zea to specific LHCs [13]. The presence of Zea has been proposed to catalyse qE quenching and for Zea-accumulating membranes faster fluorescence induction has been observed [14] [15].

The membrane protein PsbS is the only member of the LHC multi-gene family that does not bind pigments in specific locations. Instead of acting as a light harvester, this protein solely functions as a pH sensor [16]. PsbS is activated under high-light conditions, and its activation is proposed to involve protonation of specific glutamic-acid residues at low lumen pH and monomerization of PsbS dimers [16]. Recent studies showed that PsbS interacts with the LHCII polypeptides (Lhcb1, Lhcb2, and Lhcb3) or with the minor antenna proteins (Lhcb4, Lhcb5, and Lhcb6) under influence of the xanthophyll cycle [17]. The molecular mechanism for qE excitation quenching has not been resolved and the mechanistic trigger that activates the process via PsbS has not been clarified. Molecular interactions of PsbS with LHCs might induce conformational changes of the antenna proteins into quenched states. PsbS has also been suggested to induce supramolecular rearrangements of LHCs and PSII reaction center complexes [18]. According to current models, the activation of PsbS at low pH concerns the protonation of two key residues and a monomerization step [16,19]. Monomeric PsbS may disconnect LHCII from PSII after which the released LHCII complexes could form clustered aggregates that produce dissipative states via an aggregation-dependent quenching mechanism [20,21].

Liposomes form suitable model systems to investigate protein-lipid interactions in membranes of reduced complexity compared to natural biological membranes and dissect the functions of selective membrane components. Various studies have investigated the

properties of LHCII proteoliposomes [4,5,22]. Liu *et al.* demonstrated that PsbS could be refolded directly in LHCII-reconstituted membranes [23]. Wilk *et al.* co-reconstituted PsbS in liposomes with very low amounts of LHCII to prevent self-aggregation quenching, and showed that under those conditions the LHCII fluorescence was quenched in the presence of both PsbS and Zea [24]. Their work does not report on the effects of acidification though, which is known to activate PsbS *in vivo*.

The rapid qE response occurs on the time scale of seconds before the enzymatic process of xanthophyll conversion has taken place, is activated by low pH, and requires PsbS. To investigate the origin of this response mechanism, we performed a systematic fluorescence lifetime analysis on PsbS-LHCII and LHCII-only proteoliposomes at neutral and low pH. For our membrane model, we carefully choose the protein to lipids ratio, PLR expressed in mole of protein per mole lipids, so that the fluorescence of LHCII-only proteoliposomes at neutral pH would mimic the dark-adapted state of leaves *in vivo*. In dark-adapted leaves, the fluorescence of the PSII antenna is moderately quenched and LHCII has an average lifetime of ~ 2 ns, which is considerably shorter than the lifetime of ~ 4 ns that are observed for LHCII in detergent solutions [25] and suggests that LHCII exists as small aggregates in thylakoid membranes.

MATERIALS AND METHODS

LHCII EXTRACTION

Light-Harvesting Complexes were purified from spinach leaves (*Spinacia oleracea*) as described previously [5]. Briefly, LHCII trimer complexes were isolated via sucrose gradient. The trimeric green band of LHCII was extracted using a needle. Purified LHCII pigment-protein complexes were characterized by absorption spectroscopy. The buffer was exchanged into HEPES 50 mM, NaCl 100 mM, pH 7.5, n-Dodecyl β -D-maltoside (β -DM, Sigma) 0.03% and concentrated using Amicon Ultra 2 ml centrifugal filters with cut off of 30 K (Millipore) before to store the protein at -80 °C until use.

PsbS REFOLDING

PsbS genes from *Physcomitrella patens* and *Spinacia oleracea* were overexpressed in *E. coli* and purified using the protocol from Krishnan *et al.* [26]. The unfolded PsbS was stored at 4°C until further use. PsbS was refolded in presence of the detergent β -DM. According to the refolding protocol, PsbS was mixed with heating buffer (NaOAc 20 mM, NaCl 100 mM, LDS 4%, sucrose 25%, pH 7.5) and heated to 98°C for 1 minute. The appropriate amount of detergent (β -DM) was added to the mixture. The addition of 200 mM KCl and 30 minutes incubation at 4°C precipitates LDS, thus allowing β -DM to refold PsbS. Aggregated LDS was pelleted by spinning at 20000 x g for 10 minutes at 4°C. The concentration of PsbS protein in mg/ml was determined from SDS page analysis.

PREPARATION OF ASOLECTIN LIPOSOMES

Liposomes were prepared according to Crisafi & Pandit with the following adjustments [5]. Asolectin lipids from soybean (Sigma) were dissolved in chloroform to a concentration of 5 mg/ml. With a stream on N₂, the organic solvent was evaporated from the chloroform/asolectin solution collected in a round-bottom flask. To remove all traces of solvent an extra step of evaporation in a rotary evaporator (R3000, Buchi) was performed. The phospholipid bilayer was then hydrated with the desired buffer (HEPES 50 mM, NaCl 100 mM, pH 7.5) and the round bottom flask was rotated at low rpm using the rotary evaporator for 1-2 hours. After that, if the bilayer was not completely solubilized, the solution was sonicated for 1 min (2210, Branson). The liposome suspension was exposed to 10 freeze/thaw cycles followed by extrusion through polycarbonate membranes of 400 and 200 nm pore size, using a mini-extruder (Avanti polar lipids). Sizes of liposome preparations were determined by dynamic light scattering (DLS, Malvern Zetasizer Nano ZS) equipped with a Peltier controlled thermostatic cell holder.

PREPARATION OF PROTEOLIPOSOMES

For protein insertion, preformed liposomes were destabilized by the addition of 0.03% of β -DM to facilitate insertion of LHCII and PsbS into the liposome membranes. LHCII

complexes were added to the liposome suspension and incubated for 1 hour. Bio-beads were added to the suspensions in 2 steps. The first incubation step was performed at 4 °C overnight while gently rotating the sample using a roller mixer (SRT9D, Stuart). Subsequently, the Bio-beads were refreshed and the solution was again incubated for 2-3 hours. The proteoliposome suspensions were centrifuged at 20000 x g for 10 min at 4 °C using a table-top centrifuge (3K18, Sigma) to remove non-incorporated LHCII and PsbS that forms aggregate pellets [27]. LHCII insertion and removal of LHCII aggregate pellet were confirmed by running LHCII and LHCII-PsbS proteoliposomes over a sucrose gradient that showed a single green band containing the proteoliposomes [28]. The reported protein to lipid ratios (PLRs) are defined as moles of LHCII or PsbS trimers per moles of total lipids. The concentration of LHCII trimers was determined from the molar extinction coefficient for LHCII (trimers) at 670 nm, $\epsilon = 1,638,000 \text{ M}^{-1} \text{ cm}^{-1}$ [29].

CIRCULAR DICHROISM EXPERIMENTS

CD spectra were recorded on a J-815 spectropolarimeter (Jasco) equipped with a Peltier element. The wavelength range was from 350 to 750 nm, data pitch 1 nm, response 2 s, bandwidth 2 nm and scanning speed of 50 nm/min at 20 °C using a 1 cm quartz cuvette (Hellma).

UV-VIS ABSORBANCE EXPERIMENTS

Absorption spectra were recorded on a UV-1700 PharmaSpec spectrophotometer (Shimadzu) with the wavelength range set from 350 to 750 nm using 1x1cm cuvette.

STEADY-STATE FLUORESCENCE EXPERIMENTS

Fluorescence measurements were performed on a Cary Eclipse fluorescence spectrophotometer (Varian), collecting emission spectra from 660 to 720 nm using 3x3 mm quartz cuvettes. The optical density of the sample preparations varied from 0.03 to 0.07 cm^{-1} at 650 nm. The excitation wavelength was set at 650 nm or 475 nm.

TIME-RESOLVED FLUORESCENCE EXPERIMENTS

TRF measurements were performed using a FluoTime 300 (PicoQuant) time-correlated photon counter spectrometer. Samples were held in a 1x1 cm quartz cuvette that was thermostated at 20 °C and excited at 440 nm using a diode laser (PicoQuant). Fluorescence decay traces were fitted with multi-exponential using a χ^2 least-square fitting procedure.

SDS-PAGE GEL ANALYSIS

For SDS-page analysis, proteoliposomes were pelleted and re-suspended in HEPES buffer and analysed on 12,5% polyacrylamide running gel with 4% stacking gel. Gels were stained using Silver Stain Plus kit (Bio-Rad) according to the standard Bio-Rad protocol. Molecular masses were estimated via a molecular standard, precision plus protein dual colour (Bio-Rad).

RESULTS

THE RELATIONSHIP BETWEEN LHCII CONCENTRATION AND FLUORESCENCE QUENCHING

To separate the effects of PsbS and low pH from the effects of self-aggregation on the fluorescence quenching of LHCII, we aimed to have a clear overview of how concentration and quenching of LHCII in liposomes depend on the protein to lipid ratio (PLR). Several studies, including the work from the previous chapter, report on the fluorescence yields of LHCII proteoliposomes in different PLR regimes. To have an overview, we combined data results from different reports in one graph, Figure 3.1, where the quenching of LHCII proteoliposomes is plotted against the PLRs. To generate this plot, the relative fluorescence yields of the LHCII proteoliposomes were calculated, taking the reported average fluorescence lifetimes for LHCII proteoliposomes and using the fluorescence of LHCII in detergent, reported in the same studies, as a reference for 100% fluorescence.

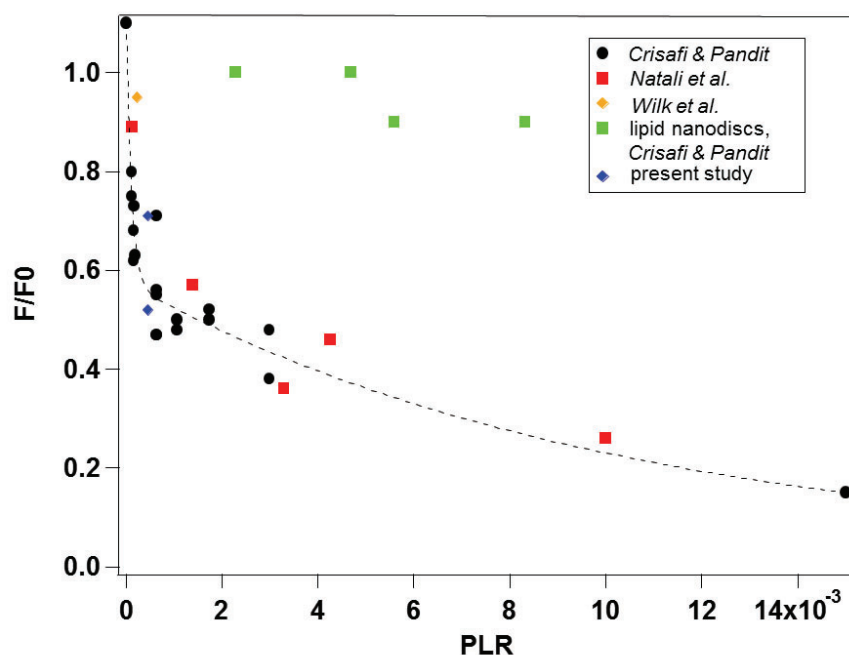


Figure 3.1 Fluorescence yield of LHCII proteoliposomes and LHCII lipid nanodiscs versus the PLRs. Data results from three different studies are plotted. Crisafi and Pandit [5] used liposomes prepared from asolectin, while Natali et al. [4] and Wilk et al. [24] used mixtures of thylakoid lipids. Data points, excluding those from lipid nanodiscs, are fitted with a double exponential fit.

As shown in Figure 3.1, the data from different sources follows a remarkably similar trend, considering that different preparation techniques were used and that our study used asolectin proteoliposomes, while other studies used liposomes prepared from thylakoid lipid mixtures of which the major content is galactolipids. At very low PLRs, a

steep dependence of the fluorescence is observed with increased LHCII concentrations that levels at ~50% quenching as described in Chapter 2. In this PLR regime, the liposomes contain only a few proteins per vesicle according to single-molecule and electron freeze-fracture microscopy [4,24].

At higher PLRs, there is a more gradual increment of quenching with the increase of LHCII concentrations. The dataset could not be fitted properly with a single exponential or sigmoidal curve and was fitted with two exponentials. The fluorescence of LHCII lipid nanodiscs is also plotted. LHCII complexes that are captured in nanodiscs are prevented from self-aggregation. Under those conditions, no significant quenching occurs, the small decrease at high PLRs is due to minor fractions of small aggregates trapped within the nanodiscs, showing that quenching in LHCII proteoliposomes is not induced by protein-lipid interactions *per se* [4,5].

The fluorescence yield of 50% around the breakpoint in the curve in Figure 3.1 corresponds to an average fluorescence lifetime of ~2 ns, which resembles the fluorescence lifetimes of dark-adapted leaves with closed reaction centres [15]. For our proteoliposome preparations, we choose to use a PLR of 6.5×10^{-4} for LHCII in lipids, which is close to the breakpoint in the slope of the curve. Note that the protein density in native thylakoids is much higher than in our proteoliposomes and we did not intend to reproduce the *in vivo* protein density, which would lead to the formation of large LHCII aggregates that strongly quench the fluorescence. In native membranes, the involvement of LHCII in super complexes may prevent the formation of such large LHCII aggregates.

ANALYSIS OF PsbS PROTEOLIPOSOMES

Proteoliposomes were prepared from asolectin lipids because those would give better reproducibility for quantitative LHCII protein insertion than liposomes prepared from galactolipid mixtures that mimic the natural thylakoid lipid composition. As shown in Figure 3.1, the trend for aggregation-dependent quenching of LHCII in asolectin liposomes (*Crisafi & Pandit*) is similar to liposomes prepared from a mixture of thylakoid lipids [5]. A PsbS: LHCII ratio of 1:1 was used. This ratio was much higher than the natural occurrence of PsbS in thylakoid membranes and was used to increase the probability that PsbS and LHCII would interact.

LHCII insertion in the liposomes was confirmed by the absence of LHCII aggregate pellet in reconstitution solutions and by sucrose gradient analysis that showed a green band containing the LHCII proteoliposomes. To test the insertion of PsbS, we performed an SDS-page gel analysis on PsbS-only proteoliposomes. Western blotting was not applied as we noticed that PsbS can give a false-positive reaction in anti-Lhcb1 Western blots (Figure A3.1).

It is recently demonstrated that PsbS forms an equilibrium of monomers and dimers in detergent solutions [26]. At low pH, the equilibrium is shifted towards the monomeric form. However, aging of the protein solutions shifts the equilibrium towards the dimeric form, both for neutral and acidic solutions. To check if the initial oligomeric state of PsbS would influence the dimerization state inside membranes, we tested PsbS insertion in

preformed liposomes under four different conditions. Proteoliposomes were prepared at pH 5.0 or pH 7.5, and for both conditions, two PsbS preparations were used containing PsbS in different monomer-dimer equilibria. One sample was three days old and contained more dimers than monomers according to SDS-page analysis. The other PsbS sample was freshly prepared and contained more monomers than dimers. The results of our insertion tests confirmed that PsbS was inserted into the liposomes under all tested conditions. Remarkably, the test shows that PsbS fractions run as a monomer band in the SDS-page gel, irrespective of the pH conditions or oligomeric state before insertion (Figure 3.2).

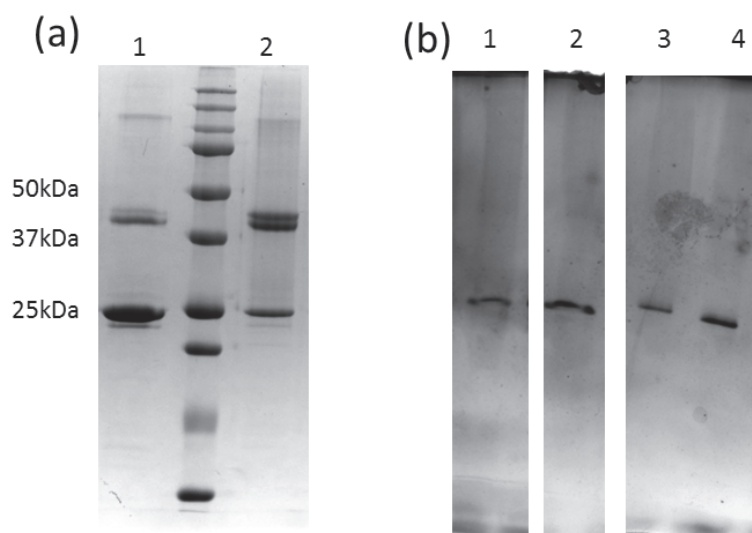


Figure 3.2 (a) SDS-page gel of PsbS in detergent solution before liposome insertion. Lane 1 contains PsbS that was predominantly in the monomeric form and lane 2 contains PsbS that is predominantly in the dimeric form. The middle lane contains the protein marker. (b) PsbS proteoliposomes confirming PsbS insertion (silver stain gel). Lane 1 and 2: proteoliposomes prepared at pH 5.0 using sample 1 (1) or sample 2 (2). Lane 3 and 4: proteoliposomes prepared at pH 7.5 using sample 1 (3) or sample 2 (4).

When the insertion was performed in pH 5.0 buffers, larger pellets of PsbS were observed containing proteins that were not inserted in the liposomes. Therefore, we proceeded with PsbS reconstitution in pH 7.5 buffer solutions. From a comparison of the gel band intensities of PsbS proteoliposomes to those of the removed pellet, we estimated that ~80% of the PsbS was inserted in the liposomes under pH 7.5 conditions (Figure A3.2).

FLUORESCENCE LIFETIME ANALYSIS OF LHCII-PsbS AT NEUTRAL AND LOW pH

TRF experiments were performed on LHCII-only and LHCII-PsbS proteoliposomes that were equilibrated at pH 7.5 or at pH 5.0. The compared LHCII-only and LHCII-PsbS proteoliposomes were always prepared using the same liposome batches since some variation in the fluorescence were found from batch to batch. To equilibrate the proteoliposome preparations at pH 5.0, we used a protocol in which suspensions prepared at pH 7.5 were acidified by injection of HCl followed by the addition of nigericin, a

liposoluble compound, in order to equilibrate pH conditions inside and outside the proteoliposomes [30]. Dynamic Light Scattering (DLS) measurements on liposomes before and after acidification and nigericin treatment confirmed that there were no significant changes in the average diameter sizes of the proteoliposomes (Table A3.1). Upon acidification, the contribution of very large particles (>500 nm), disappeared in the DLS size distribution diagrams and therefore the average diameter is slightly shifted to lower values.

Table 3.1 presents the results of TRF experiments that were performed on LHCII-only and LHCII-*patens* PsbS proteoliposomes.

Sample	A ₁ %	τ_1	A ₂ %	τ_2	A ₃ %	τ_3	τ_{av}
LHCII proteoliposomes pH 7.5	28.4	4.4	52.7	2.6	18.9	0.8	2.7
LHCII proteoliposomes pH 5.0	21.9	4.5	56.0	2.5	22.1	0.8	2.6
LHCII-PsbS proteoliposomes pH 7.5	21.5	4.6	58.0	2.6	20.4	1.0	2.7
LHCII-PsbS proteoliposomes pH 5.0	19.4	4.6	57.8	2.5	22.8	1.0	2.6
LHCII in β -DM pH 7.5	72.1	4.2	27.9	2.9	-	-	3.8
LHCII in β -DM pH 5.0	61.4	4.3	35.3	2.8	3.3	1.1	3.7

Table 3.1 Fluorescence lifetimes expressed in ns of LHCII-only and PsbS-LHCII proteoliposomes.

For comparison, the fluorescence lifetimes of LHCII in 0.03% β -DM detergent solutions equilibrated at pH 7.5 or at pH 5.0 were also collected. The presented results are the average of two reconstitution experiments using the same batch of preformed liposomes. The results show that acidification causes at most ~4% reduction of the average fluorescence lifetimes, while no differences are observed comparing LHCII and LHCII-PsbS proteoliposomes. Steady-state fluorescence spectra, as shown in Figure 3.3, collected upon 440 nm excitation show a broadening and small red shoulder for the proteoliposomes compared to LHCII in β -DM solution indicative of spectral ensembles of LHCII that are in different conformational states. In these experiments, we used PsbS from *Physcomitrella patens* since we already performed an extensive analysis of this protein, and reconstituted *patens* PsbS together with LHCII extracted from spinach leaves [26].

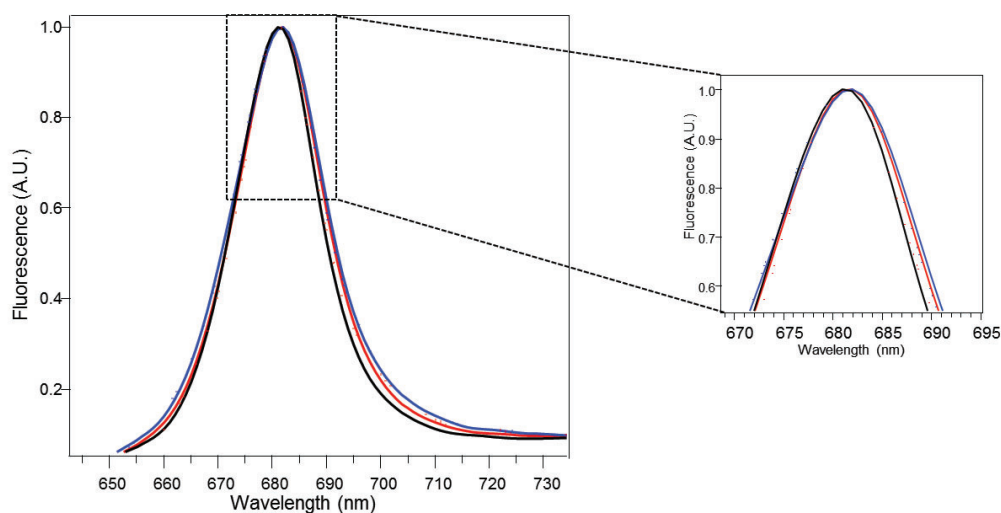


Figure 3.3 Fluorescence emission spectra of LHCII in β -DM in black, LHCII-only proteoliposomes in red and LHCII-PsbS proteoliposomes in blue at pH 7.5 normalized at the fluorescence maximum. Dashed lines: LHCII only proteoliposomes in red and LHCII-PsbS proteoliposomes blue at pH 5.0.

Because interactions between PsbS and LHCII may rely on molecular recognition sites that require protein interaction partners from the same organism, we also analysed PsbS-LHCII proteoliposomes that contained PsbS from *Spinacia oleracea*. Figures 3.4 and 3.5 show the results of a fluorescence analysis on the second set of experiments that were performed on PsbS-LHCII liposomes containing *patens* PsbS (a) or *spinach* PsbS (b). Figure 3.4 shows that the lifetime distributions of proteoliposomes containing *Patens* or *spinach* PsbS are very similar and are not significantly affected by acidification.

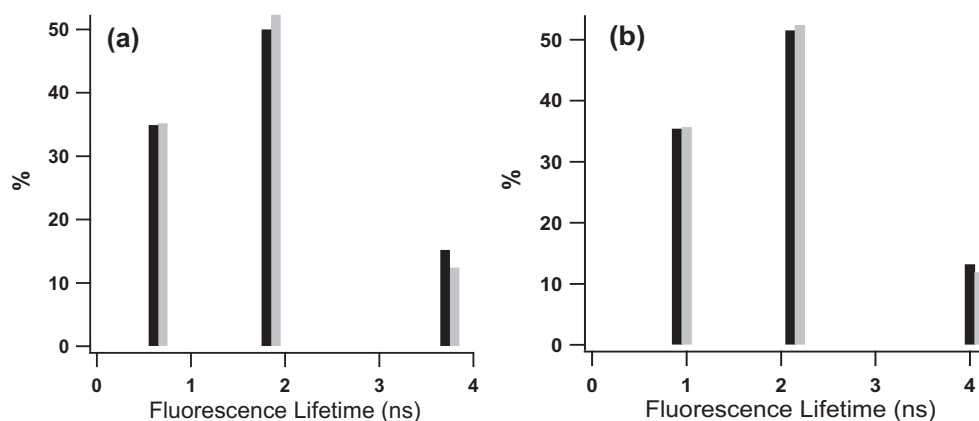


Figure 3.4 TRF analysis of PsbS-LHCII proteoliposomes containing *Patens* PsbS (a) or *spinach* PsbS (b). Black sticks: pH 7.5 conditions, grey sticks: pH 5.0 conditions.

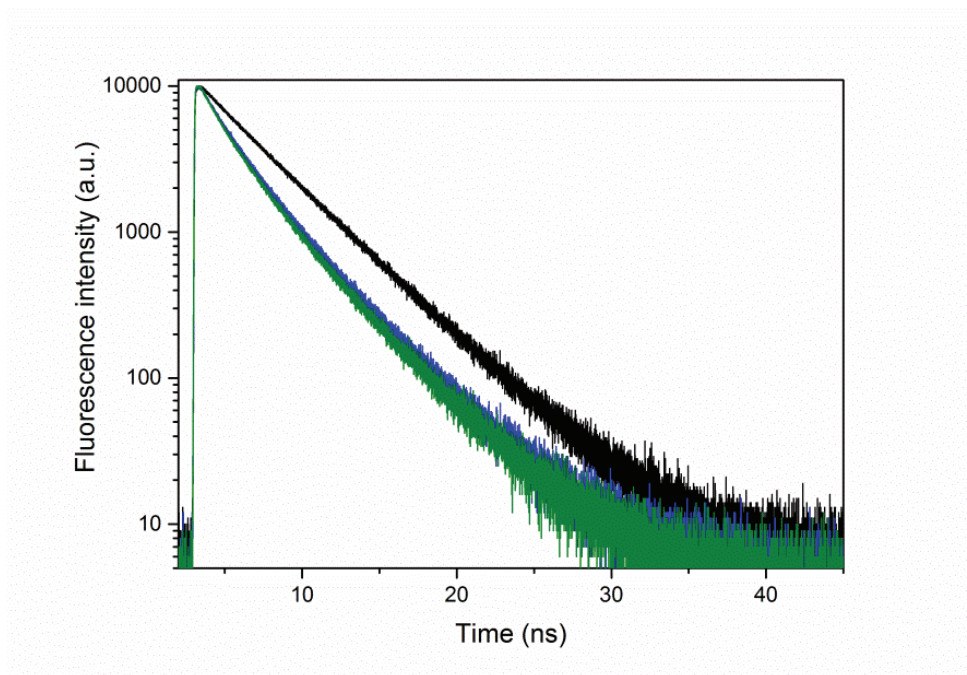


Figure 3.5 TRF experimental and fit traces of the data presented in Figure 3.3 (b). Black: LHCII in 0.03% β -DM, blue: LHCII-PsbS proteoliposomes at pH 7.5, green: LHCII-PsbS proteoliposomes at pH 5.0.

CD SPECTRAL ANALYSIS OF LHCII-PsbS PROTEOLIPOSOMES

The pigment excitonic CD spectrum of LHCII is very sensitive to the changes in the protein conformation or in the protein micro-environment. Figure 3.6 shows the excitonic CD spectra in the visible region of LHCII-only and of LHCII-PsbS proteoliposomes. PsbS does not bind any pigments and the CD bands originate from the excitonic interactions among the LHCII Chl and carotenoid pigments. The low pH CD spectra of PsbS-only and PsbS-LHCII proteoliposomes are very similar. At low pH, an increase of the negative bands at 450 nm and 461 nm is observed. The CD spectrum of LHCII in β -DM detergent is also plotted. The difference between the CD spectral shape of LHCII in β -DM and LHCII proteoliposomes is characteristic for the exchange from a detergent to lipid environment.

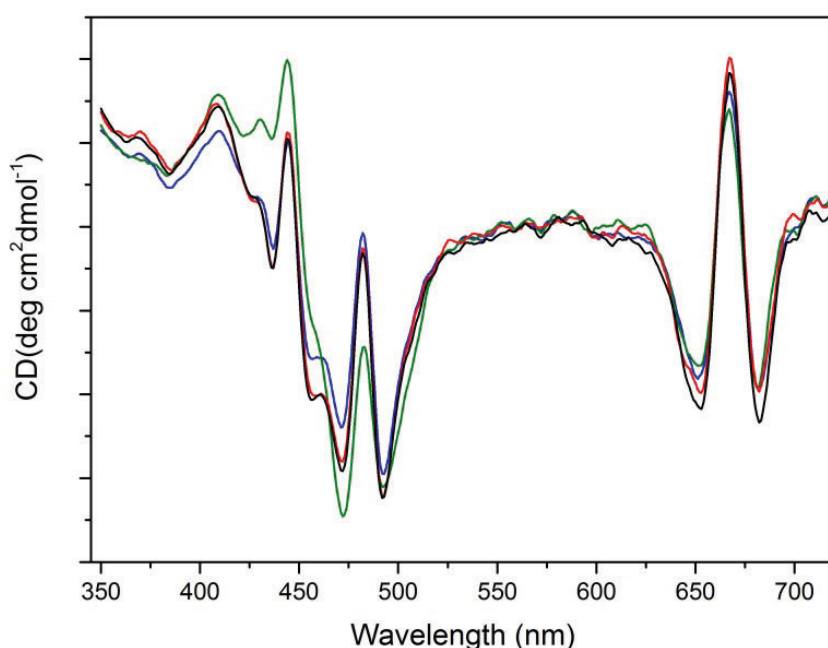


Figure 3.6 CD spectra of LHCII in 0.03% β DM at pH 7.5 (green), LHCII+ Patens PsbS proteoliposomes at pH 7.5 (blue, fluorescence τ_{av} = 2 ns), LHCII proteoliposomes at pH 5.0 (red, fluorescence τ_{av} = 1.6 ns) and LHCII+ Patens PsbS proteoliposomes at pH 5.0 (black, fluorescence τ_{av} = 1.7 ns).

Acidification of LHCII in β -DM detergent did not influence the CD spectral shape (Figure A3.3), indicating that the difference between the proteoliposome spectrum at pH 7.5 and at pH 5.0 is not due to a protonation changes at low pH that affect the LHCII conformation. The proteoliposome CD samples were obtained from different preparations that had small variations in their fluorescence lifetimes. The CD pH 5.0 samples had shorter average lifetimes, 1.6 and 1.7 ns for LHCII-only and for LHCII-PsbS proteoliposomes respectively, than the pH 7.5 sample with 2.0 ns. The small increase in quenching might have an effect on the CD spectral shape, which interestingly would

indicate that CD is a very sensitive tool for detecting quenching-related structural changes.

DISCUSSION

The analysis does not show an effect of PsbS on the LHCII Chl excited-state lifetimes, neither at neutral, nor at low pH, although the slight broadening of the fluorescence emission spectrum of PsbS-LHCII compared to LHCII-only proteoliposomes suggest that PsbS affects the LHCII fluorescence, which implies that PsbS and LHCII proteins are in physical contact with each other.

Our model aimed to mimic the fast activation of PsbS, which is presumed to rely on protonation-state changes, and we did not incorporate Zea that is responsible for the slower qZ contribution of NPQ and depends upon the activation of VDE enzymes. Wilk *et al.* performed experiments on PsbS-LHCII proteoliposomes in Zea-containing membranes [24]. On basis of their results from Western-blotting experiments, it was concluded that PsbS-LHCII heterodimers were formed, and it was shown that Zea-containing proteoliposomes were quenched via Chl-Cars interactions. We found that PsbS reacts to Lhcb1 antibodies and warn that their conclusions from Western blotting could be based on a false-positive result (Figure A3.1). Nevertheless, their data suggest that in the absence of LHCII aggregation, the combination of PsbS and Zea reduces the LHCII fluorescence yields. A much higher concentration of PsbS per lipid was used in their experiments and might be necessary to force PsbS-LHCII one-to-one interactions in an *in vitro* system.

We were not able to reproduce the results of Liu *et al.*, who detected a drop in the fluorescence intensity of PsbS-LHCII proteoliposomes upon acidification [23]. Lowering the pH of proteoliposome solutions in our case would only have a very modest effect, reducing the average fluorescence lifetimes at most ~4%, and directly monitoring the fluorescence intensity before and after acidification did not show a decrease of fluorescence intensities (*data not shown*). Liu *et al.* do not report time-resolved fluorescence experiments. Their approach consisted of direct refolding of PsbS in preformed liposome membranes [23]. We tested this method and also achieved successful refolding of PsbS directly into liposomes. However, because inspection by eye showed the presence of foam remaining in the liposome suspensions, we suspected that not all of the LDS detergent was removed with this procedure and did not continue with this approach. The negligible effect of pH on the fluorescence lifetimes of LHCII proteoliposomes predicts that lumen acidification *per se* will not influence the quenching states of LHCII. The insensitivity to pH of LHCII proteoliposomes differs from the reported pH sensitivity of pre-aggregated LHCs in low-detergent solutions, where the lowering of the pH significantly enhanced quenching [31]. It is clear that isolated LHCII is not sensitive to pH [32] and the excitonic CD spectrum of LHCII in β -DM does not change at low pH (Figure A3.3), which means that the pH does not affect the conformational energy landscapes of LHCII. The observed increased quenching of LHCII in low-detergent solutions at low pH is associated with stronger aggregation. In liposome membranes, only

lateral aggregates are formed and aggregate cluster sizes are limited to the number of LHCII complexes per vesicle [4,5]. These differences could explain why the pH sensitivity of LHCII proteoliposomes is very low.

The PsbS proteoliposomes give new information on the self-association of PsbS in lipid membranes. PsbS in detergent solutions forms monomer and dimer bands on SDS-page gels, while in PsbS proteoliposomes only forms monomer bands. It is possible that PsbS dimers in the liposome membranes did not resist the denaturing gel conditions, which would infer that PsbS dimers are destabilized in membranes compared to dimers in detergent solutions. Further experiments using cross-linkers have to be performed to determine the oligomerization states of PsbS in liposome membranes under different pH conditions and go beyond this study.

The plot in Figure 3.1 gives an overview of aggregation-dependent quenching in different fluorescence regimes. Fluorescence induction under excess light conditions reduces the average fluorescence lifetimes from ~ 2 ns in dark to ~ 0.5 ns under qE conditions. Figure 3.1 shows that starting from conditions that mimic dark-adapted states, *i.e.* average fluorescence lifetime of ~ 2 ns, qE-mimicking conditions can be achieved by increasing the LHCII density by a factor of 5 to 10; an effect that was already reported by Moya *et al.* [22]. The single-molecule study of Natali *et al.* [4] suggests that at this low PLR, liposome vesicles contain several LHCII trimers. Thus, a membrane response that would create antenna re-arrangements going from a few connected LHCII to 10-30 interconnecting LHCII would be sufficient to drive the transition from dark-adapted towards qE states. The steep dependence of the LHCII fluorescence on the PLR at very low concentrations complicates the control of LHCII fluorescence states in highly diluted LHCII proteoliposomes, such as have been employed to prevent self-aggregation [24]. We warn that a fluorescence comparison of different sample preparations under those conditions, therefore, should be taken with caution.

CONCLUSIONS

The fluorescence study of our minimal membrane model does not point toward functional quenching interactions between LHCII and PsbS, neither do they show a significant effect of pH. The results strongly suggest that the pH-dependent role of PsbS during the fast qE response lies in creating membrane rearrangements and supercomplex remodelling [28,33] that could facilitate LHCII aggregation quenching, rather than in creating direct quencher states.

REFERENCES

1. Derks A, Schaven K, Bruce D. Diverse mechanisms for photoprotection in photosynthesis. Dynamic regulation of photosystem II excitation in response to rapid environmental change. *Biochim Biophys Acta - Bioenergetics*, 1847(4), 468-485 (2015).
2. Ruban AV, Johnson CDP, Duffy. The photoprotective molecular switch in the photosystem II antenna. *Biochim Biophys Acta-Bioenergetics*, 1817(1), 167-181 (2012).
3. Kruger T, Illoia C, Johnson M *et al.* Controlled Disorder in Plant Light-Harvesting Complex II Explains Its Photoprotective Role. *Biophysical Journal*, 102(11), 2669-2676 (2012).
4. Natali A, Gruber JM, Dietzel L, Stuart MC, van Grondelle R, Croce R. Light-harvesting Complexes (LHCs) Cluster Spontaneously in Membrane Environment Leading to Shortening of Their Excited State Lifetimes. *J Biol Chem*, 291(32), 16730-16739 (2016).
5. Crisafi E, Pandit A. Disentangling protein and lipid interactions that control a molecular switch in photosynthetic light harvesting. *Biochim Biophys Acta*, 1859(1), 40-47 (2017).
6. van Oort B, van Hoek A, Ruban Alexander V, van Amerongen H. Aggregation of Light-Harvesting Complex II leads to formation of efficient excitation energy traps in monomeric and trimeric complexes. *FEBS Letters*, 581(18), 3528-3532 (2007).
7. Tian L, Dinc E, Croce R. LHCII Populations in Different Quenching States Are Present in the Thylakoid Membranes in a Ratio that Depends on the Light Conditions. *The Journal of Physical Chemistry Letters*, 6(12), 2339-2344 (2015).
8. Lambrev PH, Schmitt F-J, Kussin S *et al.* Functional domain size in aggregates of light-harvesting complex II and thylakoid membranes. *Biochim Biophys Acta - Bioenergetics*, 1807(9), 1022-1031 (2011).
9. Li X-P, Mueller-moule P, M Gilmore A, K Niyogi K. *Li XP, Muller-Moule P, Gilmore AM, Niyogi KK.* PsbS-dependent enhancement of feedback de-excitation protects photosystem II from photoinhibition. *Proc Natl Acad Sci USA* 99: 15222-15227 (2002).
10. Fan M, Li M, Liu Z *et al.* Crystal structures of the PsbS protein essential for photoprotection in plants. *Nature Structural & Molecular Biology*, 22, 729 (2015).
11. Kromdijk J, Glowacka K, Leonelli L *et al.* Improving photosynthesis and crop productivity by accelerating recovery from photoprotection. *Science*, 354(6314), 857 (2016).
12. Nilkens M, Kress E, Lambrev P *et al.* Identification of a slowly inducible zeaxanthin-dependent component of non-photochemical quenching of chlorophyll fluorescence generated under steady-state conditions in *Arabidopsis*. *Biochim Biophys Acta - Bioenergetics*, 1797(4), 466-475 (2010).
13. Morosinotto T, Baronio R, Bassi R. *Dynamics of Chromophore Binding to Lhc Proteins in Vivo and in Vitro during Operation of the Xanthophyll Cycle*, *J Biol Chem*. 277(40):36913-2 (2002)
14. Kress E, Jahns P. The Dynamics of Energy Dissipation and Xanthophyll Conversion in *Arabidopsis* Indicate an Indirect Photoprotective Role of Zeaxanthin in Slowly Inducible and Relaxing Components of Non-photochemical Quenching of Excitation Energy. *Frontiers in Plant Science*, 8, 2094 (2017).
15. Sylak-Glassman EJ, Malnoë A, De Re E *et al.* Distinct roles of the photosystem II protein PsbS and zeaxanthin in the regulation of light harvesting in plants revealed by fluorescence lifetime snapshots. *Proceedings of the National Academy of Sciences*, 111(49), 17498 (2014).
16. Correa-Galvis V, Poschmann G, Melzer M, Stühler K, Jahns P. PsbS interactions involved in the activation of energy dissipation in *Arabidopsis*. *Nature Plants*, 2, 15225 (2016).
17. Farber A, Young AJ, Ruban A, Horton P, Jahns P. Dynamics of Xanthophyll-Cycle Activity in Different Antenna Subcomplexes in the Photosynthetic Membranes of Higher Plants. *Plant Physiol.* , 115, 1609-1618 (1997).

18. Dong L, Tu W, Liu K *et al.* The PsbS protein plays important roles in photosystem II supercomplex remodelling under elevated light conditions. *Journal of Plant Physiology* (172) 33–41, (2015).
19. Bergantino E, Segalla A, Brunetta A *et al.* Light- and pH-dependent structural changes in the PsbS subunit of photosystem II. *Proceedings of the National Academy of Sciences of the United States of America*, 100(25), 15265-15270 (2003).
20. van Oort B, van Hoek A, Ruban AV, van Amerongen H. Aggregation of Light-Harvesting Complex II leads to formation of efficient excitation energy traps in monomeric and trimeric complexes. *FEBS Letters*, 581(18), 3528-3532 (2007).
21. Sacharz J, Giovagnetti V, Ungerer P, Mastroianni G, Ruban AV. The xanthophyll cycle affects reversible interactions between PsbS and light-harvesting complex II to control non-photochemical quenching. *Nature Plants*, 3, 16225 (2017).
22. Moya I, Silvestri M, Vallon O, Cinque G, Bassi R. Time-Resolved Fluorescence Analysis of the Photosystem II Antenna Proteins in Detergent Micelles and Liposomes. *Biochemistry*, 40(42), 12552-12561 (2001).
23. Liu C, Gao Z, Liu K *et al.* Simultaneous refolding of denatured PsbS and reconstitution with LHCII into liposomes of thylakoid lipids (2015).
24. Wilk M, Grunwald M, Liao PN, Wall PJ, Kuhlbrandt W. Direct interaction of the major light harvesting complex II and PsbS in NPQ. *PNAS*, 110(14), 5452-5456 (2013).
25. Belgio E, Johnson Matthew P, Jurić S, Ruban Alexander V. Higher Plant Photosystem II Light-Harvesting Antenna, Not the Reaction Center, Determines the Excited-State Lifetime-Both the Maximum and the Nonphotochemically Quenched. *Biophysical Journal*, 102(12), 2761-2771 (2012).
26. Krishnan M, Moolenaar GF, Gupta K, Goosen N, Pandit A. Large-scale *in vitro* production, refolding and dimerization of PsbS in different microenvironments. *Sci Rep*, 7(1), 15200 (2017).
27. Akhtar P, Dorogi M, Pawlak K *et al.* Pigment interactions in light-harvesting complex II in different molecular environments. *J Biol Chem*, 290(8), 4877-4886 (2015).
28. Kiss A, Ruban A, Horton P. The PsbS Protein Controls the Organization of the Photosystem II Antenna in Higher Plant Thylakoid Membranes. *Journal of biological chemistry*, 283(7), 3972-3978 (2008).
29. Butler PJG and Kuhlbrandt W. Determination of the aggregate size in detergent solution of the light-harvesting chlorophyll a/b-protein complex from chloroplast membranes. *Proc. Natl. Acad. Sci. USA*, 85, pp. 3797-3801 (1988).
30. Sigel A, Sigel H, Sigel,RKO. The Alkali Metal Ions: Their Role for Life. *Springer*, 485-548 (2016).
31. Petrou K, Belgio E, Ruban AV. pH sensitivity of chlorophyll fluorescence quenching is determined by the detergent/protein ratio and the state of LHCII aggregation. *Biochimica et Biophysica Acta - Bioenergetics*, 1837(9), 1533-1539 (2014).
32. Liguori N, Roy LM, Opacic M, Durand G, Croce R. Regulation of Light Harvesting in the Green Alga *Chlamydomonas reinhardtii*: The C-Terminus of LHCSR Is the Knob of a Dimmer Switch. *Journal of the American Chemical Society*, 135(49), 18339-18342 (2013).
33. Dong L, Tu W, Liu K *et al.* The PsbS protein plays important roles in photosystem II supercomplex remodeling under elevated light conditions. *Journal of Plant Physiology*, 172, 33-41 (2015).
34. <https://www.antibodies-online.com/antibody/93510/anti-Chlorophyll+a-b+binding+protein+lhcb1+antibody/1>

APPENDIX

Western blot analysis of *spinach* LHCII and *patens* PsbS

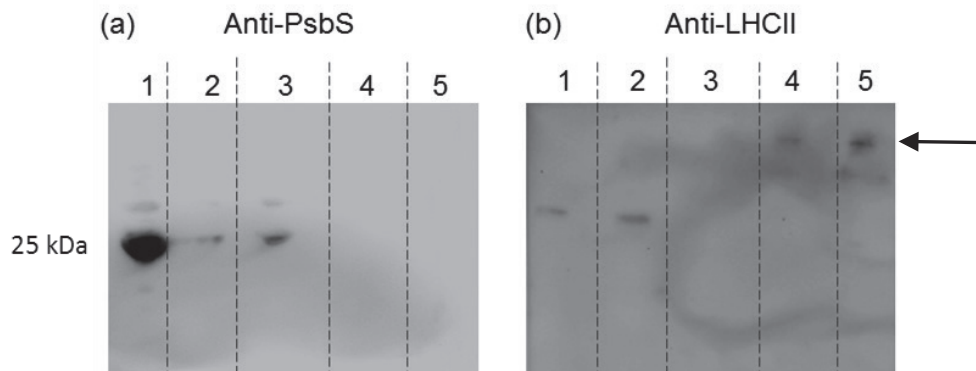


Figure A3.1. Western blotting against PsbS in (a) and against Lhcb1 in (b). In (a), lane 1 contains unfolded PsbS, lane 2 contains refolded PsbS, lane 3 contains both LHCII and PsbS and lane 4 contains LHCII proteoliposomes. Lane 5 is the marker. In (b), lane 1 contains LHCII, lane 2 contains both LHCII and PsbS, lane 3 is the marker, lane 4 contains folded PsbS and lane 5 contains unfolded PsbS. Lane 4 and 5 in (b) show that blotting against Lhcb1 detects high molecular-weight bands of PsbS aggregates (at the arrow) which is due to the unspecific binding of anti-Lhcb1 to PsbS [34].

Estimation of the efficiency of PsbS insertion into asolectin liposomes

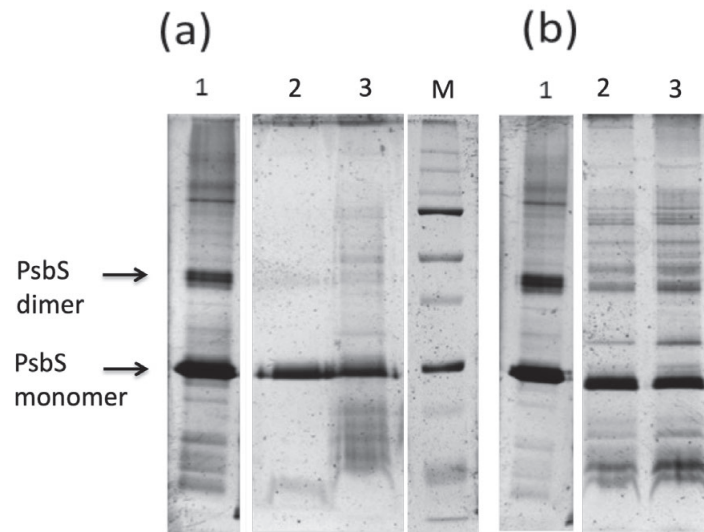


Figure A3.2 SDS-page analysis of two PsbS proteoliposome preparations. (a) 1, PsbS in β -DM, 2 and 3: PsbS proteoliposomes, M, marker. (b): 1, PsbS in β -DM, 2 and 3: PsbS aggregate pellet.

PsbS proteoliposomes prepared at pH 7.5 were separated from non-inserted protein pellet and loaded on a denaturing SDS page silver staining gel. The intensities of the bands of (a) lane 2 and 3 (PsbS proteoliposomes) and (b) 2 and 3 (PsbS pellet) were compared and corrected for the difference in original volume. The pellet was solubilized in a total volume of 41 μ l of 4x crack solution from which 20 μ l was loaded on the SDS-page denaturing gel. The PsbS proteoliposomes were solubilized in a total volume of 130 μ l from which 15 μ l was loaded. Comparing the band intensities of (a) and (b) and correcting for the difference in loading concentration, the insertion efficiency was estimated to be ~80%. The pellets in (b) contain some low-molecular-weight bands that could be of degraded protein.

Dynamic Light Scattering analysis of liposomes before and after acidification and nigericin treatment

	Z-Average (Diameter nm)	PdI Width (Diameter nm)
liposomes pH 7.5	175.7	60.1
liposomes pH 7.5 + nigericin	171.1	78.1
liposomes pH 5.0	159.8	59.1
liposomes pH 5.0 + nigericin	169.4	87.1

Table A3.1 DLS-determined diameter sizes of liposomes, confirming that acidification and nigericin treatment did not lead to destabilization of the liposomes.

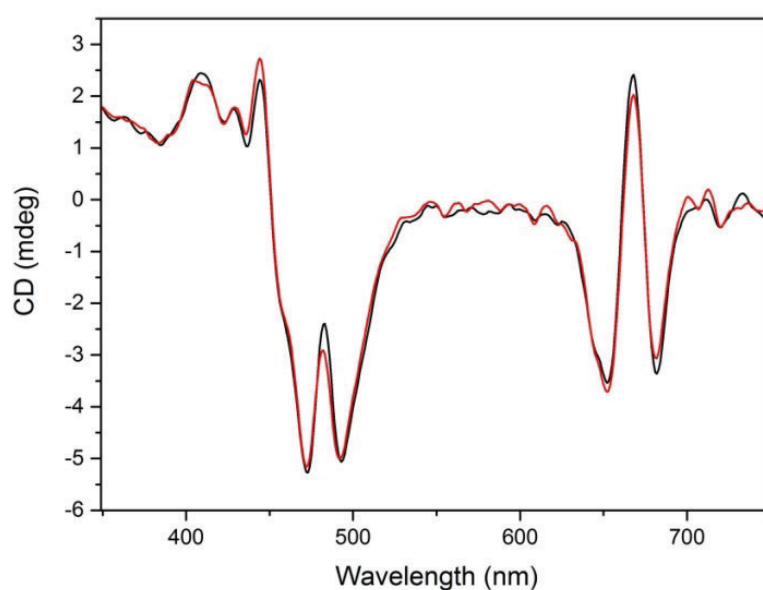


Figure A3.3 CD spectra of LHCII in 0.03% β -DM at pH 7.5 (red) and at pH 5.0 (black).

CHAPTER 4

*Production of ^{13}C Lutein *rLhcb1* for NMR studies*

ABSTRACT

In this chapter, we employed recombinant expression to design a selectively labelled LHCII pigment-protein complex with only lutein ^{13}C isotope-labelled among all the pigments participating to the protein refolding. We overexpressed in *E. coli* to obtain high amounts of the apoprotein Lhcb1 from *Arabidopsis thaliana*, which is one of the most abundant polypeptides of the Light-Harvesting Complex LHCII.

To achieve selective lutein labelling, the unlabelled purified Lhcb1 apoprotein from *E. coli* was refolded in the presence of pigment mixture which consisted of unlabelled Chl *a* and *b*, violaxanthin and neoxanthin and uniformly ^{13}C -labelled lutein. Unlabelled Chlorophylls and carotenoid pigment mixtures were extracted from spinach leaves and the carotenoids were further purified via HPLC, while ^{13}C lutein was obtained from biosynthetically ^{13}C enriched *C. reinhardtii* cells by total pigment extraction and purification via HPLC. The labelling efficiency of the recombinant protein was determined by mass spectrometry (MS) and estimated to be ~38%. The reconstituted ^{13}C lutein-rLhcb1 complexes were purified using Ni^{2+} -column purification and sucrose gradients and subsequently analysed by UV-Vis, CD spectroscopy and size-exclusion chromatography (SEC). These characterizations confirmed that the recombinant protein is well folded and in monomeric form.

INTRODUCTION

In the previous chapters the attention was focused on the native trimeric form of LHCII from *Spinacia oleracea*, here the focus is shifted towards a recombinant system to study the characteristics of selective carotenoids in LHCII. In this chapter, we describe an approach that combines biosynthetic isotope labelling and pigment purification from green algae, recombinant expression, and pigment reconstitution to obtain ^{13}C lutein-rLhcb1 for characterization by NMR spectroscopy. An important advantage of using recombinant protein, as alternative to native ones, is the possibility to label one specific component of the protein-pigment complex that otherwise could not have been possible with the standard growing procedure. In this case, we aimed to have unlabelled protein and among all pigments components only the lutein to be ^{13}C labelled.

Recombinant LHCs have been a great tool to study the protein function. Site-selective mutagenesis has been used to block specific pigment binding sites of interest to understand how the relative pigments were interacting, and how their presence could affect the folding [1,2]. It has been investigated the selectivity of the binding pockets towards specific pigments varying the compositions of the pigments mixture, without site-selective mutagenesis [3].

The recombinant LHCII so produced has the characteristic to have the backbone of the protein and all the cofactors non-isotopically labelled ad exception of only one, the lutein. The steps involved in the protocol of the recombinant proteins are pretty straightforward. The gene is cloned in the vector, transformed in the host and induced in the culture. At this point, the protein overexpressed is ready to be purified and characterized. Over the past twenty decades, many attentions were given to the importance of this technique which is widely documented in many reviews [1-9]. For most recombinant expression studies, *E. coli* is used as a host organism due to the fast growth. The duplication time is 20 minutes, which means that in a few hours the host is ready to be induced, although; in some occasion; it has been noticed that the expression of the recombinant protein might cause a sensible decrease of the duplication time [10]. When the foreign gene is introduced in the new host it will be expressed in a different environment regarding pH, osmolarity and redox potential which might interfere. In addition to it, the expressed protein with low or null solubility in water leads to the formations of build-ups of protein aggregated named inclusion bodies (IBs) [11]. In some case, therefore, the formation of IBs can be an advantage especially when the protein can be easily refolded *in vitro*.

The apoprotein Lhcb1 once purified from the *E. coli* cells does not have the proper folding because the host organism is unable to produce the cofactors essential to transform the apoprotein in the final pigment-protein complex. The Lhcb1, therefore, is folded in presence of a pool of cofactors such as Chls, carotenoids, and lipids, which are arranged accordingly to the protein backbone.

LARGE SCALE OVEREXPRESSION AND PURIFICATION OF Lhcb1 APOPROTEIN IN E. coli

OVEREXPRESSION

Lhcb1 apoprotein was overexpressed in *E. coli* BL21 pLysS. Tests were performed at different temperatures, 18°C and 37°C, in a range of time between 3 hours and overnight. As shown in Figure 4.1 the vector at 18°C overnight does not give any overexpression after induction of the cells with IPTG, while the same vector at 37°C, after 3 hours from induction, shows overexpression of 10 mg starting from 200 ml of culture.

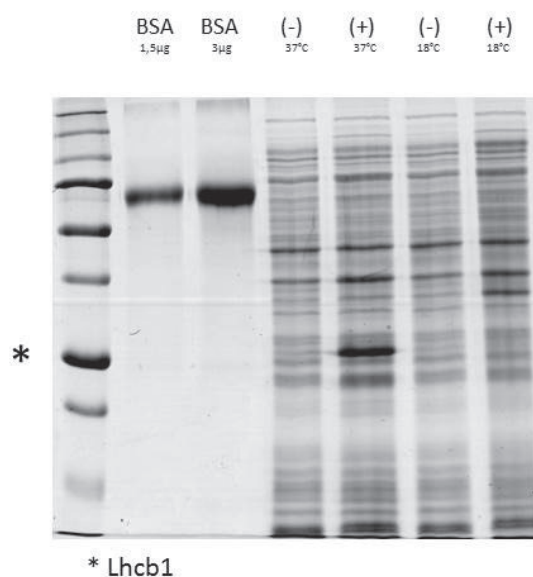


Figure 4.1 SDS page of overexpressed Lhcb1 in BL21 pLysS. From left to right: ladder, BSA 1.5 ug, BSA 3ug, 37°C (-) IPTG, 37°C 3hr (+) IPTG, 18°C (-) IPTG, 18°C O/N (+) IPTG

To improve the overproduction yield, two more strains were tested. These two strains, BL21-CodonPlus and BL21-RP*, showed an increase in the yield because of better compatibility between their tRNA and the one of the apoprotein. Therefore we decided to put aside the first tested strain, BL21-pLys, due to codon bias effect [12]. In Figure 4.2 a denaturing SDS gel is shown with the tested conditions. As for the previous strain, the strains were tested using different growing conditions from 3 hours after induction until overnight. The best yield was given by the strain BL21-codonPlus with the optimum conditions of 37°C and 3 hours growing time from induction. Overnight growing was disregarded to avoid protein degradation, which is more likely to happen after a long time from the induction due to *E. coli* stress [13,14]. For the BL21-CodonPlus at 37°C after 3 hours from induction, the estimated yield was about 30 mg of protein from 200 ml of cells culture. The final estimation was done after the purification of inclusion bodies from the cells.

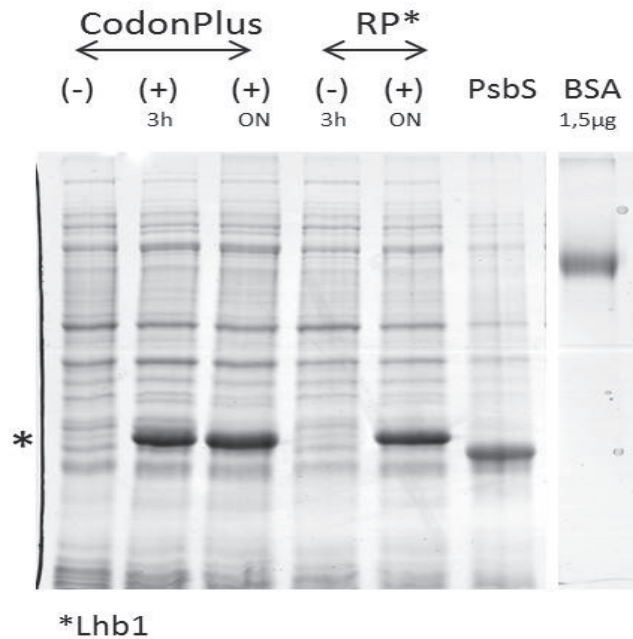


Figure 4.2 SDS page of overexpressed *Lhcb1-pExp5* in *BL21-codonPlus* and *BL21-RP**. From left to right, *CodonPlus* 37°C (-) ITPG, *CodonPlus* 37°C 3h, (+) ITPG, *CodonPlus* 37°C O/N, (+) ITPG, *RP** 37°C (-) ITPG, *RP** 37°C O/N (+) ITPG, control *PsbS* at 22 kDa, *BSA* 1.5 µg

Under equal conditions, both strains are suitable for the protein growth giving a similar yield. The strain *CodonPlus* was chosen, over *RP**, for the overexpression of *Lhcb1*.

The final overexpression of the apoprotein, *Lhcb1* gene from *Arabidopsis thaliana*, was performed in 500 ml of *E. coli* *BL21-CodonPlus*, using 1 L Erlenmeyer flask, of preheated at 37°C, LB medium [15] with antibiotics, ampicillin and chloramphenicol, inoculating with ~300 µl of pre-culture, from -80°C glycerol stock ($OD_{600} \sim 0.6$). The culture was grown at 37°C in flasks while stirring with a speed of 220 rpm until the OD_{600} reached 0.6. At this stage, the cells were supplied with IPTG and kept growing until the OD_{600} was around 3, which corresponds to 3-4 hours after induction. All cells were pelleted down and stored at -80°C until the next step of purification. The overexpression yield was in a range between 150 and 200 mg per 1 L of culture.

With the intention of increasing the overexpression yield, *E. coli* cells were grown using a 2 L bioreactor (Schott-Buran). The bioreactor allows a better overproduction due to change in the growing conditions. In particular, with the set-up we are equipped with, via the use of an external pump, air was constantly supplied to the culture and the internal culture temperature was monitored with a thermometer in contact with the culture. Higher culture oxygenation allows for a longer growing time because the stationary phase is reached later than in normal conditions [16,17]. Because the set-up was not provided with a channel for feeding the culture, the maximum growing tested time was up to overnight after the induction. Similarly, for the growth of bacteria in the flask, cells were harvested after 3-4 hours of growing from induction in order to prevent any food stress which will have a negative impact in the overall of the protein production. In particular, food stress is responsible for the arrest of all metabolic activity and growth. This leads to the production of new enzymes, such as protease, lipases, and substrate capturing [18-

20]. Under these optimized conditions, the overproduction yield was around 300 mg per 1 L of culture.

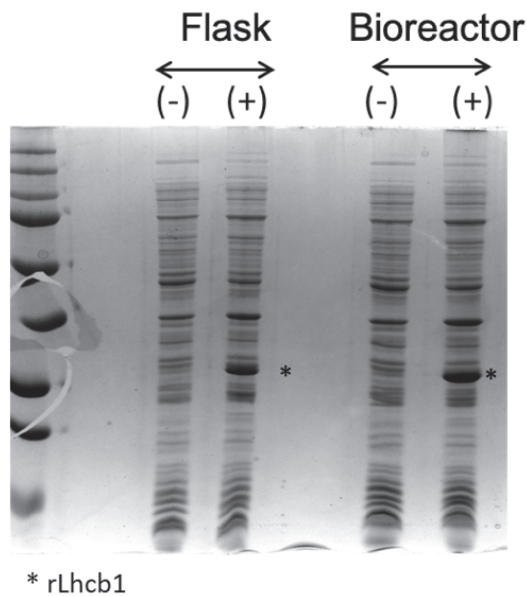


Figure 4.3 SDS polyacrylamide gel of rLhcb1 overexpression at 37°C. From left to right, Marker, flask (-) IPTG, flask (+) IPTG, bioreactor (-) IPTG, bioreactor (+) IPTG

PURIFICATION

As already mentioned, eukaryotic membrane proteins are often accumulating in cells in the form of protein adducts called inclusion bodies (IBs) [21].

The IBs, hosting Lhcb1 were purified from pelleted cells accordingly to the protocol of Krishnan *et al.* [22,23]. Several washing steps using Triton buffer (Tris 20 mM, Triton x-100 0,5 % w/v, β -Mercapto-ethanol 1 mM) were performed in order to solubilize most of the impurity as showed in Figure 4.4. The pelleted cells have been solubilized in lysis buffer (Tris 50 mM, sucrose 2.5% w/v, EDTA 1 mM, Lysozym 10 mg/ml pH 8). The total sample (T) was taken after have added detergent buffer (NaCl 20 mM, Deoxycholic acids 1% w/v, Tris 20 mM, EDTA 2 mM, β -Mercapto-ethanol 10 mM, pH 7.5). The solution was spun down and separated from the supernatant (S_n) while the pellets were dissolved in fresh Triton buffer (P_n).

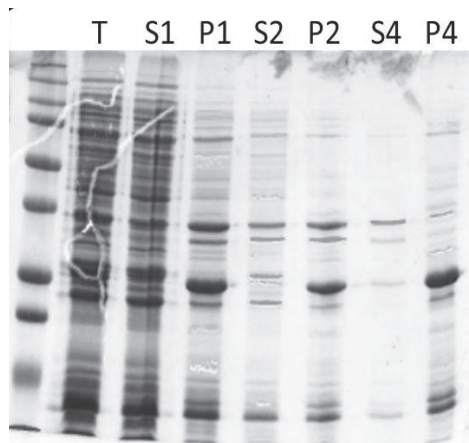


Figure 4.4 SDS page of purified Lhcb1 from left to right: Marker, total protein, S₁, P₁, S₂, P₂, S₄, P₄.

Following 3 washing steps, the apoproteins pelleted in inclusion bodies was solubilized in TE buffer (Tris 50 mM, EDTA 1 mM, pH 8, β-Mercapto-ethanol) and stored at -20°C (P₄) until refolding. From a total amount of 125 mg of protein in cell pellet, 90 mg of total protein in inclusion bodies was purified.

¹³C LABELLING OF CHLAMYDOMONAS REINHARDTII

C. reinhardtii cells, (strain JVD-1B[pGG1]) were grown in our laboratory using a home-built growth chamber. Algae were grown under constant light intensity consisting of eight individual cool white LEDs that gave approximately 50 μmol/m²s of light in the photosynthetically active region equipped with a LED outputs of 3 watts and a temperature colour of 6500K [24]. The growth temperature was set at 25°C ± 0.2 °C, in Tris-acetate-phosphate medium at pH 7.0 (TAP medium) [25] as food source. *C. reinhardtii* algae were isotope labelled using acetic acid_{1,2-¹³C₂} (99% ¹³C, Cambridge Isotope Laboratories, Inc.) replacing the acetic acids as component of the TAP medium. Green algae are classified as a mycotrophic system, which means that they are able to use several carbon sources. In this case, the available carbon sources were both the ¹³C labelled acetic acid from the medium and ¹²C from CO₂ coming from the air that is naturally dissolved in the medium and that will be taken up during the respiration process. The availability of both carbon sources reduces the ¹³C label efficiency because ¹²C will also be present [26].

The algae were grown starting from a plate culture, and then with the use of a sterile inoculating loop, a single colony was harvested and diluted in a 5 ml volume of TAP medium. From the stock culture, 1 ml (with OD₇₅₀ of 1) was used to inoculate 500 ml of ¹³C labelled TAP medium. After approximately 4-5 days, with the optical density equal to 2-2,5 at 750 nm, the culture was ready to be harvested.

PIGMENT EXTRACTION

Unlabelled pigments were extracted from fresh market spinach leaves.

In the total pigments extraction both Chls and carotenoids are presents while with the carotenoids extraction these are separated from the Chls. Labelled pigments were extracted from ^{13}C isotopic labelled *C. reinhardtii* [27].

In short, chloroplasts were extracted from homogenized spinach leaves and washed with wash buffer (Sorbitol 50 mM, Tricine 5 mM and EDTA 1 mM with pH 8) which allowed to purify the thylakoid membrane. Pigments were subsequently extracted from the pelleted thylakoid using acetone buffered with di-sodium carbonate. The cellular components were taken out from the dissolved pigment in acetone via centrifugation. Dissolved pigments were then extracted using diethyl ether which was evaporated using a rotary evaporator. After extraction, pigments were quantified [28], dried and stored at -80° under a nitrogen stream until further use. For the carotenoids extraction, the procedure was almost the same with the exception of the carotenoids saponification performed overnight by potassium hydroxide. After this treatment, carotenoids were separated from Chls because do the latter are not soluble in diethyl ether but rather in the water phase. Carotenoids content in the mixture was determined using the respective extinction coefficients [29].

HPLC ISOLATION

Individual pigments were purified from the -80°C stock of total Chls and carotenoids using high-pressure liquid chromatography (HPLC). The sample was dissolved in acetone and spun down prior to column injection (Gemini 5 μm NX-C18 110, LC column 250 x 10 mm), to prevent any pigments aggregates or salts (NaCl or NaSO_4 used during the pigments extraction) from going into the column and occlude it. The separation was performed using an Agilent technical 1200 connected in series with an Agilent technical quadrupole LC/MS 6130, protected with a guard column 10 x10 mm. The protocol used refers to what Gilmore *et al.* [30] described in their paper with some adjustments. The pigments were eluted using a gradient between 2 different eluent mixture, A and B. Eluent A is composed of 70% acetonitrile, 20% methanol, and 10% water while eluent B contained 32% ethyl acetate and 68% methanol. A flow rate of 5 ml/min was used. One purification run from the total pigment extraction took 48 minutes with a gradient of 0-80%. Additional 6 minutes were used to clean the column before the next injection. During the purification, from the total mixture of pigments, four main elution peaks were identified combining the information from MS and UV-Vis spectroscopy.

	Time (minutes)	%A	%B
1	0	100	0
2	2	20	80
3	47	20	80
4	48	0	100
5	54	0	100

Table 4.1 Scheme of gradient elution going from 100% A at time zero to 100% B in 54 minutes.

The first peak with the mass of 600 g/mol, is in agreement with the mass of violaxanthin and neoxanthin. Lutein is the second peak with a mass of 568,871 g/mol. The third peak with a mass of 900 g/mol, is Chl *b*, and the last peak with a mass of 893 g/mol, is Chl *a*.

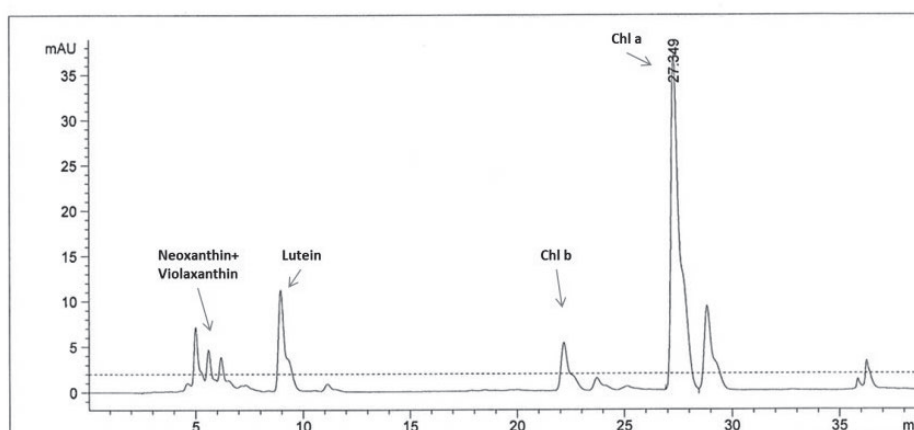


Figure 4.5 HPLC elution profile of pigment isolation from total pigments extracted from spinach. In the y-axis is report the absorption intensity measured at 440 nm.

During the run, a small aliquot of the sample was collected and dissolved in 50% acetonitrile/water solution. The sample was injected in LC/MS using as eluent 1% of acetic acid with a flow rate of 0,5 ml/min. Pigments are not only light sensitive but also oxygen sensitive. In fact, the presence of oxygen activates processes as epoxidation or bleaching [31] and the MS analysis, of the eluted aliquot, was a great tool to discriminate oxidized pigments from the non-oxidized. The two species of the same compound had different elution times, therefore multiple bands were observed which means different MS spectra and absorption profiles. Pure fractions were dried under a stream of nitrogen and stored at -80°C until further use. Chlorophylls content was quantified accordingly to Porra *et al.* [28], while the carotenoid content was determinate accordingly to [29].

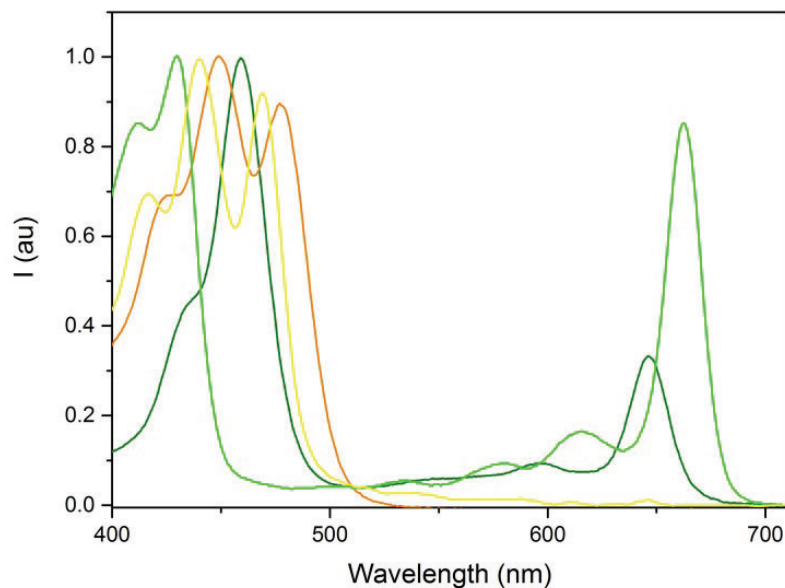


Figure 4.6 UV-Vis absorbance spectra of isolated pigments, normalized for the maxima of absorption. Chl a in light green, Chl b in dark green, lutein in orange and Vio+ Neo in yellow.

¹³C QUANTIFICATION

A small aliquot of the eluted fractions was analysed via MS to get their mass profile. This was an essential tool not only to identify the pigment types but also to determine the ¹³C labelling profile. In this context, we concentrate our attention on the lutein sample. Before to proceed with the analysis of the mass spectra of ¹³C lutein, we had to verify that the mass visible in the spectra is the real mass minus one water molecule, which has a mass of 18,01 g/mol. This means that in case of ¹²C Lutein, of which the molecular weight is 568,871 g/mol, the expected mass is around 550,86 g/mol, to which corresponds a peak in the mass spectra profile with a relative intensity percentage of 100. A small percentage of the compound with the real mass around 568.1 g/mol is also visible as shown in Figure 4.7.

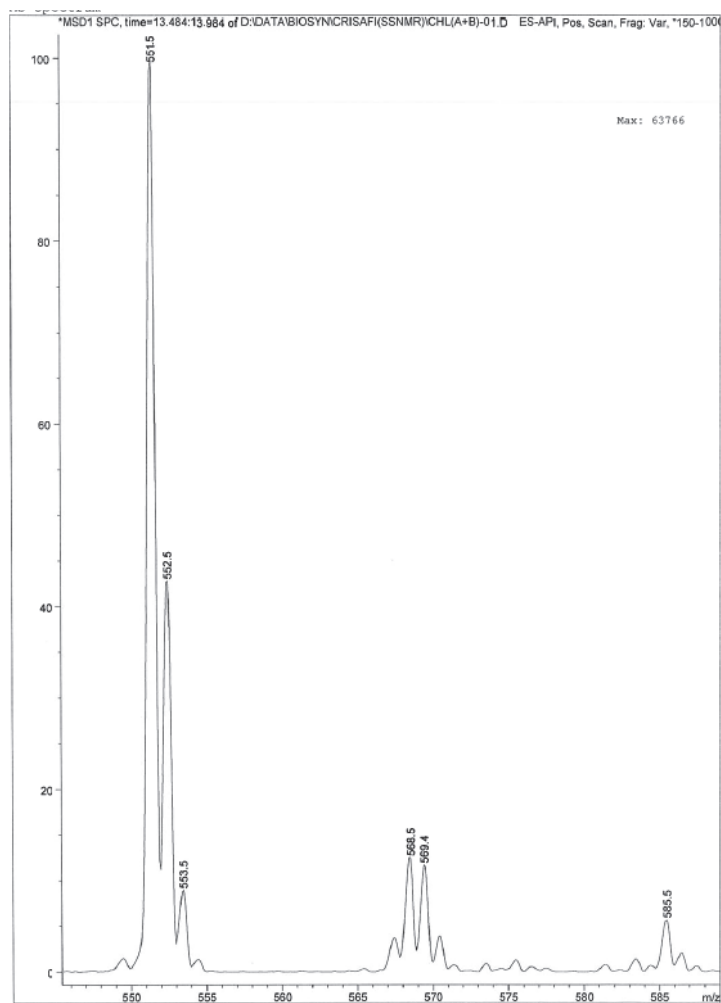


Figure 4.7 MS profile of *na lutein*.

Very much different is the profile of the labelled lutein. Ideally, for a molecule that is synthesized, we would have expected an increase in the total mass equal to $1 \times C_n$, corresponding to about 100% of ^{13}C labelling. In the case of lutein, from the chemical formula, $C_{40}H_{52}O_2$, there are forty atoms of carbon which means an increase equal to 40 g/mol, for a final mass of 608,871 g/mol. From a simulation of the expected profile of the compound, we would have expected only one peak with mass of 590,86 g/mol (608,871-18,01 g/mol).

Algae were grown under constant light, which increased the probability of fixating the CO_2 from air [32].

The proof that the algae not only take up carbons from ^{13}C acetic acid in the medium but also fixate carbons from CO_2 is shown in the MS spectra of ^{13}C lutein, as reported in Figure 4.8.

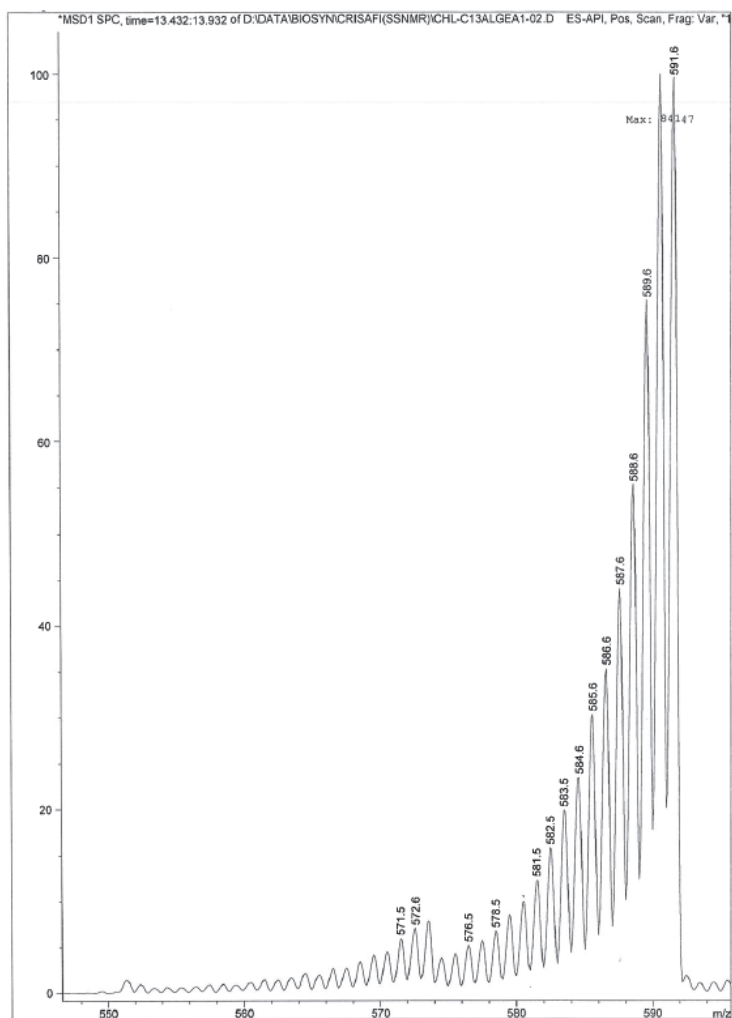


Figure 4.8 MS profile of ^{13}C lutein.

It is fascinating to observe the mass distribution profile of the ^{13}C lutein. The peaks distributions starting from the fully ^{13}C labelled compound toward the natural abundance are observed in Figure 4.8 going from right to left. Two peaks with equal relative intensity, of 100, are visible and correspond to 40 and 39 carbon atoms labelled and left from these there is a series of peaks, precisely 38 more, which correspond to molecules with one less ^{13}C labelled carbon each, until the very last peak which has 40 ^{12}C carbons. To estimate the percentage of labelling, the ^{13}C abundance of the different peaks with the occurrence of more than 10 in intensity was taken into account. Below this threshold, the values of peaks with less than 29 ^{13}C carbons were neglected. From the mass spectra profile shown in Figure 4.8 the total intensity of the peak fractions above the threshold is indicated by the formula:

$$\text{Total intensity} = \sum_{i>18}^n I_n$$

Giving a total intensity of 518.

The contribution of each fraction above the threshold was calculated according to the formula reported below

$$\text{Relative Intensity} = I_n / \sum_{i>18}^n I_n$$

In conclusion, the $^{13}\text{C}_{40}$ and $^{13}\text{C}_{39}$ lutein molecules together account for 38,61% of the total peak fractions. After that we have 14,5% of $^{13}\text{C}_{38}$, 10,61% of $^{13}\text{C}_{37}$, 8,5% of $^{13}\text{C}_{36}$ and so on.

REFOLDING AND CHARACTERIZATION OF ^{13}C LUTEIN *rLhcb1*

REFOLDING OF *Lhcb1* USING WHOLE-PIGMENT EXTRACT

Refolding of recombinant *Lhcb1* was first tried as the protocol reported by Natali *et al.* [27]. Briefly, ~800 μg of protein in inclusion bodies was pelleted and solubilized in 400 μl of TE buffer (Tris 20 mM, EDTA 1 mM, HEPES 200 mM, sucrose 5% w/v) with 400 μl of recombinant buffer (Sucrose 5% w/v, LDS 4% w/v, HEPES 200 mM, pH 7.5). The protein was denatured at 98°C in 1 minute. While the protein solution was cooling down, pigments were prepared, 500 μg of Chl (*a+b*) and 80 μg of carotenoids. The new detergent, OG, was added with the final concentration of 2% and kept on ice for 10 minutes. In order to precipitate the LDS present from the inclusion bodies purification, KCl was added, with a final concentration of 200 mM and the sample was kept on ice for 20 minutes before it was pelleted at 15800 x g for 10 minutes at 4°C. After that, the refolded protein was separated from unbound pigments using Ni^{2+} column and by using linear sucrose gradients. In order to minimize protein losses by skipping the Ni^{2+} column step, also a variation on the protocol was tried using *Lhcb1* apoprotein that was first purified with urea wash, as Krishnan *et al.* [22] optimized for *PsbS*. In this case, the protein was purified from the inclusion bodies with the use of urea buffer (100 mM sodium phosphate, Tris 100 mM, Urea 8M, LDS 0,05% pH 8).

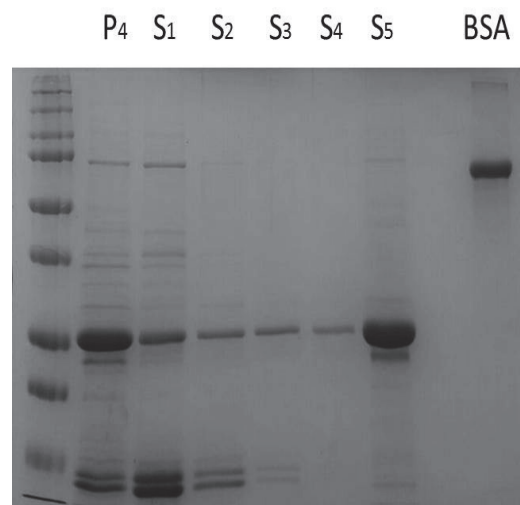


Figure 4.9 SDS page of urea wash purification of *Lhcb1* from left to right: Marker, *P4*, *S1*, *S2*, *S4*, *S5* and BSA ~3 μg

With the help of the urea, all the impurity will be washed away in the supernatant (S₁-S₄) while the apoprotein will be present in the pellet. The Lhcb1 apoprotein was solubilized in buffer (sodium phosphate 100 mM, Tris 100 mM, Urea 8M, pH 8) with high amount of LDS (0,5%). After the overnight incubation, the apoprotein was fully solubilized (S₅), and the buffer was exchanged to TE buffer, the same one used for the protein refolding, using a PD10 column. Figure 4.9 shows that until wash S₄ there is some inevitable loss of the Lhcb1, however, the apoprotein is recovered in S₅.

REFOLDING OF Lhcb1 USING MIXTURE OF HPLC-PURIFIED PIGMENTS

In a first trial, the LHCII pigment mixture for reconstitution was created by mixing stoichiometric amounts of HPLC purified Cars and Chl pigments. I compared, pigment-refolded, rLhcb1 samples that had the same apoprotein and were differing only for the pigment mixtures used for reconstitution. The “rLhcb1 standard” was prepared as in the published protocol [27], using total pigment extraction from spinach and “rLhcb1 mix pigments” was prepared using a mixture of HPLC purified pigments in stoichiometric ratios. As shown in Figure 4.10a, the absorption and CD profiles of the “rLhcb1 mix pigments” sample is not in agreement with the profile of “Lhcb1 standard” obtained using the standard protocol and indicates incomplete pigment reconstitution.

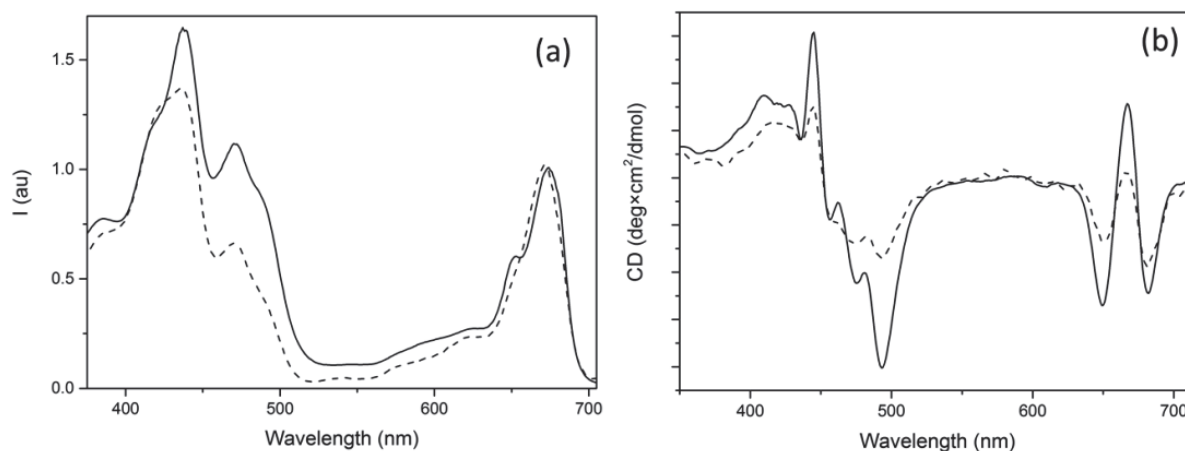


Figure 4.10 (a) UV-Vis spectra normalized for the peak at 674 nm. Dash is the rLhcb1 refolded with HPLC purified pigments, solid line is rLhcb1 with a mixture of extracted pigments. (b) CD spectra normalized for the concentration. Solid line is the rLhcb1 refolded with whole pigments extractions, dash line is rLhcb1 with the mixture of HPLC purified pigments

The refolded Lhcb1 with the HPLC-purified pigment mixture is lacking in Chl *b*. This result might be explained by the absence of lipids that are extracted together with the pigments in total-pigment mixtures used to reconstitute the Lhcb1 standard, but that was lost during the HPLC purification. To our knowledge, previous studies were performed using pigment mixtures extracted from thylakoids [23] or the apoprotein was reconstituted in presence of lipids in order to have the folded pigment-protein sample in liposomes [33,34] and lipids might be essential for correct folding and pigment binding *in*

vitro. Proteins in native environments are folded in presence of lipids, of which phosphatidylglycerol is also essential for trimer formation. Also, membrane proteins are, per definition, more stable in the presence of lipids than in a detergent environment, which might explain as well why refolding the protein in a mixture without lipids does not lead to a correct folding.

REFOLDING OF Lhcb1 USING Chl WHOLE-PIGMENT EXTRACTS AND HPLC-PURIFIED CAROTENOIDS

The pigment mixture for the reconstitution was changed in consequence of the previous results. The mixture consisted of Chls from a whole-pigments extraction, while the Cars mixture mimicked the native ratio between Neo, Vio, Lut using HPLC purified Cars. In this way, from the whole pigments extraction, eventual co-extracted lipids would be available to allow proper refolding while the carotenoids mixture was made combining the HPLC purified pigments of interest. Excess of Cars, especially ^{13}C lutein, should promote a preferential binding of the ^{13}C lutein to the lutein L1 and L2 binding pockets [35,36]. CD and UV-Vis absorption confirmed the success of the refolding and the protocol was up-scaled for the need of producing milligrams of ^{13}C lutein-rLhcb1 for study by NMR. In particular, for each preparation 4.8 mg of protein in inclusion bodies were refolded as in the protocol in presence of 3 mg of chlorophylls, from the whole pigments extraction, and 480 μg of HPLC purified carotenoids of which half is ^{13}C Lutein. After the Ni^{2+} purification, the sample was purified via sucrose gradient.

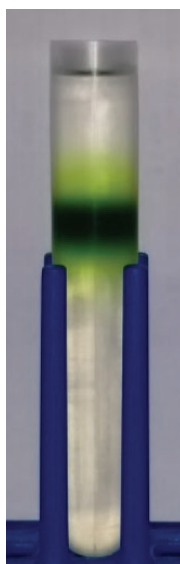


Figure 4.11 Sucrose gradient with 0.06% βDM , 0.01 M HEPES, pH 7.6 of rLhcb1 after purification with Ni^{2+} column.

Aliquots from the fraction were loaded on an SDS denaturing gel page to verify the presence of the protein as showed in Figure 4.12 below.

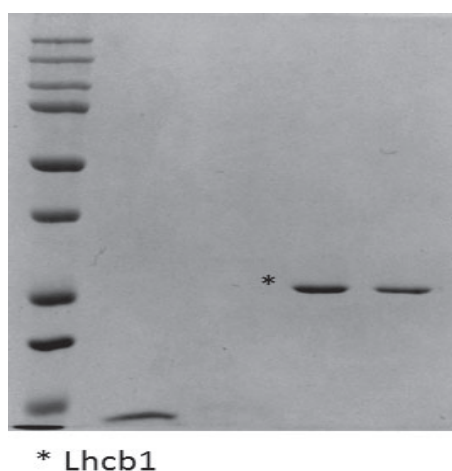


Figure 4.12 Denaturing SDS gel page of rLhcb1. From left to right Ladder, Wash I, Flow through, Fraction II and Fraction I.

From the SDS gel page analysis, in both fractions, I and II, the presence of the Lhcb1 protein is verified which has a band around 25 kDa. Figures 4.13 and 4.14 show the UV-Vis absorption and CD profiles of pooled fractions of ^{13}C -lutein rLhcb1, confirming that the pigment-protein complexes were properly folded.

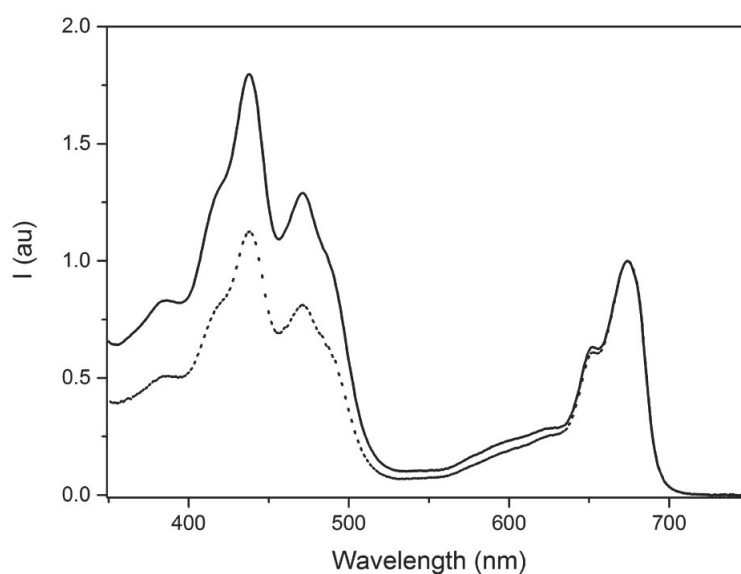


Figure 4.13 UV-Vis spectra of the final sample of ^{13}C lutein-rLhcb1. The spectra are normalized for the peak at 674 nm, Fraction I in the solid line and Fraction II in the dotted line.

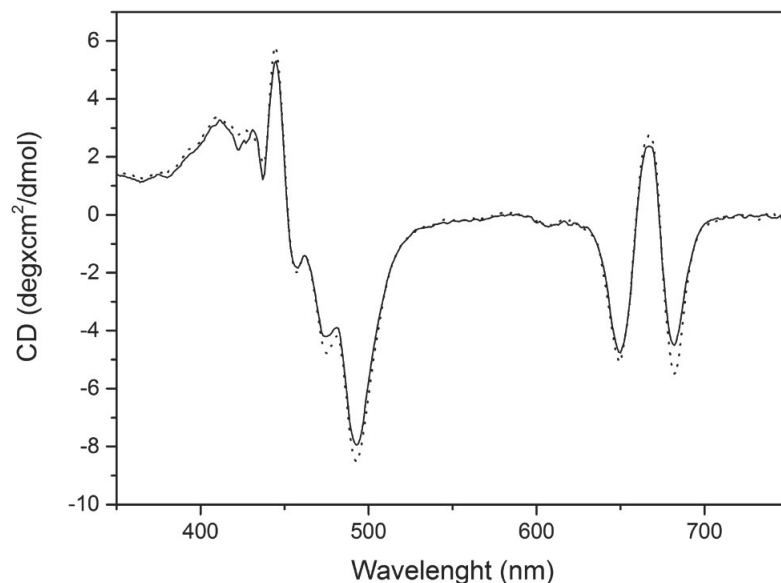


Figure 4.14 CD spectra normalized for the concentration of recombinant ^{13}C lutein-rLhcb1. Fraction I is the solid line and fraction II is the dotted line.

The CD spectrum, Figure 4.14, is in agreement with literature data for recombinant, monomeric LHCII which has a characteristic profile in comparison to the trimeric state [33]. The monomeric oligomer state is further confirmed from size exclusion chromatography [33,37].

The elution profile of rLhcb1 was compared with the one from LHCII monomers that were extracted from spinach leaves, collecting the monomer band from a sucrose gradient. From the elution profile in Figure 4.15, we can conclude that indeed the rLhcb1 is present as a monomer. The elution profile of rLhcb1 was compared with the profile from a mixture of gel-filtration protein standards (data not showed) with molecular weights in the range between 670 kDa and 1350 Da (Bio-rad) [38], estimating a monomer size around 90 kDa for the monomer pigment-protein complex embedded in detergent micelles.

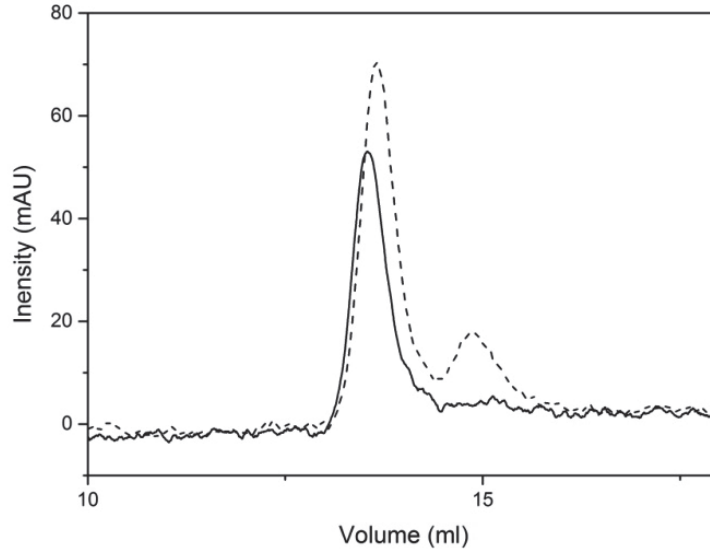


Figure 4.15 SEC chromatogram at 280 nm of rLhcb1 from *A. thaliana* in solid line compared with native monomeric LHCII extracted from spinach in dashed line.

Pigments composition was checked using HPLC on reverse phase C18 analytical column (Phenomenex) using a protocol based on Gilmore *et al.* [39]. The HPLC chromatogram in Figure 4.16 was compared with the pigment profile of native LHCII trimer from spinach, as the standard. We can conclude that all the pigments got inserted with the observation of a slight difference in the insertion of Lut and Vio. The amount of Vio inserted is less but this is acceptable because the pigment for monomer is loosely bounded at the periphery of the pigment-complex which likely can be lost in the insertion/purification process, in addition, this site does not have selective affinity, while Neo binding site is 100% selective for this pigments with interacts of Chl *b* [1,40]. From the chromatogram it seems that more lutein got inserted occupying other binding sites maybe, the Vio binding site was more likely occupied by the Lut rather than from the Vio [1,40].

The amount of pigments inserted, see Table 4.2, was estimated from the HPLC. Chl (*a/b*) is equal to 1.38 which is close to the theoretical of 1.33 The estimation was compared with the literature of native LHCII, in which it has been reported a value for Chl (*a/b*) around 1.33 for higher plants [41,42].

	Neo	Vio	Lut	Chl b	Chl a
rLhcb1	0.8 ±0.04	0.3 ±0.015	2.3 ±0.115	5.8 ±0.29	8 ±0.4

Table 4.2 In the table amount of pigment estimated from HPLC measurements. With the assumption that the Chl *a* content of 8 molecules.

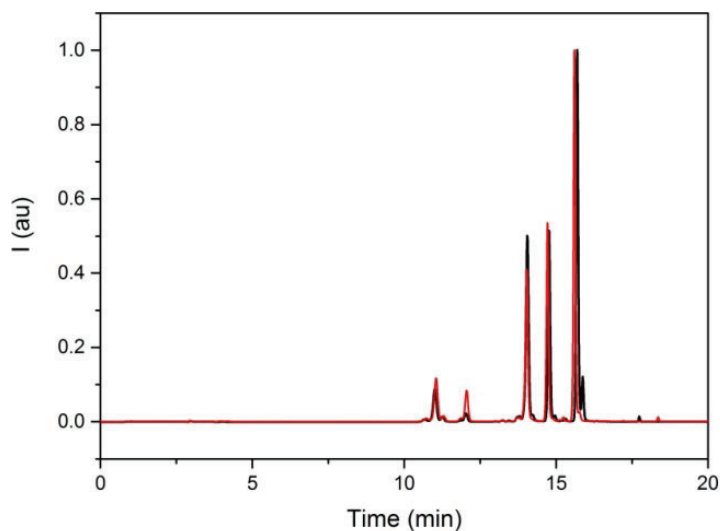


Figure 4.16 HPLC Chromatogram, with a detection wavelength of 440 nm, of rLhcb1 black line and native LHCII trimer from spinach leaves in red line. Spectra were normalized for the Chl a peak.

The collected bands of different fractions were flash-frozen and stored at -80°C in the presence of sucrose as a cryo-protectant, until use.

CONCLUSIONS

We can conclude that the recombinant and reconstituted ^{13}C lutein rLhcb1 was correctly refolded and the upscaling of the production was successful to yield 12 milligrams of protein to be further study with solid-state NMR spectroscopy.

REFERENCES

1. Croce R, Weiss S, Bassi R. Carotenoid-binding Sites of the Major Light-harvesting Complex II of Higher Plants. *The Journal of Biochemistry and Molecular Biology* 274 (42), 29613–29623 (1999).
2. Remelli R, Varotto C, Sandona D, Croce R and Bassi R. Chlorophyll Binding to Monomeric Light-harvesting Complex. A mutation analysis of chromophore/binding residues. *The Journal of biological chemistry*. 274(47), 33510–33521 (1999).
3. Hobe S, Niemeier H, Bender A and Paulsen H. Carotenoid binding sites in LHCIIb Relative affinities towards major xanthophylls of higher plants. *Eur. J. Biochem.* , 267, 616-624 (2000).
4. Markrides SC. Strategies for Achieving High-Level Expression of Genes in *Escherichia coli*. *Microbiological reviews*, 512-538 (1996).
5. Baneyx F. Recombinant protein expression in *E. coli*. *Current opinion in biotechnology*, 10, 411-421 (1999).
6. Stevens RC. Design of high-throughput methods of protein production for structural biology. *Structure* 8(9), 187-195 (2000).
7. Jana S, Deb JK. Strategies for efficient production of heterologous proteins in *Escherichia coli*. *Appl Microbiol Biotechnol*, 67(3), 289-298 (2005).
8. Sorensen HP, Mortensen KK. Advanced genetic strategies for recombinant protein expression in *Escherichia coli*. *J Biotechnol*, 115(2), 113-128 (2005).
9. Rosano GL, Ceccarelli EA. Recombinant protein expression in *Escherichia coli*: advances and challenges. *Front Microbiol*, 5, 172 (2014).
10. Bentley WE, Mirjalili N, Andersen DC, Davis RH, and Kampala DS. Plasmid-Encoded Protein: The Principal Factor in the “Metabolic Burden“ Associated with recombinant bacteria. *Biotechnology and Bioengineering*, 35, 668-681 (1990).
11. Carrió MM, Villaverde A. Construction and deconstruction of bacterial inclusion bodies. *Journal of Biotechnology* 96, 3–12 (2002).
12. Carstens CP, Bonnardel J, Allen R, Waesche A. BL21-CodonPlus Cells Correct Expression Problems Caused by Codon Bias. *Strategies*, 14, 50-52.
13. Kuroda A, Nomura K, Ohtomo R, Kato J, Ikeda T, Takiguchi N, Ohtake H, Kornberg A. Role of Inorganic Polyphosphate in Promoting Ribosomal Protein Degradation by the Lon Protease in *E. coli*. *Science*, 293, 705-707 (2001).
14. Podolski RJ. Protein Degradation in Bacteria, *Archives of Biochemistry and Biophysics*, 327-340 (1953).
15. Bertani G. The mode of phage liberation by *Escherichia coli*. *J Bacteriol.* ,62, 293-300 (1951).
16. Smith MW, Neidhardt FC. Proteins Induced by Anaerobiosis in *Escherichia coli*. *Journal of bacteriology*, 154 (1), 336-343 (1983).
17. Smith MW, Neidhardt FC. Proteins Induced by Aerobiosis in *Escherichia coli*. *Journal of Bacteriology*, 154 (1), 344-350 (1983).
18. Chung HJ, Bang W, and Drake MA. Stress Response of *Escherichia coli*. *Comprehensive in Food Science and Food Safety Reviews*, (5), 52-64 (2006).
19. Matin A, Auger EA, Blum PH, Schultz JE. Genetic basis of staf survival in non differentiating bacteria. *Annu. Rev. Microbiol.* , (43), 293-316 (1989).
20. Kjelleberg S, Hermansson M, Marden P. The transient phase between growth and non growth of heterotrophic bacteria with empi-iasis on the marine enviromnet. *Ann. Rev. Microbio*. 41 25-49 (1987).
21. Nagai K, Thøgersen HC. Synthesis and Sequence-Specific Proteolysis of Hybrid Proteins Produced in *Escherichia coli*. *Methods in enyzmology*, 153, 461-481 (1987).

22. Krishnan M, Moolenaar GF, Gupta K, Goosen N & Pandit A. Large-scale *in vitro* production, refolding and dimerization of PsbS in different microenvironments. *Sci Rep*, 7(1), 15200 (2017).
23. Paulsen H, Rümmler U, Rüdiger W. Reconstitution of pigment-containing complexes from light-harvesting chlorophyll a/b-binding protein overexpressed in *Escherichia coli*. *Planta*, 181, 204-211 (1990).
24. <http://www.ledshighpower.nl/index.php>
25. Gorman DS and Levine RP. Cytochrome *f* and plastocyanin: their sequence in the photosynthetic electron transport chain of *Chlamydomonas reinhardtii*. 54, 1665-1669 (1965).
26. Roach T, Sedoud A, Krieger-Liszak A. Acetate in mixotrophic growth medium affects photosystem II in *Chlamydomonas reinhardtii* and protects against photoinhibition. *Biochim Biophys Acta*, 1827(10), 1183-1190 (2013).
27. Natali A, Gruber JM, Dietzel L, Stuart MC, van Grondelle R, Croce R. Light-harvesting Complexes (LHCs) Cluster Spontaneously in Membrane Environment Leading to Shortening of Their Excited State Lifetimes. *J Biol Chem*, 291(32), 16730-16739 (2016).
28. Porra RJ, Thompson WA, Kriedemann PE. Determination of accurate extinction coefficients and simultaneous equations for assaying chlorophylls *a* and *b* extracted with four different solvents: verification of the concentration of chlorophyll standards by atomic absorption spectroscopy. *Biochimica et Biophysica Acta*, 975, 384-394 (1989).
29. Davies BH. Identification of carotenoids by their absorption characteristics. *Biochem.J.* , 103(2) (1967).
30. Gilmore AM, Yamamoto HY. Resolution of lutein and zeaxanthin using a non-encapped, lightly carbon-loaded C 18 high-performance liquid chromatographic column. *Journal of Chromatography*, 543(137-145) (1991).
31. Pessaraki M. Handbook of Photosynthesis. *Taylor & Francis Group*, second edition (2005).
32. Rabinowitch EI. Photosynthesis. *Interscience publisher*, 2 (1956).
33. Rogl H, Schödel R, Lokstein H, Kühlbrandt W, and Schubert A. Assignment of Spectral Substructures to Pigment-Binding Sites in Higher Plant Light-Harvesting Complex LHC-II. *Biochemistry* 41, (7) 2281-2287 (2002).
34. Croce R, Weiss S, Bassi R. Carotenoid-binding Sites of the Major Light-harvesting Complex II of Higher Plants. *Journal of Biological Chemistry*, 274(42), 29613-29623 (1999).
35. Dall'Osto L, Lico C, Alric J, Giuliano G, Havaux M, Bassi R. Lutein is needed for efficient chlorophyll triplet quenching in the major LHCII antenna complex of higher plants and effective photoprotection *in vivo* under strong light. *BMC Plant Biol*, 6, 32 (2006).
36. Hobe S, Prytulla S, Kühlbrandt W and Paulsen H. Trimerization and crystallization of reconstituted light-harvesting chlorophyll a/b complex. *The Embo Journal*, 13(15), 3423-3429 (1994).
37. Ruban AV, Berera R, Illiaia C *et al.* Identification of a mechanism of photoprotective energy dissipation in higher plants. *Nature*, 450(7169), 575-578 (2007).
38. Gilmore AM, Yamamoto HY. Zeaxanthin Formation and Energy-Dependent Fluorescence Quenching in Pea Chloroplasts under Artificially Mediated Linear and Cyclic Electron Transport. *Plant Physiol.*, 96, 635-643 (1991).
39. Croce R, Remelli R, Varotto C, Breton J, Bassi R. The neoxanthin binding site of the major light harvesting complex (LHCII) from higher plants. *FEBS Letters* 456, 1-6 (1999).
40. Liu Z, Yan H, Wang K, Kuang T, Zhang J, Gui L, An X & Chang W. Crystal structure of spinach major light-harvesting complex at 2.72 Å resolution. *NATURE*, 428, 287-292 (2004).
41. Standfuss J, van Scheltinga ACT, Lamborghini M, Kühlbrandt W. Mechanisms of photoprotection and nonphotochemical quenching in pea light-harvesting complex at 2.5 Å resolution. *Embo J*, 24(5), 919-928 (2005).

CHAPTER 5

NMR studies on ^{13}C lutein- rLhcb1

ABSTRACT

We applied selective lutein ^{13}C isotope labelling to study the structure and plasticity of the two luteins in the Light-Harvesting Complex II (LHCII) pigment-protein complex. In Chapter 4 we used recombinant expression and pigment reconstitution for selective isotope pigment labelling, allowing us to obtain selective ^{13}C labelled lutein monomeric LHCII using recombinant monomeric Lhcb1 from *A. thaliana* without the signals coming from the protein amino acids or from other carotenoids, Chls or lipids. In this chapter, we investigate the structure and dynamics of the two luteins in LHCII in with high-resolution Magic Angle Spinning (MAS) NMR. The pigment-protein complex is prepared in detergent micelles or in the aggregated state [1,2], in which the protein respectively forms fluorescent and fluorescence-quenched states.

Our results show that we, for the first time, could obtain structural information of the luteins in LHCII in the unquenched, fluorescent state, which is not accessible by X-ray crystallography. By analysis of ^{13}C - ^{13}C and ^1H - ^{13}C correlation NMR spectra we could obtain NMR ^{13}C chemical shift assignments of the lutein head atoms.

INTRODUCTION

Carotenoids in photosynthesis are essential both for increasing the light-harvesting absorption range and for photoprotection against photodamage. Among the pool of photosynthetic pigments in plants, the lutein counts for the 60% of the xanthophylls and the 40% of all the carotenoids, which makes this pigment the most abundant xanthophyll species [3]. Lutein has a structural role in the stability of Light-Harvesting Complexes (LHCs) and his presence is essential for correct folding of the proteins [3-5]. *In vitro* reconstitution shows that the lack of lutein *per se* is sufficient to prevent trimerization [3]. Carotenoid triplets have a photoprotective role in quenching long-lived $^3\text{Chl}^*$, which can react with O_2 forming harmful singlet oxygen [3]. In higher plants, recent studies show that lutein is involved in a lutein epoxidation (LutE) cycle which converts lutein to epoxidase lutein. Both reactions of the LutE cycle are catalysed by the violaxanthin de-epoxidase enzyme (VDE) and zeaxanthin epoxide (ZEP), which are involved as well in more well-known violaxanthin cycle [6].

LHCs protein of plants and algae are responsible for sunlight absorption and under moderate light conditions, transfer excitations to the reaction center. Instead, in the presence of intense light, LHCs associated with Photosystem II dissipate the excess of light energy to prevent photodamage by rapid quenching of excitations. The LHC proteins, of which Light-Harvesting Complex II is the most abundant, have the intrinsic property to alternate between light-harvesting, fluorescent and photoprotective, quenched states by reversible switching of their conformations [7,8].

The molecular mechanism that triggers the photoprotective switch of the protein has not been resolved yet [9-12]. In LHCII, Lut1, which occupies the L1 site, has been proposed to function as a quencher in the photoprotective state. This lutein is close to Chl *a*610, Chl *a*611 and Chl *a*612 that are the reddest Chls in LHCII [3]. Because these Chls have the lowest excitation energy [3], excitations will accumulate here and this site is assumed to be the site of energy dissipation in the photoprotective state. The switch into a photoprotective state has been proposed to involve a change in the interaction between lutein and those Chls, producing a quenched state via energy transfer from the Chls to the Cars S1 state, or via Chl-Cars excitonic interactions [11].

Lut1 is also involved in energy transfer to Chl *a* in light-harvesting conditions [9], and its presence is required for efficient Chl triplet quenching as demonstrated by Dall' Osto *et al.* [3].

The presence of lutein in the L1 site is essential since the non-occupancy of site L2 did not significantly affect photobleaching in recombinant LHCII [5,13].

In this chapter, we explore the role of lutein in the conformational switch of LHCII by comparing the lutein conformations in fluorescent and quenched LHCII states. Hereto, rLhcb1 from *A. thaliana* has been refolded in the presence of ^{13}C labeled lutein together with all the other pigments unlabeled. This selective labelling strategy allows to simplify the NMR spectra and concentrate specifically on the lutein signals. We mimic LHCII in unquenched and quenched state, by preparing the protein in detergent solution (β -DM) and in the aggregated state. In the aggregated state, the LHCII proteins interact with each other, which is known to produce quenched states as reported in Chapter 2. To reveal

the lutein conformational structures and understand how the lutein pigment molecules interact with their environment, we perform a MAS NMR study on ^{13}C lutein-rLhcb1. In Figure 5.1, we take a closer look into the LHCII protein, highlighting the two luteins (in orange), which are sandwiched between the transmembrane-helices A and B.

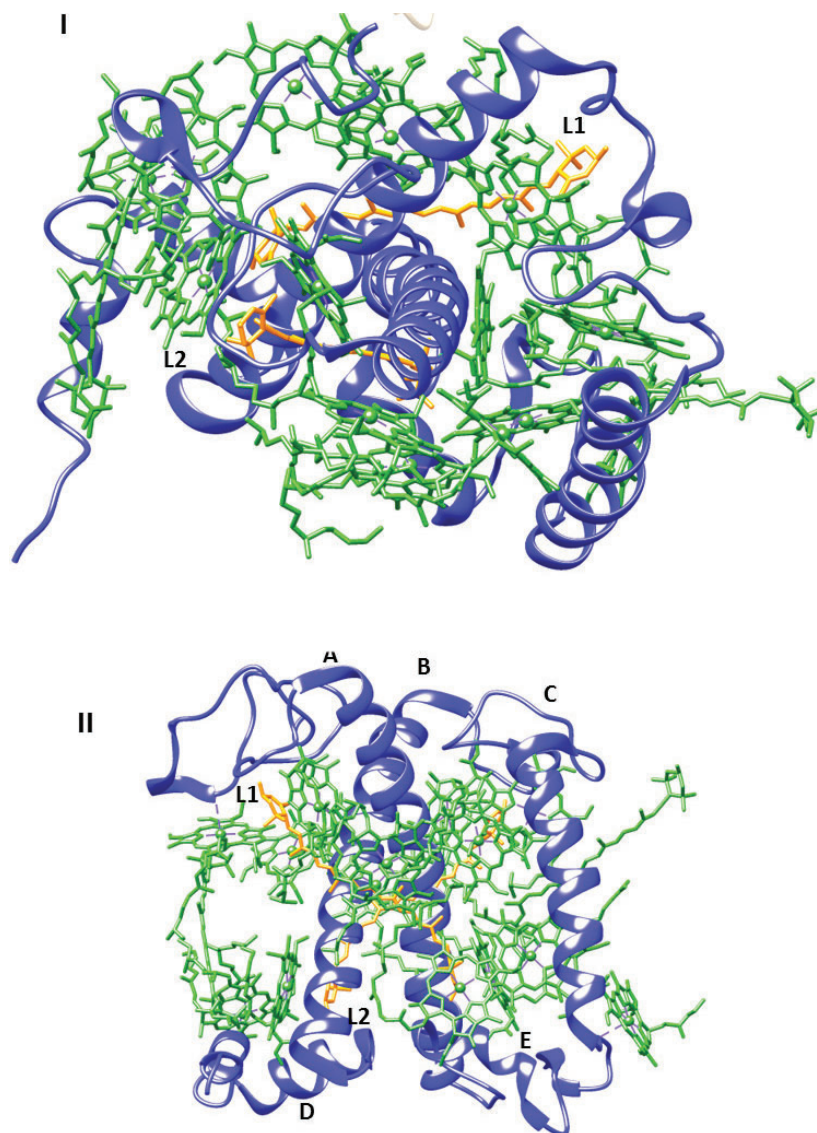


Figure 5.1 The top and side view of LHCII from spinach (PDB-1RWT) are respectively I and II. In green all the Chls, Neo and Vio are presented while in orange the luteins are presented (L1 and L2 accordingly to nomenclature of Standfuss *et al.* [14]).

The two X-ray structures that have been published of LHCII in 2004 and 2005, by Liu *et al.* and by Standfuss *et al.* respectively, have a resolution of 2.75 Å and 2.5 Å [14,15]. This resolution is not enough to determine atomic bond lengths, and for instance, distinguish between the chemical structures of the two lutein heads. With NMR spectroscopy, in contrast, it is possible to distinguish between signals from the two head groups because of the different position of the double bonds. Another advantage of NMR over X-ray crystallography is the possibility to investigate samples in different physical states, *i.e.*

liquid, solid, gel like, *etc.* This is an enormous advantage if we consider that for X-ray the sample should be crystallized and that long-range crystalline order is required. LHCII in crystalline form adopts a quenched like state which per definition does not give opportunity to study its conformational switch [10,16]. With NMR instead, we can prepare samples in different conditions to reproduce the two switch states. Furthermore NMR, in general, offers the possibility of probing samples at a wide range of temperatures, which helps to determine dynamic features of molecules.

MATERIALS AND METHODS

SAMPLE PREPARATION

DETERGENT SAMPLE PREPARATION

The preparation of recombinant Lhcb1 with ^{13}C lutein has been described in Chapter 4. All the purified fractions, previously characterized and stored at -80°C , were combined together for characterization by NMR. The total sample volume was concentrated, using Corning Spin-X UF 20 ml concentrators with 10 kDa pore size. The final volume was 150 μl and the sample was split in two fractions. One fraction was used to mimic the unquenched state of rLhcb1 by solubilizing the protein in β -DM detergent. 70 μl of this sample were loaded in a 4mm rotor, which corresponded to ~ 6 mg Chl ($a+b$). The sample was carefully packed in the rotor via several short spinning steps.

AGGREGATE SAMPLE PREPARATION

The remaining sample was used to mimic the quenched state via protein aggregation. Pandit *et al.* showed that aggregated LHCII after detergent removal remains its tertiary structure because the pigment-protein complexes have a comparable NMR profiles [2]. As already demonstrated in previous work, in result of the detergent dilution, LHCII aggregates are formed, and the consequent dramatic decrease in the fluorescence of LHCII was shown to resemble, in several aspects, the *in vivo* NPQ state [7,17,18]. The ^{13}C lutein-rLhcb1 sample was diluted until the detergent concentration was below the critical micelle concentration (CMC). The CMC of β -DM detergent in water is around 0.17 mM which corresponds with 0,0087 % [19]. This means that in order to aggregate the protein, the final concentration of β -DM should be at least less than the CMC above indicated. To achieve the aggregation state, the protein sample was diluted accordingly. The sample was concentrated using the same Corning Spin-X UF 20 ml concentrators used as described above. The volume sample was reduced to 2 ml and dialyzed against 3 L of HEPES buffer, 0.01 M, devoid of detergent. Finally, the aggregated sample was successfully pelleted by ultracentrifugation (Optima L, Beckman Coulter). By adding of few microliters of the buffer, the solid aggregates could be transferred to the 4 mm rotor. The sample was packed using short spinning steps as described above.

UV-VIS ABSORPTION

UV-Vis measurements were performed with a Cary 60 spectrophotometer (Agilent technologies). Spectra were collected between 350 nm and 750 nm using 0,1 or 1 cm quartz cuvettes.

TIME RESOLVED FLUORESCENCE

Time-resolved fluorescence measurements were performed using a FluoTime 300 (PicoQuant) time-correlated photon counter spectrometer. Samples were held in a 1x1 cm quartz cuvette that was thermostated at 20°C and excited at 440 nm using a diode laser (PicoQuant). Fluorescence decay traces were fitted with a multi-exponential decay curve using a χ^2 least-square fitting procedure.

NMR EXPERIMENTS

NMR measurements were performed on a Bruker avance-I 750 MHz wide bore solid-state NMR spectrometer with 17.6 Tesla magnetic field. In this field, ^{13}C and ^1H resonate at 188.66 and 750.23 MHz respectively. Standard 4mm triple resonance MAS probe was used for the experiments. All the samples were packed in 4mm zirconium rotors with a spacer and top insert and were spun at the magic angle (54.74°) at a spinning frequency of 14 kHz. The temperature was kept constant at 220 K.

Approximately 70 μl of sample volume containing ~ 6 mg of Chl ($a+b$) was loaded in the 4mm rotor.

^{13}C spectra were obtained through cross-polarization magic-angle spinning (CP-MAS) technique with SPINAL64 decoupling [20]. ^1H and ^{13}C were irradiated with 80.6 kHz and 62.5 kHz radio frequency pulses with a contact time of 2 ms used to achieve the CP condition. For an acquisition time of 20 ms, a recycle delay of 1 s was used and more than. The line broadening function of 50 Hz was applied while processing the spectra. All the ^{13}C spectra were externally referenced to $^{13}\text{COOH}$ resonance of *U* [^{13}C - ^{15}N]-tyrosine/HCl which was referenced to tetramethylsilane (TMS). After optimizing the conditions for 1D ^{13}C CP MAS spectra, 2D ^1H - ^{13}C HETCOR and ^{13}C - ^{13}C PARIS experiments were implemented. For ^1H - ^{13}C HETCOR, different contact times, i.e. 256 μs , 1024 μs , and 3072 μs were used. For ^{13}C - ^{13}C PARIS experiments, mixing times of 10 ms, 25 ms or 30ms were used. The basis of the applied pulse sequences is explained below.

CP-MAS

Cross-Polarized Magic Angle Spinning (CP-MAS) is a technique which is applied to detect low gamma (γ) of rare nucleus such as ^{13}C or ^{15}N . Obtaining a good spectrum of low gamma nuclei is challenging due to their low abundances, low spin polarization, low signal intensity and their characteristic long relaxation times compared to protons leading to long acquisition times. All these aspects can be overcome by CP technique, where the magnetization is transferred from abundant nuclei to rare nuclei. CP is achieved via dipolar couplings and is obtained through the simultaneous application of

two external radio-frequency fields satisfying the Hartmann-Hahn condition [21]. When protons are in the proximity of ^{13}C nuclei, magnetization is transferred, which increases the sensitivity for detecting the ^{13}C nuclei, and the relaxation delays are reduced by exciting the ^1H and ^{13}C together with matching spin lock pulses. CP goes via dipolar coupling and is always combined with MAS. In the MAS experiment, the sample is spun rapidly in a cylindrical rotor around a spinning axis oriented at the magic angle 54.74° with respect to the applied magnetic field [22] [23]. MAS averages the hetero-nuclear dipolar coupling and chemical shift anisotropy (CSA) interactions to zero. Thus, at higher spinning speeds, the inhomogeneous anisotropic line broadenings are removed resulting in narrow central lines. Although MAS removes the main effects of the anisotropic dipolar interactions on the linewidths, higher order effects must be still removed by spin decoupling. This can be achieved through the application of radio-frequency irradiation schemes on the non-observed spins for heteronuclear interactions. Among the several techniques available for heteronuclear decoupling, small phase incremental alternation with 64 steps (SPINAL-64) has been used for the experiments described in this chapter [24].

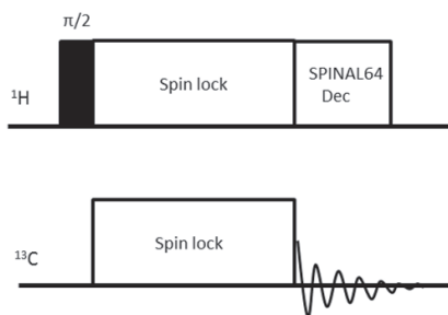


Figure 5.2 Schematic representation of CP-MAS pulse sequence.

HETCOR

Heteronuclear correlation spectroscopy (HETCOR) is a multidimensional experiment [25] that correlates heteronuclear resonances, typically ^{13}C or ^{15}N with ^1H resonances, by transferring polarization between the heteronuclear ^{13}C or ^{15}N and ^1H spins. For solids, obtaining narrow lines in the proton dimension is challenging and this is overcome by the using frequency switched Lee-Goldburg irradiation technique (FSLG) [26].

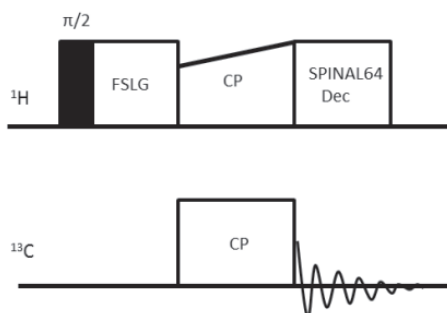


Figure 5.3 Schematic representation of HETCOR pulse sequence.

In our 2D HETCOR experiments, the indirect dimension is the proton while the direct dimension is ^{13}C . By varying the CP contact times, it is possible to get information from directly-bounded proton and carbons using shorter contact times such as $128\ \mu\text{s}$, while the longer contact times, 1072 or $3072\ \mu\text{s}$, give rises to correlated peaks coming from correlations over several bond distances.

PARIS

Phase Alternated Recoupling Irradiation Schemes (PARIS) was used as dipolar recoupling scheme in ^{13}C - ^{13}C experiments.

2D ^{13}C - ^{13}C correlation experiments are essential for defining the tertiary structure of proteins, through space correlation [27].

The efficiency in the magnetization transfer between two carbon nuclei during a recoupling experiment depends from several factors: spatial proximity (r), chemical shift ($\Delta\delta$) and strength of ^1H - ^1H dipolar couplings present in the surrounding proton bath. The last two parameters are sensitive to the specific experimental conditions that are applied [28].

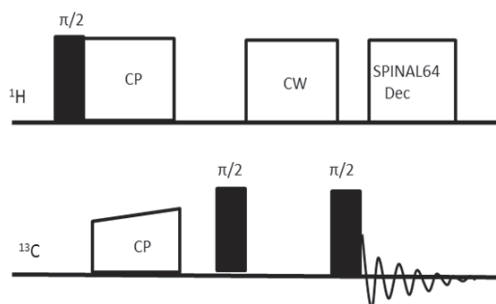


Figure 5.4 Scheme of PARIS pulse sequence.

Using short mixing time, $\tau_m = 10$ ms, the spin diffusion, ^{13}C - ^{13}C is restricted to the closest atoms, while with the increasing of $\tau_m = 30$ ms the spin diffusion is extended to the farther atoms.

RESULTS AND DISCUSSION

The quenched and unquenched ^{13}C lutein-rLhcb1 samples were characterized by UV-Vis absorption and time-resolved fluorescence spectroscopy. The quenched sample shows some scattering in the absorption spectrum due to the aggregate particles suspended in the solution which interferes with the absorption. The samples were compared to the spectra of native LHCII monomer and trimer extracted from market fresh spinach leaves as displayed in Figure 5.5.

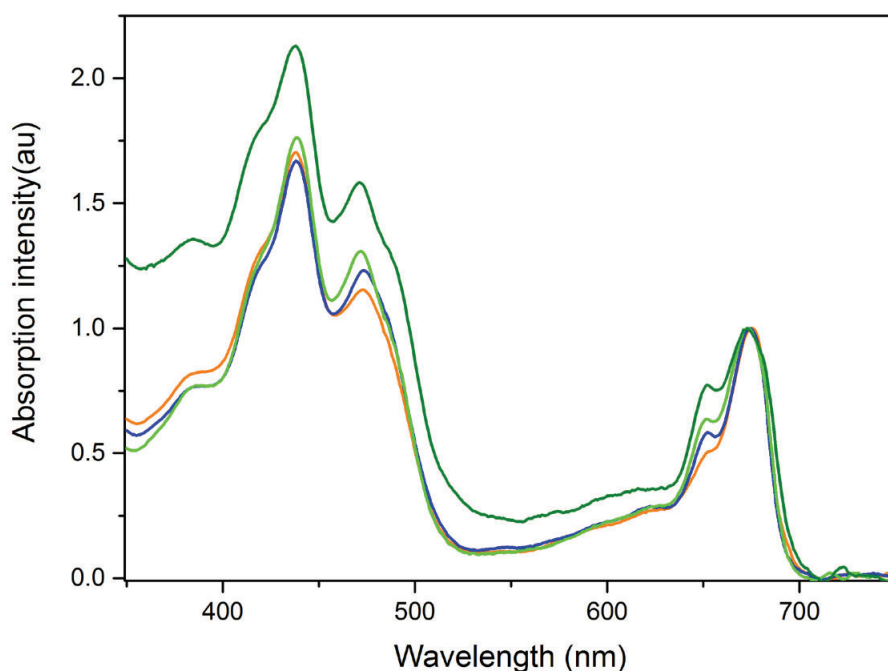


Figure 5.5 In blue LHCII trimer in β -DM, in orange LHCII monomer in β -DM, in light green ^{13}C lutein-rLhcb1 in β -DM and in dark green the ^{13}C lutein-rLhcb1 aggregate. Spectra are normalized to the intensity at 680 nm.

As shown in Figure 5.6 and Table 5.1, the Chl excited-state lifetimes are drastically reduced in aggregated ^{13}C lutein-rLhcb1 compared to detergent-solubilized ^{13}C lutein-rLhcb1, which indicates that the aggregated protein is in a strongly quenched state.

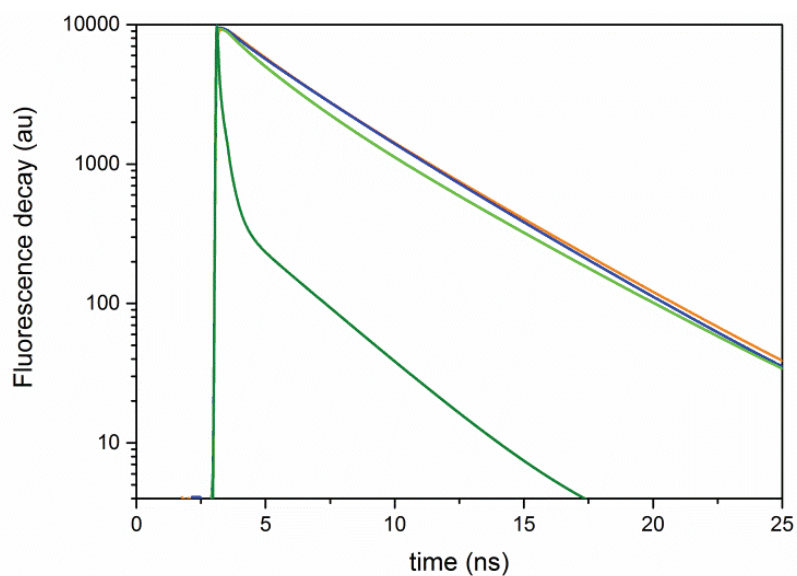


Figure 5.6 Time resolved fluorescence decay spectra. In blue LHCII trimer in β -DM, in orange LHCII monomer in β -DM, in light green ^{13}C lutein-rLhcb1 in β -DM and in dark green the ^{13}C lutein-rLhcb1 aggregate.

	$A_1(\%)$	$\tau_1(\text{ns})$	$A_2(\%)$	$\tau_2(\text{ns})$	$A_3(\%)$	$\tau_3(\text{ns})$	$\tau_{av}(\text{ns})$
LHCII monomer	63.1	4.2	36.9	2	-	-	3.3
LHCII Trimer in β-DM	51.4	4.2	36.5	2.6	12.1	0.5	3.2
^{13}C lutein-rLhcb1 in β-DM	42.5	4.3	43.7	1.9	13.8	0.4	2.7
^{13}C lutein-rLhcb1 aggregate	38.3	0.3	55.6	0.1	6.1	2.7	0.3

Table 5.1 Fitted fluorescence lifetimes of decay traces shown in Figure 5.6.

NMR SPECTROSCOPY

1D ^{13}C CP-MAS EXPERIMENTS

Temperature dependence of ^{13}C CP-MAS NMR spectral intensities of ^{13}C lutein Lhcb1 in β -DM

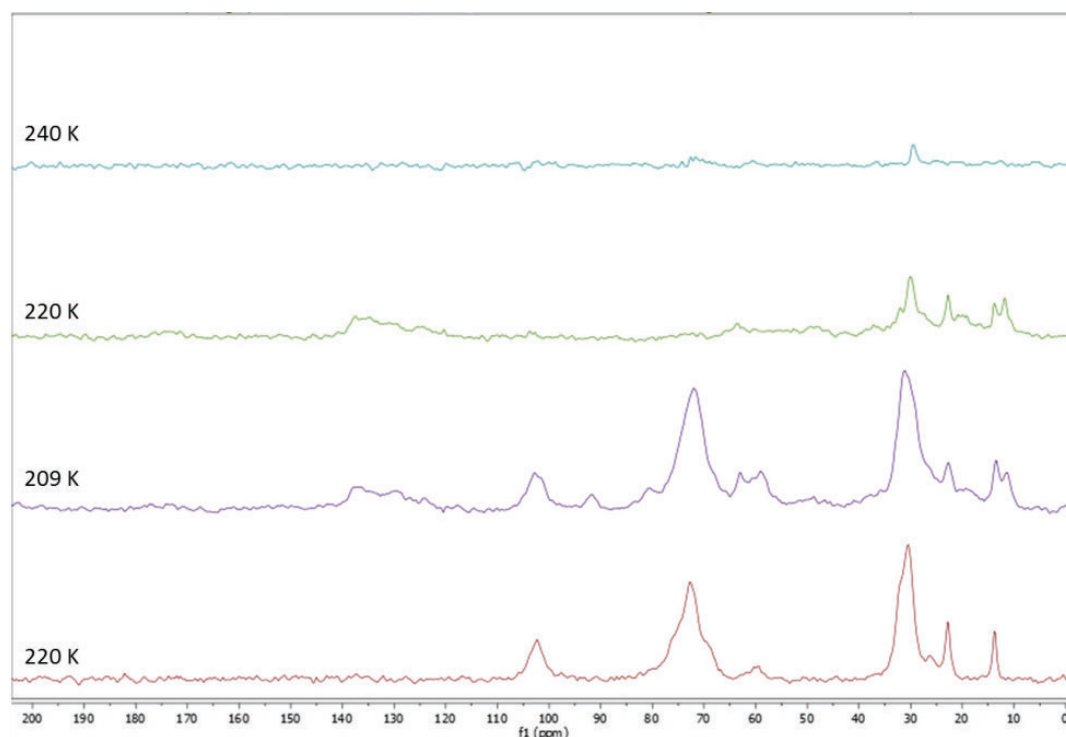


Figure 5.7 CP-MAS spectra of ^{13}C lutein-rLhcb1 in β DM at 240K in blue, 220K in green, 209K in purple. The spectrum of β DM at 220K is presented in red.

For the unquenched sample, lutein ^{13}C chemical shifts are only visible if the temperature is lowered below 240 K due to dynamics of the lutein molecules that makes cross polarization inefficient because of averaging of the dipolar couplings to zero (Figure 5.7). The 1D CP-MAS spectra presented in Figure 5.7 were collected with the same number of scans (NS=512). Following the signal intensities as function of temperature, we observe that going from 240 to 220 K, signal intensities increase, from which we can conclude that the lutein dynamics is reduced. Below 220 K the signal intensities decrease again and are obscured by strong signals of the β -DM detergent molecules (purple spectrum) that become immobilized. Therefore, 220 K was chosen as the optimal temperature.

Comparison of the ^{13}C CP MAS NMR spectra of ^{13}C lutein-rLhcb1 in β -DM, ^{13}C lutein-rLhcb1 aggregates and ^{13}C lutein as crystalline powder.

Spectra of ^{13}C lutein-rLhcb1 in quenched and unquenched states collected at 220K are shown in Figure 5.8, together with the 1D spectrum from lutein as crystalline powder as a reference (Sigma). The spectra show that lutein -CH, -CH₂ and -CH₃ signals can be detected in the ^{13}C lutein-rLhcb1 sample in the two conditions. In the ^{13}C lutein-rLhcb1 spectra, we observe natural abundance ^{13}C signals from the protein, including the backbone -CO peak at ~175 ppm. The asterisks indicate the peaks coming from the detergent, which are clearly visible at ~100 ppm and 70 ppm.

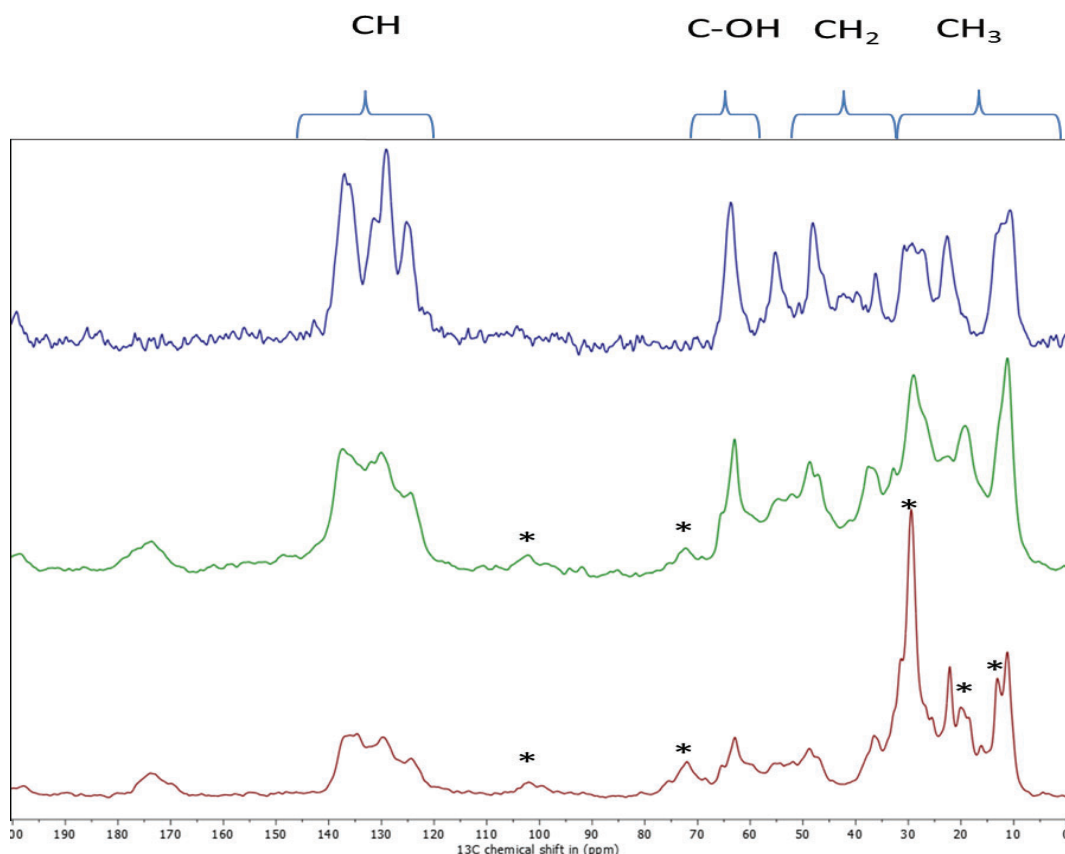


Figure 5.8 CPMAS experiment showing in blue ^{13}C lutein in crystalline form, in green the aggregate ^{13}C lutein-rLhcb1 and in red the ^{13}C lutein-rLhcb1 in β -DM. Asterisk indicate peaks from the β -DM.

^1H - ^{13}C HETCOR NMR EXPERIMENTS

^1H - ^{13}C HETCOR experiments of ^{13}C lutein-rLhcb1 in β -DM and of ^{13}C lutein-rLhcb1 aggregates were recorded at 220 K using different mixing times. Figure 5.9 shows the comparison of HETCOR spectra different two mixing time, 256 and 3072 μs , for the detergent sample. A similar pattern is observed for the HETCOR experiment of only lutein (data shown in Figure A5.6).

Interestingly, in the HETCOR spectra with long mixing times a narrowing of the peaks is observed, compared to the 256 μs spectrum, which is correlated with the extension of the correlations. Notably, an up-field shifted ^1H peak with a chemical shift around -2 ppm

(ω_1 , ^1H), correlating with 16 ppm (ω_2 , ^{13}C) is present in the HETCOR spectrum of ^{13}C lutein-rLhcb1 in β -DM with the mixing time of 256 μs that is not visible in spectra collected with longer mixing time.

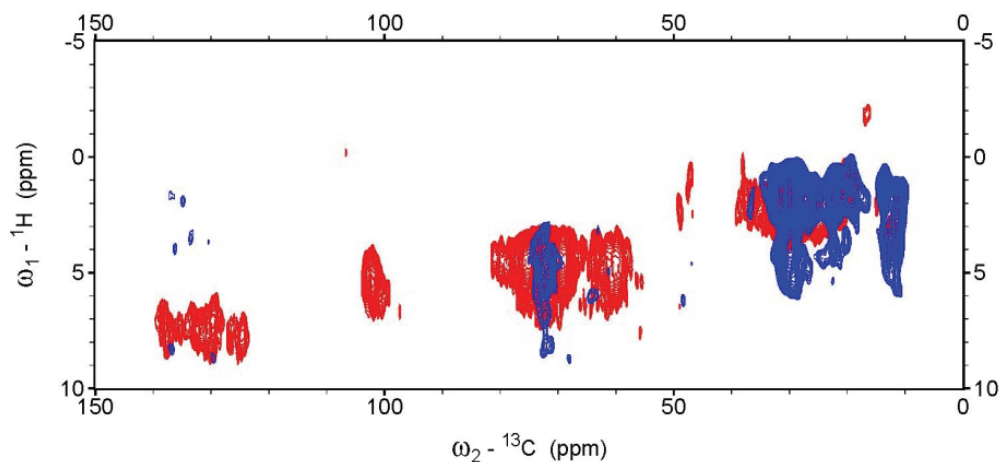


Figure 5.9 HETCOR ^1H - ^{13}C spectra of ^{13}C lutein-rLhcb1 in β -DM collected with 256 μs mixing time (red) and with 3072 μs mixing time (blue).

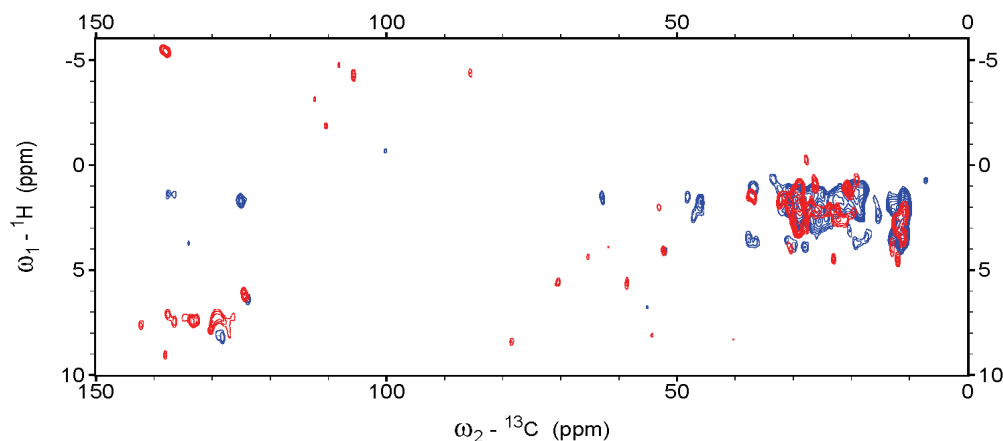


Figure 5.10 HETCOR ^1H - ^{13}C spectra of aggregated ^{13}C lutein-rLhcb1 collected with 256 μs mixing time (red) and with 3072 μs mixing time (blue).

With the short mixing time, only one-bond correlations are observed, while with the long mixing time it can be deduced that up to three-bond correlations are observed. For instance, correlations between the acyl-chain methyl protons and -CH carbons are observed in the region between 0-5 ppm (ω_1) and 120-150 ppm (ω_2). In Figure 5.10 the HETCOR spectra of the aggregate ^{13}C lutein-rLhcb1 at short and long mixing times are overlaid. Figure 5.11 shows a comparison of the detergent and aggregate sample at 256 μs mixing time.

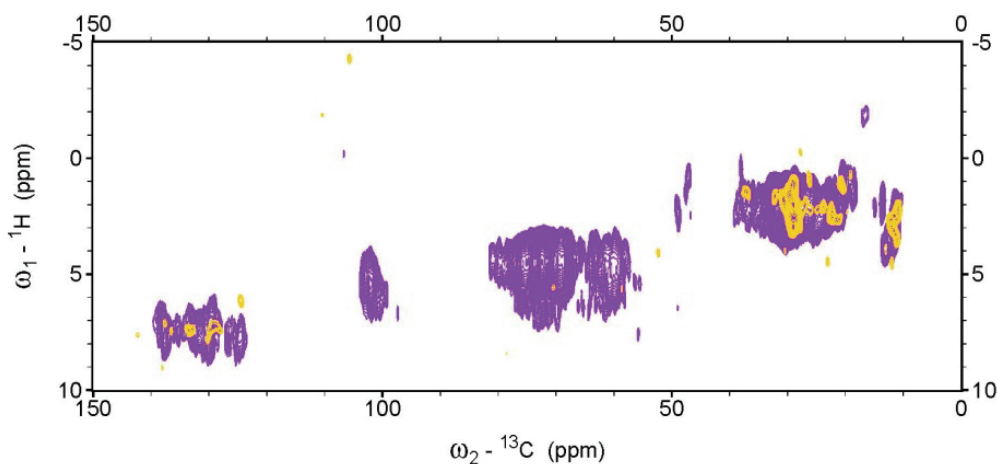


Figure 5.11 HETCOR ^1H - ^{13}C spectra with 256 μs mixing time. Spectra of ^{13}C lutein-rLhcb1 in βDM (purple) and of aggregated ^{13}C lutein-rLhcb1 (yellow).

However, the signal intensities of the aggregate sample were too weak for a proper comparison with the detergent sample and in our further analysis, we continued with the detergent sample of ^{13}C lutein-rLhcb1 in unquenched state.

Assignment of the ^{13}C lutein head atoms in ^{13}C -lutein rLhcb1 in βDM .

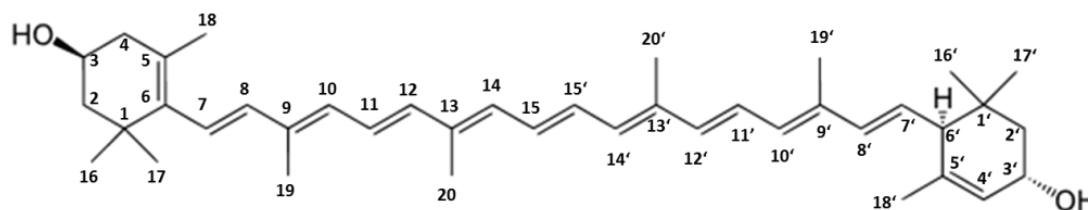


Figure 5.12 Chemical structure of lutein and atom numbering used for the assignments.

Through the combined analysis of the ^1H - ^{13}C HETCOR and ^{13}C - ^{13}C CP PARIS experiments, it has been possible to perform an assignment of the ^{13}C carbons in the lutein heads, that have better dispersion than the signals from the lutein polyene chains. The overlay of the spectrum of ^{13}C lutein-rLhcb1 in $\beta\text{-DM}$ with the spectrum of only $\beta\text{-DM}$ (Figure A5.3) confirms that the peaks coming from the $\beta\text{-DM}$ detergent are not interfering with the lutein signals in the aliphatic region between 30-60 ppm and the aromatic region between 125-140 ppm.

^{13}C - ^{13}C PARIS spectra of ^{13}C lutein-rLhcb1 in $\beta\text{-DM}$ with 25 and 30 ms mixing time in combination with the HETCOR spectrum at 256 μs mixing time was used for NMR assignment of the lutein head atoms as shown in Figure 5.13 and summarized in Table 5.2.

The connections between vicinal atoms have been built starting from the peaks relative to the C18 and C18'. The lutein ^{13}C chemical shift assignments are presented in Table 5.2 and the lutein chemical structure with the atoms numbered is presented in Figure 5.12. We could distinguish the two lutein heads, owing to the double-bond character of carbons in the head-groups. For some correlations, peak doubling is observed due to the fact that the two luteins are in non-equivalent protein environments.

As mentioned above, in the HETCOR spectrum an up-field shifted peak is observed around -2 ppm. Closer inspection shows a doubling of this peak, -1.7 ppm and -2 ppm, indicating that signals of the two luteins are distinguished. We can assign the cross peaks to the -CH₃ in position C18' in the lutein head for both the luteins. The origin of this shift lies in the proximity of this methyl group of Lut1 to the ring of Chl *a*610, and of the head methyl group of Lut2 to the ring of Chl *a*602. Ring-current shifts are very sensitive to changes in the lutein orientation and therefore these NMR signals could be used as a marker in further experiments to compare lutein orientation and interactions in the unquenched and quenched state.

The -CH signals coming from the conjugated lutein chain accumulate in the region between 125-140 ppm, hampering unambiguous assignments.

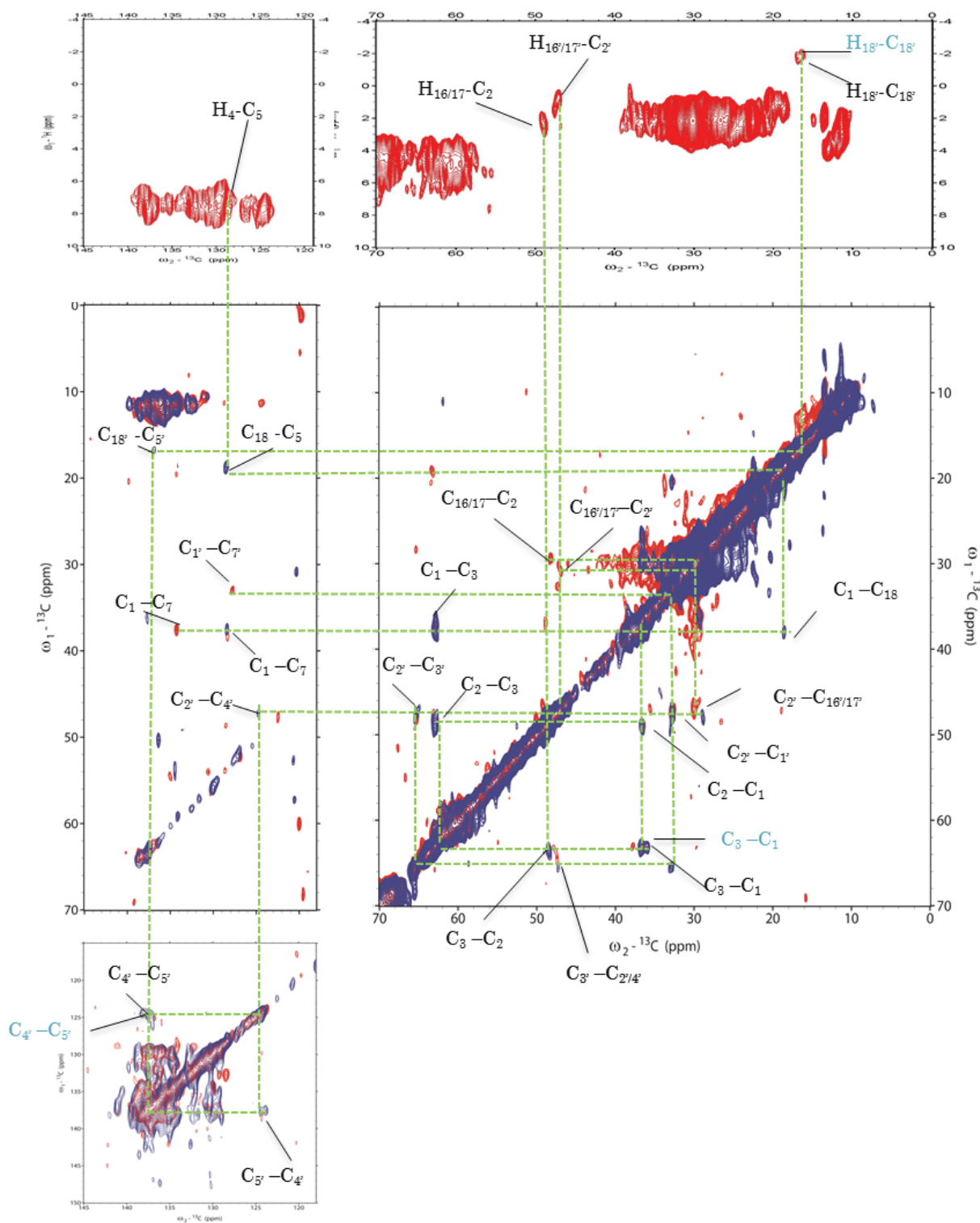


Figure 5.13 ^{13}C - ^{13}C CP PARIS NMR spectra of ^{13}C lutein-rLhcb1 in βDM detergent collected with 25 ms in blue with and 30 ms in red, together with the ^1H - ^{13}C HETCOR spectrum collected with 256 μs mixing time (in red).

Atom	i	δ	ii	δ	i'	δ	ii'	δ
C1, C1'	36.0	2.0	36.7	2.7	32.7	-4.4		
C2, C2'	48.5	2.9			47.5	-0.9		
C3, C3'	62.7	0.8			65.6	-0.3		
C4, C4'					124.5	0.0		
C5, C5'	128.5	-0.7			136.8	-0.9	136.1	-1.6
C6, C6'	134.3	-3.7						
C7, C7'	128.2	2.4			127.6	-1.1		
C16/17, C16'/17'	29.4	0.7			32.8	3.3	30.3	0.8
C18, C18'	18.9	-1.5			16.4	-6.5	16.9	-6.0

Table 5.2 ^{13}C chemical shifts of ^{13}C lutein-rLhcb1 in β -DM are compared to the chemical shifts of lutein in CDCl_3 . *i* and *ii* represent double peaks, for carbons having different chemical shifts for the two luteins. The column identified with δ represents the chemical shift difference between the ^{13}C lutein-rLhcb1 in β -DM and lutein in CDCl_3 .

Figure 5.14 maps the chemical-shift differences between ^{13}C lutein-rLhcb1 in β -DM and lutein in CDCl_3 solution and represents the influence of the protein environment on the lutein ground-state electronic structure.

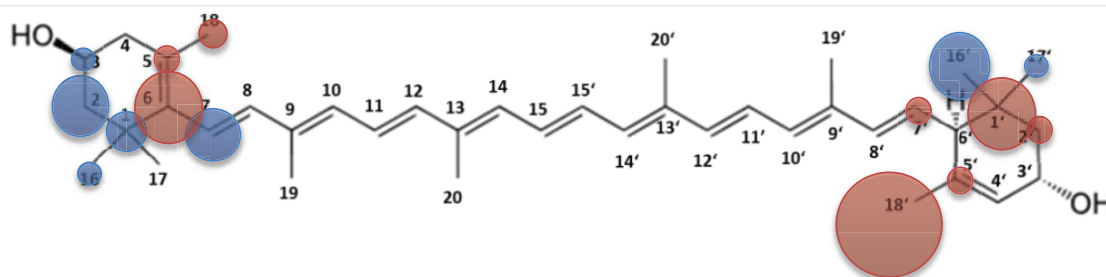


Figure 5.14 Lutein chemical structure mapping chemical shift differences δ between ^{13}C lutein-rLhcb1 in β -DM and lutein in CDCl_3 solution. Blue: downfield shifts; red: up-field shifts. The circle sizes represent the magnitudes of the shift differences.

DISCUSSION

From the crystal structure of LHCII, Lut1 is close to Chl *a*610 and Chl *a*612, while Lut2 is close to Chl *a*602 and Chl *a*603. The Chls *a*610 and *a*602 are close to the heads of the two luteins.

Both Chls *a*610 and *a*602 are ligated via an Arg-Glu ion pair in LHCII. The Arg-Glu ion pairs also have a structural role in stabilizing the two intersecting transmembrane helices of LHCII. In Sunku *et al.*, it was concluded that the Arg-Glu interactions do not change comparing the unquenched and quenched state of LHCII that was prepared respectively in β -DM and aggregated form [2]. Moreover, it was concluded that the orientation of Chl *a*610 and Chl *a*602 with respect to the ligating Arg does not change. From the results, it was predicted that any change in Lut-Chl interactions producing a quenched state, as has been proposed by several studies [9,15,29], should involve a movement of lutein relative to the adjacent Chls that are held in place in the protein.

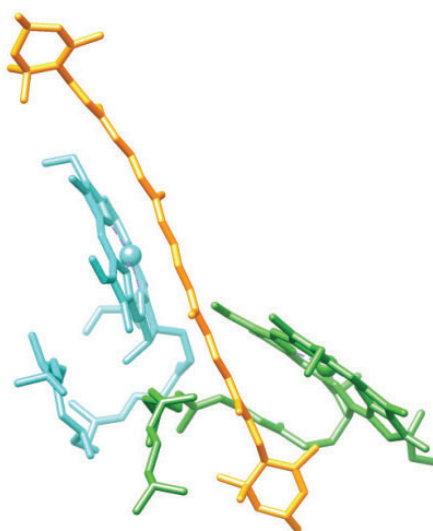


Figure 5.15 Pigments view of LHCII from spinach (PDB- 1RWT). Lut1 in orange, Chl *a*610 in green and Chl *a*612 in cyan.

From the representative structure shown in Figure 5.15 is visible how the lutein chain is almost parallel to Chl *a*612, while the methyl group from the lutein head is pointing toward the center of Chl *a*610. As Balevicius *at al.* predicted using simulation, the lutein moves accordingly to the protein functional state, which is translatable in a change of the interaction with both the Chls [30]. The luteins are stabilized by the stromal and luminal loops of LHCII that may undergo conformational changes in the quenched state. Indeed, the work of Sunku *et al.* showed a change in backbone conformation of an Arg located in the stromal loop [2]. Lut1 is stabilized by the helix D and the loop connecting helix A and D [1] (Figure 5.1). If any conformational change occurs in this loop region, the lutein position may be affected but not the Chls which are bound to the transmembrane helices A and B. Furthermore, chemical-shift changes that were observed in Chl *a* macrocycle

atoms (C4, C5 and C6) between the quenched and unquenched form of LHCII could tentatively be explained by a movement of Lut1 with respect to Chl α 612 [1].

In support for the importance of carotenoids as one of the agents involved in the regulation of light harvesting in the photosystems under high-light conditions there is recent work from Balevicius *et al.* [30] Their study investigated the dependence of the energy-transfer inducing electronic coupling on the mutual orientation of Chl α 612 and Lut1. Their model used a starting point in which Chl α 612 is close to the middle section of the lutein (the C15=C15' bond in Figure 5.12), because that is the center of their transition density [30] and with the chlorine ring maximally parallel to the conjugation plane of the Car, which is a condition for efficient interaction due to the overlap of transition densities [31]. From the simulation, it is clear that the Chl-Car interaction is sensitive to the mutual orientation of the Car and Chl pigments [30]. The relative excitation transfer rate can be driven from excitation-preserving to quenching configurations within physical boundaries. This, according to them, supports the idea of Cars acting as one of the agents regulating energy density in the photosystems under high-light conditions, and presents the most realistic molecular switching pathway [30].

Our work reports for the first time on the structure of the luteins in LHCII in unquenched state, complementing the crystallographic structures of LHCII in the quenched state. Our finding that lutein C18' methyl NMR chemical shift is affected by ring-currents induced by Chl α 610 (Lut1) and Chl α 602 (Lut2) provides us now with a highly sensitive probe for comparing the distances and orientations of the lutein heads in unquenched and quenched states. With this approach, we can experimentally test if the photoprotective switch indeed involves a movement of lutein.

From the representative structure shown in Figure 5.15 it is visible how the lutein chain is almost parallel to Chl α 612, while the methyl group from the lutein head is pointing toward the center of Chl α 610. Balevicius *at al.* predicted that the lutein moves with respect to Chl α 612 accordingly to the protein functional state, which should be translatable in change of the interaction with both the Chls [30].

Moreover, the ring-current effects allow us to compare lutein structures of LHCII in β -DM with lutein in the LHCII crystal structures, as we can predict crystal-structure-based lutein-Chl ring-current shifts and compare those with the experimentally assigned chemical shifts of ^{13}C lutein-rLhcb1 in β -DM [32-34].

Although LHCII contains two luteins, we obtained only one set of lutein head correlations, with doubling of some of the peaks. This suggests that the two lutein molecules are similarly affected by the surrounding pigment-protein environment. Specifically, doubling of the C18' peaks indicates that the Lut1-Chl α 610 and Lut2-Chl α 602 interactions are similar and that there is a high degree of symmetry between the two pigment sites.

The appearance of lutein signals in the detergent sample only below 240 K indicates that at higher temperatures the lutein molecules undergo dynamic, internal motions on a (sub)microsecond timescale. As the lutein positions are correlated with their role as a light harvester or quencher, such dynamics might enable LHCII to switch between quenched and unquenched states.

CONCLUSIONS

In this work, we for the first time could detect the structure and dynamics of lutein in LHCII in unquenched state in a detergent environment. With this preliminary work, we opened the way for an investigation of the interaction between Lut1-Chl α 610 (1), or Lut2-Chl α 602, in quenched and unquenched states to test if the photoprotective switch involves a change in lutein-Chl interactions.

The C18' and H18' NMR chemical shifts are influenced by Chl ring currents and thereby can be used as markers that should be very sensitive to changes in the position and orientation of lutein in the protein. MAS NMR investigations of aggregated, quenched ^{13}C lutein-rLhcb1 are underway.

REFERENCES

1. Pandit A, Reus M, Morosinotto T, Bassi R, Holzwarth AR, de Groot HJ. An NMR comparison of the light-harvesting complex II (LHCII) in active and photoprotective states reveals subtle changes in the chlorophyll a ground-state electronic structures. *Biochim Biophys Acta*, 1827(6), 738-744 (2013).
2. Sunku K, de Groot HJ, Pandit A. Insights into the photoprotective switch of the major light-harvesting complex II (LHCII): a preserved core of arginine-glutamate interlocked helices complemented by adjustable loops. *J Biol Chem*, 288(27), 19796-19804 (2013).
3. Dall'Osto L, Lico C, Alric J, Giuliano G, Havaux M, Bassi R. Lutein is needed for efficient chlorophyll triplet quenching in the major LHCII antenna complex of higher plants and effective photoprotection in vivo under strong light. *BMC Plant Biol*, 6, 32 (2006).
4. Plumley FG, Schimdt W. Reconstitution of chlorophyll a/b light-harvesting complexes: Xanthophyll-dependent assembly and energy transfer. *Cell Biology*, 84, 146-150 (1987).
5. Formaggio E, Cinque G, Bassi R. Functional Architecture of the Major Light-harvesting Complex from Higher Plants. *J. Mol. Biol.*, 314, 1157-1166 (2001).
6. García-Plazaola JI, Matsubara S, Osmond CB. The lutein epoxide cycle in higher plants: its relationships to other xanthophyll cycles and possible functions. *Functional Plant Biology* 34(9), 759-773 (2007).
7. Horton P, Ruban AV, Walters RG. Regulation of Light Harvesting in green plants. *Annu. Rev. Plant Physiol. Plant Mol. Biol.*, 47, 655-684 (1996).
8. Natali A, Gruber JM, Dietzel L, Stuart MCA, van Grondelle R, Croce R. Light-harvesting Complexes (LHCs) Cluster Spontaneously in Membrane Environment Leading to Shortening of Their Excited State Lifetimes. *Journal of biological chemistry* 291(32), 16730-16739 (2016).
9. Ruban AV, Berera R, Iliaia C *et al.* Identification of a mechanism of photoprotective energy dissipation in higher plants. *Nature*, 450(7169), 575-578 (2007).
10. Pascal AA, Liu Z, Broess K *et al.* Molecular basis of photoprotection and control of photosynthetic light-harvesting. *Nature*, 436(7047), 134-137 (2005).
11. S. Bode, Quentmeier CC, Liao P-N, Hafi N, Barros T, Wilk L, Bittner F, and Wall PJ. On the regulation of photosynthesis by excitonic interactions between carotenoids and chlorophylls. *PNAS* 106(30), 12311-12316 (2009).
12. Miloslavina Y, Wehner A, Lambrev PH *et al.* Far-red fluorescence: a direct spectroscopic marker for LHCII oligomer formation in non-photochemical quenching. *FEBS Lett*, 582(25-26), 3625-3631 (2008).
13. Croce R, Weiss S, Bassi R. Carotenoid-binding Sites of the Major Light-harvesting Complex II of Higher Plants. *J. Mol. Biol.* 274(42), 29613-29623 (1999).
14. Standfuss J, van Scheltinga ACT, Lamborghini M, Kühlbrandt W. Mechanisms of photoprotection and nonphotochemical quenching in pea light-harvesting complex at 2.5 Å resolution. *EMBO J*, 24(5), 919-928 (2005).
15. Liu Z, Hanchi Y, Wang K, Kuang T, Zhang J., Gui L, An X & Chang. W Crystal structure of spinach major light-harvesting complex at 2.72 Å resolution. *NATURE*, 428, 2887-2292 (2004).
16. van Oort B, Marechal A, Ruban AV *et al.* Different crystal morphologies lead to slightly different conformations of light-harvesting complex II as monitored by variations of the intrinsic fluorescence lifetime. *Phys Chem Chem Phys*, 13(27), 12614-12622 (2011).
17. Wentworth M, Ruban AV, Horton P. Chlorophyll fluorescence quenching in isolated light harvesting complexes induced by zeaxanthin. *FEBS Lett*, (471), 71-74 (2000).
18. Wentworth M, Ruban AV, and Horton P. Kinetic Analysis of Nonphotochemical Quenching of Chlorophyll Fluorescence. 2. Isolated Light-Harvesting Complexes. *Biochemistry*, 40, 9902-9908 (2001).
19. Alpes H, Apell H-J, Knoll G, Plattner H and Riek R. Reconstitution of Na⁺/K⁺-ATPase into phosphatidylcholine vesicles by dialysis of nonionic alkyl maltoside detergents. *Biochimica et Biophysica Acta*, 946, 379-388 (1988).

20. Fung BM, Khitryn AK, Ermolaev K. An Improved Broadband Decoupling Sequence for Liquid Crystals and Solids. *Journal of Magnetic Resonance*, 142(1), 97-101 (2000).
21. Hartmann SR, Hahn EL. Nuclear Double Resonance in the Rotating Frame. *Physical Review*, 128(5), 2042-2053 (1962).
22. Andrew ER, Bradbury, A. and Eades, R. G. Nuclear magnetic resonance spectra from a crystal rotated at high speed. *Nature*, 182, 1659-1659; (1959).
23. Lowe IJ. Free Induction Decays of Rotating Solids. *Physical Review Letters*, 2 (7), 285-287 (1959).
24. Fung BM, Khitryn AK, and Ermolaev K. An Improved Broadband Decoupling Sequence for Liquid Crystals and Solids. *Journal of Magnetic Resonance*, 142, 97-101 (2000).
25. <http://chem.ch.huji.ac.il/nmr/techniques/2d/hetcor/hetcor.html>.
26. Tian D, Li T, Zhang R *et al.* Conformations and Intermolecular Interactions in Cellulose/Silk Fibroin Blend Films: A Solid-State NMR Perspective. *J Phys Chem B*, 121(25), 6108-6116 (2017).
27. Miao Y, Cross TA. Solid state NMR and protein-protein interactions in membranes. *Curr Opin Struct Biol*, 23(6), 919-928 (2013).
28. Mithu VS, Bakthavatsalam S, Madhu PK. ¹³C-¹³C homonuclear recoupling in solid-state nuclear magnetic resonance at a moderately high magic-angle-spinning frequency. *PLoS One*, 8(1), e50504 (2013).
29. Ilioaia C, Johnson MP, Liao PN *et al.* Photoprotection in plants involves a change in lutein 1 binding domain in the major light-harvesting complex of photosystem II. *J Biol Chem*, 286(31), 27247-27254 (2011).
30. Balevicius V Jr., Fox KF, Bricker WP *et al.* Fine control of chlorophyll-carotenoid interactions defines the functionality of light-harvesting proteins in plants. *Sci Rep*, 7(1), 13956 (2017).
31. Dreuw A, Fleming GR, Head-Gordon M. Role of electron-transfer quenching of chlorophyll fluorescence by carotenoids in non-photochemical quenching of green plants. *Biochemical Society Transactions*, 33(4), 858-862 (2005).
32. Abraham RJ, Smith KM. NMR Spectra of Porphyrins. 21. Applications of the Ring-Current Model to Porphyrin and Chlorophyll Aggregation1. *J. Am. Chem. Soc.*, 105, 5734-5741 (1983).
33. Janson TR, Kane AR, Sullivan JF, Knox K, and Kenney ME. The Ring-Current Effect of the Phthalocyanine Ring. *Journal of the American Chemical Society*, 91(19), 5210-5212 (1969).
34. Mizoguchi T, Sakamoto S, Koyama Y, Ogura K and Inagak F. The Structure of the Aggregate Form of Bacteriochlorophyll *c* Showing the Q_y Absorption above 740 nm as Determined by the Ring-current Effects on ¹H and ¹³C Nuclei and by ¹H-¹H Intermolecular NOE Correlations. *Photochemistry and Photobiology*, 67(2), 239-248 (1998).
35. Ragasa CY, Levida RM, Don MJ and Shen CC. Cytotoxic Isothiocyanates from *Moringa oleifera* Lam Seeds. *Philippine Science Letters*, 5(1) (2012).
36. La Fountain AM, Pacheco C, Prum RO, Frank HA. Nuclear magnetic resonance analysis of carotenoids from the burgundy plumage of the Pompadour Cotinga (*Xipholena punicea*). *Arch Biochem Biophys*, 539(2), 133-141 (2013).
37. Mathur A. Extraction, isolation and purification of Lutein, Zeaxanthin, Meso-Zeaxanthin and β-Cryptoxanthin. CHAPTER-3.

A.5 Liquid and Solid-State NMR of lutein

^{13}C NMR lutein spectra were assigned accordingly to Ragasa *et al.* [35] while proton assignment is accordingly to [36,37] Even though this value comes from protein in CDCl_3 this is the best guess to start were to look for the pigment peaks. We expected indeed a shift of the ppm because the lutein in the protein is exposed to a different protein environment which reflect in shifts of the peaks.

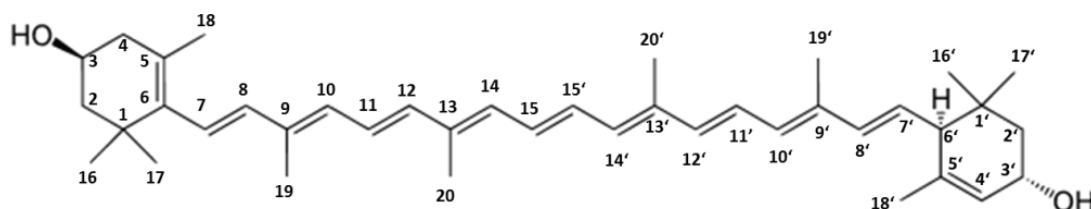


Figure A5. 1 Chemical structure of lutein.

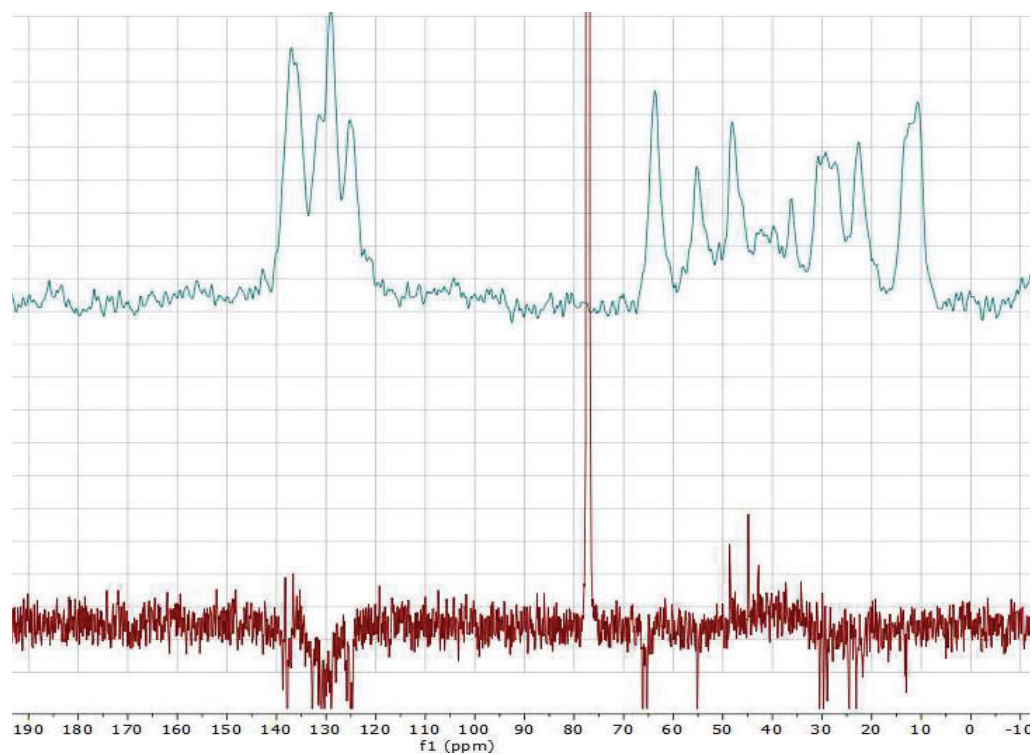


Figure A5.2 In blue 1D solid state NMR of na lutein powder compared with its liquid (dissolved in CDCl_3) NMR spectrum in red.

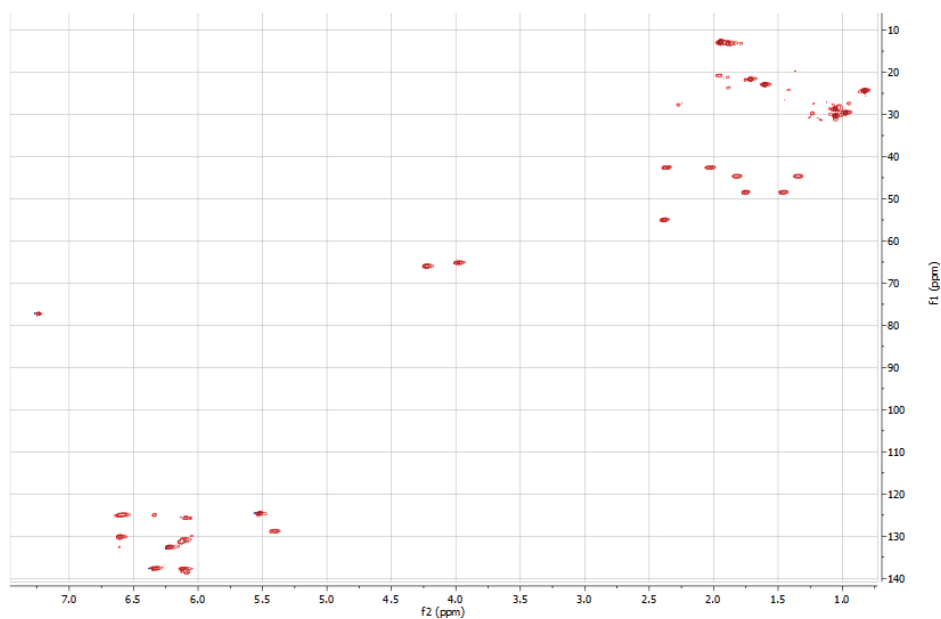


Figure A5.3 HSQC-EDETPG of lutein in $CDCl_3$. In blue -CH and - CH_3 and in red - CH_2 and -C.

Atoms	Functional group	^{13}C Chemical shift ppm	1H Chemical shift ppm
x	CH	65.10	N/A
C ₁₆	CH ₃	28.70	1.07
C ₁₇	CH ₃	30.30	1.07
C ₁₈	CH ₃	21.60	1.74
C ₁₉	CH ₃	12.70	1.97
C ₂₀	CH ₃	12.70	1.967
C _{20'}	CH ₃	12.80	1.967
C _{19'}	CH ₃	13.10	1.91
C _{18'}	CH ₃	22.90	1.64
C _{16'}	CH ₃	29.50	0.85
C _{17'}	CH ₃	24.70	0.99
C _{1'}	C	34.00	N/A
C _{2'}	CH ₂	44.60	1.37 and 1.85
C _{3'}	CH (-OH)	65.90	N/A
C _{4'}	CH	124.50	6.64
C _{5'}	C	137.70	n/A
C _{6'}	CH	55.00	N/A
C _{7'}	CH	128.70	5,43
C _{8'}	CH	130.80	6.63
C _{9'}	C	135.10	N/A
C _{10'}	CH	137.60	6.26

C _{11'}	CH	124.80	6.64
C _{12'}	CH	137.70	6.36
C _{13'}	C	136.50	N/A-
C _{14'}	CH	132.60	6.14
C _{15'}	CH	130.10	6.63
C ₁₅	CH	130.10	6.63
C ₁₄	CH	132.60	6.26
C ₁₃	C	136.40	N/A
C ₁₂	CH	137.50	6.35
C ₁₁	CH	124.90	6.64
C ₁₀	CH	131.30	6.15
C ₉	C	135.7	N/A
C ₈	CH	138.50	6.15
C ₇	CH	125.60	6.10
C ₆	C	138.00	N/A
C ₅	C	126.20	N/A
C ₄	CH ₂	42.50	2.04 AND 2.39
C ₃	CH(-OH)	65.10	?
C ₂	CH ₂	48.40	1.45 and 1.77
C ₁	C	37.10	N/A

Table A5.1 ¹³C and ¹H chemical shift table of lutein in CDCl₃.

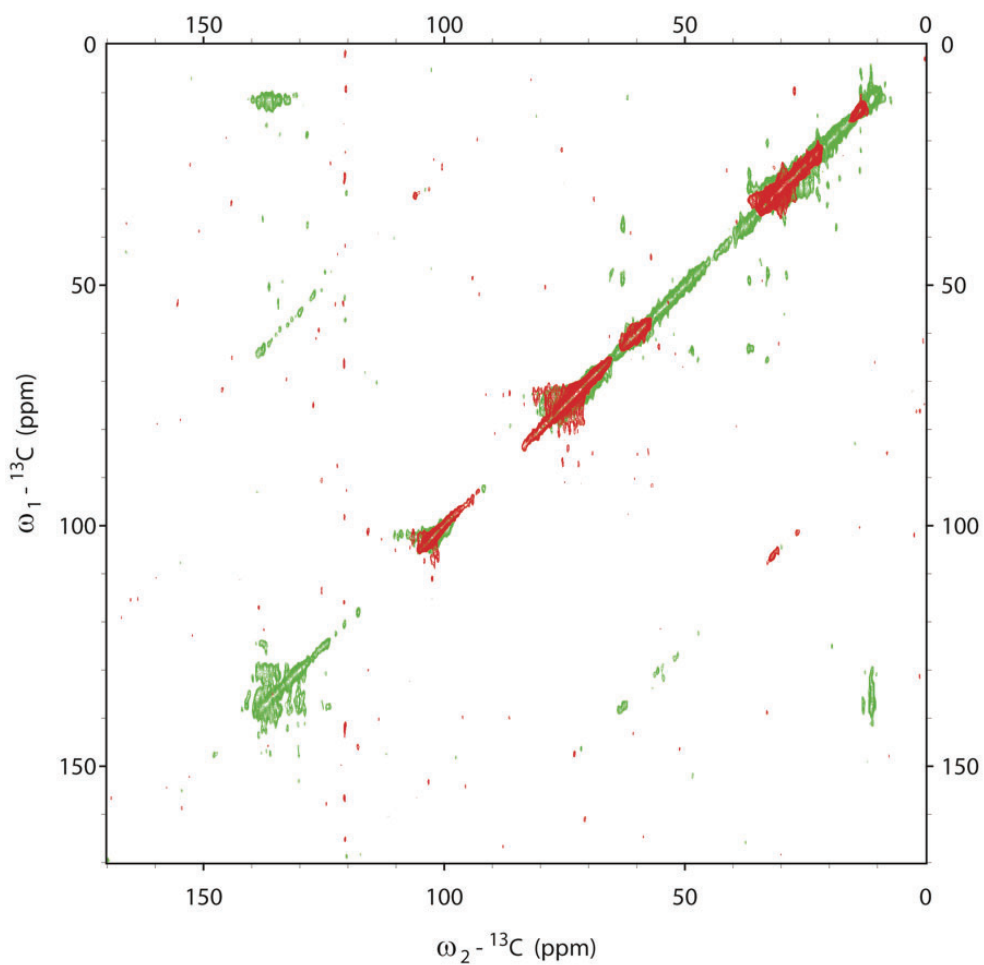


Figure A5.4 Overlaid ${}^{13}\text{C}$ - ${}^{13}\text{C}$ PARIS NMR spectrum collected with 25ms mixing time. In red: NMR spectrum of β -DM and in green ${}^{13}\text{C}$ lutein-rLhcb1 in β -DM.

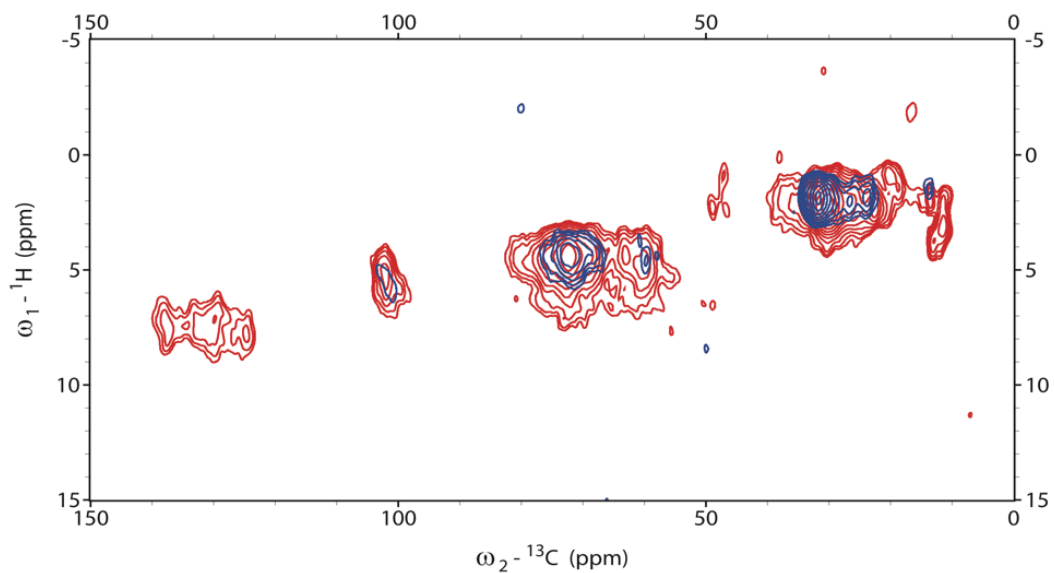


Figure A5.5 ${}^1\text{H}$ - ${}^{13}\text{C}$ HETCOR spectra of the unquenched ${}^{13}\text{C}$ lutein-rLhcb1 in red and β -DM in blue using 256 μs contact time.

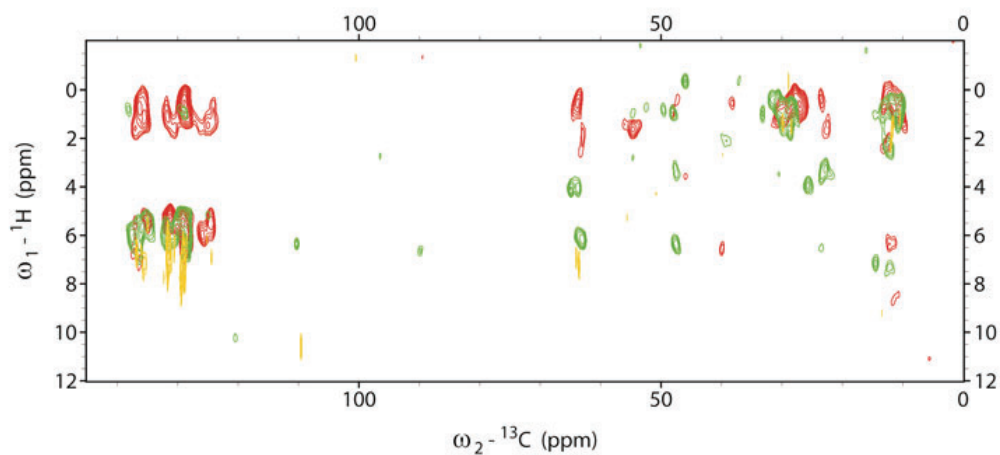


Figure A5.6 ^1H - ^{13}C HETCOR spectra of ^{12}C lutein powder at different mixing time. In yellow 256 μs , in green 1024 μs and in red 3072 μs .

With the increase of the mixing time the correlation between ^1H and ^{13}C goes from 1 bond up to 3 bonds.

CHAPTER 6

CONCLUSIONS and OUTLOOK

CONCLUSIONS

The Light-Harvesting Complex II is the most abundant Light-Harvesting Complex in nature and is involved in both photoprotection and light harvesting processes.

By comparing the fluorescence characteristics of LHCII in liposomes and in lipid nanodiscs the effects of protein and lipid interactions have been discriminated in the presented approach.

LHCII fluorescence quenching is not the result of a specific thylakoid lipid microenvironment but is driven by LHCII protein-protein interactions. We also demonstrated that LHCII is unidirectional inserted in proteoliposomes, according to the analysis of enzyme cleavage products, which is a significant achievement in membrane protein reconstitution that has importance for mimicking protein functions *in vitro*.

The transition from a light-harvesting to a quenching state is associated with LHCII pigment-protein conformational changes. To understand the role of the lutein in this process, recombinant Lhcb1 from *A. thaliana* with ^{13}C lutein was successfully refolded and investigated by solid state NMR. By this approach, we could assign the lutein heads of ^{13}C lutein-rLhcb1 and for the first time obtain structural information of lutein in LHCII in the active, fluorescent state.

In vivo Chl excited-state quenching of the photosynthetic antenna associated with photoprotection is the result of a series of events and has been proposed to involve the interaction between LHCII and PsbS. The time-resolved fluorescence study of our minimal PsbS-LHCII membrane model do not point toward functional quenching interactions between LHCII and PsbS, neither show a significant effect after lowering the pH. The results strongly suggest that the pH-dependent role of PsbS during the fast qE response lies in creating membrane rearrangements and super complex remodelling that could facilitate LHCII quenching, rather than in creating direct quencher states.

OUTLOOK

By complementing the solid-state NMR experiments on ^{13}C lutein-rLhcb1 in unquenched state with NMR experiments on quenched ^{13}C lutein-rLhcb1 aggregates, it will be possible to reveal if the photoprotective switch of LHCII involves a change in lutein interactions. Further studies can be performed on the protein inserted in liposomes or nanodiscs to mimic the *in vivo* environment and reproduce *in vitro* different protein functional states. To address the role of lutein-Chl *a* interactions in forming a quencher state, it would be of interest to refold Lhcb1 in presence of ^{13}C labelled Chl *a* and compare NMR spectra of ^{13}C Chl *a*-rLhcb1 in quenched and unquenched state. With this experiment will be possible to specifically investigate if any changes are involved in the surrounding of the Chl *a*, which pigments so far have only been detected in NMR spectra of uniformly labelled LHCII sample.

The experiments presented in Chapter 3 show that interaction between PsbS and LHCII is not sufficient to induce the photoprotective switch of LHCII. It would be of interest to

test the interaction between PsbS and zeaxanthin-binding LHCII, which is naturally present in the protein under stress conditions due to the depoxidation of violaxanthin as the presence of Zea seems to be indispensable to induce qE quenching *in vivo*.

SUMMARY

Solar energy is an intermittent light-source, and is used by photosynthetic organisms to drive energy required cellular processes. Solar energy is primarily absorbed by two groups of pigments, chlorophylls and carotenoids, which are mainly located in the light harvesting complex proteins (LHCs). These proteins are essential for the performance of photosynthesis, not only because they are involved in harvesting the light, but also because they protect the photosynthetic system from excess of light that can cause photodamage.

In **Chapter 2**, I performed *in vitro* studies mimicking the two functions of LHCII by inserting the protein in nanodiscs and in liposomes to mimic respectively the light-harvesting and the photoprotector activity. I demonstrate that Chl excitation quenching is dependent on protein-protein interactions, and not on protein-lipid interactions, by performing fluorescence experiments on proteoliposomes with different PLRs and using thylakoids lipids or asolectin.

For mimicking native-like protein interactions, LHCII should be inserted unidirectionally in the membranes, like *in vivo*. Using enzymatic digestion, I show that there is a preferential insertion of the LHCII proteins in our model membranes.

Using asolectin model membranes, I investigated the specific interactions of LHCII with PsbS which are known to play a key role in quenching excitations under light-stress conditions *in vivo*. **Chapter 3** was dedicated to explore whether only the interaction between the two proteins, in acidified environments, is sufficient to promote LHCII fluorescence quenching. CD and TRF studies were performed on PsbS-LHCII proteoliposomes at different pH conditions. The fluorescence study of our minimal membrane models strongly suggests that the pH-dependent role of PsbS, during the fast qE response, lies in creating membrane rearrangements and supercomplex remodeling that could facilitate LHCII aggregation quenching, rather than in creating direct quencher states.

In **Chapters 4 and 5** the focus shifts from an intermolecular approach toward an intramolecular approach to understand how the protein in the quenched state changes the pigment conformations in comparison to the unquenched state. I successfully obtained ^{13}C lutein-rLhcb1 by refolding recombinant Lhcb1 from *Arabidopsis thaliana* in the presence of non-isotopically labelled pigments from fresh market spinach with excess of ^{13}C labelled lutein extracted from isotopically labelled *Chlamydomonas reinhardtii* and isolated via HPLC. The ^{13}C lutein-rLhcb1 protein in detergent, mimicking the unquenched state, and protein aggregates, mimicking the quenched state, were biochemically and spectroscopically characterized and further analysed with solid state NMR. The lutein ^{13}C chemical shifts could be assigned for LHCII in detergent. Ring current shifts of the lutein head signals indicate that the heads are in close proximity to specific Chls (Chl *a*610 and Chl *a*602), providing for the first-time structural information about lutein-Chl interactions in LHCII in its unquenched state.

SAMENVATTING

Zonne-energie is een fluctuerende lichtbron die gebruikt wordt door fotosyntheseorganismen om cellulaire processen aan te drijven. Zonne-energie wordt primair geabsorbeerd door twee groepen pigmenten, het chlorofyl en de carotenoiden, welke voornamelijk voorkomen in eiwitcomplexen (LHC's). Deze eiwitten zijn essentieel voor de werking van fotosynthese, niet alleen omdat ze betrokken zijn bij het opvangen van licht, maar ook omdat ze het fotosynthesesysteem beschermen tegen schade door overmatige lichtinval.

In **Hoofdstuk 2** heb ik in vitro studies uitgevoerd om de twee functies van LHCII na te bootsen, door het eiwit in nanodiscs en liposomen in te voegen, waarmee respectievelijk de lichtopvangactiviteit en de lichtbeschermingsactiviteit nagebootst worden. Ik heb aangetoond dat Chl fluorescentiedoving afhankelijk is van eiwit-eiwit interacties, en niet van eiwit-lipide interacties, door fluorescentie-experimenten uit te voeren op proteoliposomen met verschillende PLR's en gebruik te maken van thylakoïd lipiden of asolectin. Om natuurgetrouwe eiwitinteracties na te bootsen is vereist dat LHCII unidirectioneel in de membranen ingevoegd wordt, zoals in vivo. Door gebruik te maken van enzymatische vertering heb ik gedemonstreerd dat er een preferentiële invoeging bestaat van de LHCII-eiwitten in onze modelmembranen.

Met behulp van modelmembranen gemaakt van asolectine heb ik de specifieke interactie van LHCII met PsbS onderzocht, waarvan bekend is dat ze in vivo een sleutelrol spelen in fluorescentiedoving onder invloed van lichtinval. In **Hoofdstuk 3** is onderzocht of de interactie tussen alleen de twee eiwitten, in een aangezuurde omgeving, genoeg is om LHCII fluorescentiedoving te doen plaatsvinden. CD en TRF studies zijn uitgevoerd naar PsbS-LHCII proteoliposomen bij verschillende pH condities. Fluorescentieonderzoek naar ons modelmembraan wijst er sterk op dat de pH-afhankelijke rol van PsbS, gedurende de snelle qE respons, ligt in het herschikken van het membraan en het opnieuw modelleren van het supercomplex dat LHCII-aggregatie-uitdoving faciliteert, in plaats van het creëren van uitdovingstoestanden.

In **Hoofdstukken 4 en 5** verschuift de focus van een intermoleculaire aanpak naar een intramoleculaire aanpak, om te kunnen begrijpen hoe het eiwit in de uitgedoofde toestand de pigmentconformaties verandert, in vergelijking tot de niet-uitgedoofde toestand. Ik heb op succesvolle wijze ¹³C luteïne-rLhcb1 verkregen door het opnieuw vouwen van recombinant Lhcb1 eiwit uit *Arabidopsis thaliana* in de aanwezigheid van niet-isotopisch gelabeld pigment uit verse spinazie met een overmaat van ¹³C-gelabeld luteïne, dat via HPLC geëxtraheerd is uit isotoop verrijkt *Chlamydomonas reinhardtii*.

Het ^{13}C luteïne-rLhcb1 eiwit in detergens, dat de niet uitgedoofde toestand nabootst, en eiwitaggregaten, die de uitgedoofde toestand nabootsen, zijn biochemisch en spectroscopisch gekarakteriseerd en verder geanalyseerd met vaste stof-NMR. De chemische verschuiving voor ^{13}C luteïne kon worden toegekend voor LHCII in detergens. Ringstroomverschuivingen van de luteïne-kopsignalen geven aan dat de koppen zich dicht bij specifieke Chls bevinden (Chl a610 en Chl a602), waarmee voor de eerste keer structurele informatie over de luteïne-Chl interactie in LHCII in zijn niet-uitgedoofde staat geleverd wordt.

RIASSUNTO

L'energia solare è una sorgente fluttuante di luce, usata da sistemi fotosintetici per portare avanti processi cellulari richiedenti energia chimica. L'energia solare è principalmente assorbita da due gruppi di pigmenti, clorofille e carotenoidi, maggiormente localizzati nei complessi collettori di luce (LHCs). Queste proteine sono essenziali per la fotosintesi non solo perché coinvolte nell'assorbimento della luce ma anche perché proteggono il sistema da danni provocati dall'eccesso di energia solare.

Nel **Capitolo 2**, ho condotto studi *in vitro*, al fine di mimare le due principali funzioni della proteina LHCII. Quest'ultima è stata inserita in liposomi e nano dischi ricreando rispettivamente lo stato collettore di luce e foto-protettore. Ho dimostrato che il quenching dello stato eccitato delle Chls dipende essenzialmente da interazioni proteina-proteina e non da interazioni proteina-lipidi. L'obiettivo è stato raggiunto analizzando la fluorescenza di proteo-liposomi con differente contenuto di proteina usando asolectina e lipidi tilacoidi. Per riuscire a creare interazione simile a quella *in vivo*, LHCII dovrebbe essere inserita unidirezionalmente nella membrana lipidica. Attraverso una digestione enzimatica, ho mostrato un'inserzione preferenziale della proteina LHCII nelle nostre membrane modello.

Usando membrane modello con asolectina lipidi, ho provato ad investigare le specifiche interazioni tra la proteina LHCII con PsbS, nota per il suo ruolo fondamentale nel quenching dello stato eccitato in caso di stress *in vivo*. Il **Capitolo 3** è, quindi, dedicato ad investigare che il solo ambiente acido possa essere sufficiente per la promozione del quenching della fluorescenza. Gli esperimenti di CD e TRF sono stati condotti su PsbS-LHCII proteo-liposomi a pH 5 e 7.5. Il ruolo dipendente dal pH del PsbS durante la veloce risposta al qE, risiede nel promuovere arrangiamenti della membrana lipidica facilitando l'interazione LHCII-LHCII piuttosto che attivare direttamente lo stato di quenching.

Nei **Capitoli 4 e 5** il focus è spostato dalla sfera intermolecolare alla sfera intramolecolare per capire come la proteina cambi la distribuzione spaziale dei pigmenti a causa dello stato di quenching. Ho ottenuto con successo ¹³C lutein-rLhcb1, tramite il refolding della proteina con clorofille e carotenoidi estratti da spinaci freschi e, in presenza di un eccesso della sola luteina estratta da *Chlamydomonas reinhardtii* marcate isotopicamente e purificato tramite HPLC. La ¹³C lutein-rLhcb1 così ottenuta, solubilizzata in presenza di detergente, mima lo stato di non quenching mentre la proteina aggregate, mima lo stato di quenching. Ambedue sono state caratterizzate dal punto di vista biochimico e spettroscopico. Indagini più specifiche sono state condotte con NMR allo stato solido. I dati ottenuti da quest'ultimo sono stati comparati con quelli del chemical shift ottenuti dall'indagine della sola luteina. La corrente di anello prodotta nelle strutture cicliche provoca un chemical shift quando la testa della luteina è nelle vicinanze delle Chls (Chl *a*610 e Chl *a*602), dando per la prima volta informazioni strutturali riguardo le interazioni specifiche luteina-Chl nella proteina LHCII nello stato di non quenching.

CURRICULUM VITAE

My name is Emanuela Crsafi and I was born in Brindisi the 22nd November 1988. I grew up in my parent' s home town, Catania, in the beautiful Italian region of Sicily, where I have completed all my studies. My, early discovered, passion for science drove me to start, in the 2007, the Bachelor program of Science in Chemistry after which I decided to proceed with a Master in Material Chemistry. During the two years of my master I realized deep interest in all what concerned biochemistry, therefore I decided to invest my master internship in the group of the Prof. Dr. C. La Rosa studying stability of DNA quadruplexes. After having graduated with honors in the 2013 I undertook the challenging path of the PhD in Leiden, in the 2014 in the group of Dr. Anjali Pandit promoted by Prof. Dr. Huub J.M. de Groot, with the aim of studying the molecular plasticity of LHCII.

In my academic career, I have been accepted to participate to the SSNMR school in Munich (GE, 2014) and to the XX School of Pure and Applied Biophysics in Venice, with the focus in Molecular and biophysical aspects of photosynthesis (IT, 2016).

During the past years my work was selected to be presented as posters in several conferences: Dutch Biophysics (NL, 2014), Reedijk symposium (NL 2014), SSNMR school (GE, 2014), Dutch Biophysics (NL, 2015), Chain (NL, 2015), 17th International Congress on Photosynthesis Research, PS17 and Light Harvesting satellite meeting (NL ,2016), Dutch Biophysics (NL, 2016), Chain (NL, 2016), Gordon research conference and Gordon research seminar in Photosynthesis (USA,2017).

PUBLICATIONS

- V. Romanucci, D. Milardi, T. Campagna, M. Gaglione, A. Messere, A. D'Urso, E. Crisafi, C. La Rosa, A. Zarrelli, J. Balzarini, G. Di Fabio (2014) *Synthesis, biophysical characterization and anti-HIV activity of novel 5'-Hydrophobic-conjugated G-quadruplex forming oligonucleotides*, *Bioorganic & Medicinal Chemistry*, 22, (3), 960–966
- E. Crisafi & A. Pandit (2017) *Disentangling protein and lipid interactions that control a molecular switch in photosynthetic light harvesting*. *BBA Membrane*
- E. Crisafi, M. Krishnan & A. Pandit, *Time-resolved fluorescence analysis of LHCII in the presence of PsbS at neutral and low pH*. (Submitted).

ACKNOWLEDGMENT

I want to thank my supervisor Dr. A. Pandit for the given opportunity. During these years of Ph.D., I have grown learning that is essential to be open to change point of view, each small achievement is a very big step in our development and we should be proud of. Thanks to my promotor Prof. dr. H.M.J. de Groot, whom never misses an opportunity to have nice and challenging discussion and from whom I have learned that we **MUST ALWAYS THINK**.

Thanks to Geri and Nora, it has been a pleasure to be supported from you. Your passion and dedication to science has been inspirational. Geri, your structure and strong mind made me feel safe and comfortable.

A special thanks to Karthick, without whom I could not manage to let it go. You are an endless source of inspiration and management. You helped me during the most difficult and challenging period of my Ph.D.

TOA, Arian, Trudi, Marco you have been really kind with helping me when needed and willing to slow down in your busy day to let me practice my Dutch. I will never forget your kind souls.

Liesbeth, dear Liesbeth... at the beginning of our journey you were there willing to help us for everything and anything. Later stage, you became the solid pillar that each of us need in our Ph.D. experience.

Thanks to ALL the BOPC group, with whom I enjoyed very lovely lunch breaks colored with all the possible discussion topics, most frequently regarding food. What to say we like to eat ☺. Never forget that LUNCH time is 12:30 no matter what...

A special thanks to my good and old LCP2, Jessica, Remco and Dieuwertje. I miss so much our time there. Finally, after 3 years from that new year proposition I could fulfill the point: "Have Dutch discussion with Emanuela". Better later than never :P Vidya, you introduced me to a new vision of life, science and food...Thanks a lot I will always remember the first time that I met you.

Thanks to Kassi, you always make my days unpredictable.

An unconditional thanks to Rubin. You were always there listening and thinking with me. You helped me a lot and supported since you joined the group. Your passion for science knowledge in all its peculiarity is admirable.

Fatemeh and Maithili. We started together this journey, I am pleased that with the time our bonding increased. We shared so much during this experience, from work to personal life.

Thanks to Nicola who always had to deal with my peculiar character which made our days full of surprise.

Thanks to my family who gave me the opportunity to study and made me grow resolute and strong minded as I am.

Thanks to all my friend who, in Leiden, are as a second family, making me feel at home. Stefania, even if far from each other we shared this life experience together. Lontane ma vicine sempre!